JOSÉ CARLOS DE MORAES SILVA

THEORETICAL INVESTIGATION OF EPIDEMIC DISEASES WITH WANING IMMUNITY

Thesis presented to the Universidade Federal de Viçosa, as part of the requirements of the Graduate Program in Physics, to obtain the degree of *Doctor Scientiae*.

Adviser: Silvio da Costa Ferreira Junior

Co-adviser: Diogo Henrique da Silva

VIÇOSA - MINAS GERAIS
2024

Ficha catalográfica elaborada pela Biblioteca Central da Universidade Federal de Viçosa - Campus Viçosa

T
S586t
2024

Silva, José Carlos de Moraes, 1989-
Theoretical investigation of epidemic diseases with waning immunity / José Carlos de Moraes Silva. – Viçosa, MG, 2024.
1 tese eletrônica (107 f.): il. (algumas color.).

Texto em inglês.
Inclui apêndices.
Orientador: Silvio da Costa Ferreira Junior.
Tese (doutorado) - Universidade Federal de Viçosa, Departamento de Física, 2024.
Referências bibliográficas: f. 96-107.
DOI: https://doi.org/10.47328/ufvbbt.2025.437
Modo de acesso: World Wide Web.

1. Redes (Matemática). 2. Markov, Processos de. 3. Epidemias - Modelos matemáticos. I. Ferreira Junior, Silvio da Costa, 1976-. II. Universidade Federal de Viçosa. Departamento de Física. Programa de Pós-Graduação em Física. III. Título.

CDD 22. ed. 514.223

Bibliotecário(a) responsável: Euzébio Luiz Pinto CRB-6/3317

JOSÉ CARLOS DE MORAES SILVA

THEORETICAL INVESTIGATION OF EPIDEMIC DISEASES WITH WANING IMMUNITY

Thesis presented to the Universidade Federal de Viçosa, as part of the requirements of the Graduate Program in Physics, to obtain the degree of *Doctor Scientiae*.

APPROVED: December 19th 2024.

Assent:

Documento assinado digitalmente
gov.br
JOSE CARLOS DE MORAES SILVA
Data: 01/07/2025 21:53:39-0300
Verifique em https://validar.iti.gov.br

José Carlos de Moraes Silva
Author

Documento assinado digitalmente
gov.br
SILVIO DA COSTA FERREIRA JUNIOR
Data: 01/07/2025 14:47:31-0300
Verifique em https://validar.iti.gov.br

Silvio da Costa Ferreira Junior
Adviser

I dedicate this work to my beloved wife Amanda Cristina Santos Dias and my parents, Vergínia Cristina de Moraes Silva (in memorian) and Antônio Carlos Muniz da Silva.

Acknowledgments

First of all, I would like to thank my father Antônio Carlos for all support and unconditional willingness to help and in memorian, my beloved mother Verginia Cristina, who is not among us anymore, but has still been a major inspiration, a source of wisdom in unclear moments and whose voice and memories bring me to a safe place. I would also like to thank my wife and friend Amanda Christina, whose support and love were indispensable throughout my whole PhD. Thanks also to my friend Ethe Costa, for all support and friendship demonstrated throughout these almost 7 years. To Wesley Cota and Thamires Cordeiro for their friendship and special moments lived throughout my whole stay in Viçosa. I would also like to thank all the people from the "Salinha"(Small room), specially Gabriel, Hugo, Juliane and Thainá for the nice moments, sharing valuable advice and also for showing their most human side in all its spectrum. This last part helped me a lot in important moments. I would like to thank specially my adviser Silvio Ferreira and my co-adviser Diogo Henrique da Silva for all support, even emotionally, when I lacked self-confidence. I am lost for words when it comes to their knowledge and wisdom shared, which were truly indispensable. Special thanks to Professor Clodoaldo for the opportunity to work in the LabSpin in the period my scholarship came to an end, enabling me to carry on my research.
I would like to thank GISC, NSSC and Jupiter clusters for all computational support.

I would also like to thank CNPq and FAPEMIG for all the financial support. This study was financed in part by the Coordenação de Aperfeiçoamento de Pessoal de Nível Superior Brasil (CAPES) Finance Code 001.

A vida imita o vídeo, garotos inventam um novo inglês vivendo num país sedento um momento de embriaguez - Somos quem podemos ser. Engenheiros do Hawaii

Abstract

SILVA, José Carlos de Moraes, D.Sc., Universidade Federal de Viçosa, December, 2024. **Theoretical investigation of epidemic diseases with waning immunity** Adviser: Silvio da Costa Ferreira Junior. Co-adviser: Diogo Henrique da Silva.

Among prototypical epidemic models, we can highlight the *susceptible*, *infected* and *susceptible* model (SIS), possessing a transition to an absorbing state, and the *susceptible*, *infected* and *recovered* model (SIR), possessing a transition between outbreaks spanning finite and vanishing fractions of a population. They represent models without immunization and with permanent immune period, respectively, and have drawn much attention from researchers interested in their critical behavior in heterogeneous networks with *power-law* degree distributions, $P(k) \sim k^{-\gamma}$. However, much less attention has been devoted to its general counterpart, the *susceptible*, *infected*, *recovered* and *susceptible* model ($SIRS$), which presents finite immunity periods $1/\alpha$, where α is a rate of waning immunity. While SIR ($\alpha = 0$) is accurately described by a *recurrent dynamic message passing* (rDMP), an adaptation of this theory to the SIS ($\alpha \to \infty$) model, is not capable of capturing basic features as the vanishing of the epidemic threshold λ_c in the thermodynamic limit on top of heterogeneous networks with $\gamma > 3$. An open question is whether the rDMP theory is capable of predicting the correct behavior of the $SIRS$ model. We discovered that epidemics with immunity period in heterogeneous topologies are better described by the rDMP theory, which accounts for correlations only in the non-backtracking aspect, than the pQMF theory. Conversely, the pQMF theory outperforms rDMP theory in homogeneous networks. Markovian processes are valuable for the study stochastic models, presenting Poisson (exponential) distribution. However, regarding real epidemics, recovery data are best fitted by Gamma or Weibull distributions. In this thesis we analyze the impact of non-Markovian recovery distribution on the epidemic activation of the SIS and $SIRS$ models by employing $\eta > 1$ recovery compartments, leading to Gamma distributions for the recovery time. We found that the $SIRS$ model on top of star-graphs, with finite α and the case $\eta \to \infty$, leads to a finite lifespan, while the increasing of compartments η in the SIS model keeps the lifespan exponentially increasing with network size unaltered, as found in the Markovian SIS model. Extensive numerical simulation do not show any significant changes in the scenario of power-law networks with $\gamma < 3$, while it presents only small changes for $\gamma > 3$, regarding activation and localization patterns.

Keywords: Complex networks. Critical phenomena. Epidemic spreading. Mean-field theories.

Resumo

SILVA, José Carlos de Moraes, D.Sc., Universidade Federal de Viçosa, dezembro, 2024. **Investigação teórica de doenças epidêmicas com período imune.** Orientador: Silvio da Costa Ferreira Junior. Coorientador: Diogo Henrique da Silva.

Dentre os modelos epidêmicos prototípicos, destacam-se o modelo *suscetível*, *infectado* e *suscetível* (SIS), o qual possui uma transição para o estado absorvente, e o modelo *suscetível*, *infectado* e *recuperado* (SIR), que possui uma transição entre surtos cobrindo frações finitas e ínfimamente pequenas de uma população. Ambos representam modelos sem imunização e com imunidade permanente, respectivamente, e atraíram muita atenção de pesquisadores interessados em seu comportamento crítico em redes heterogêneas com distribuições de grau em *lei de potência*, $P(k) \sim k^{-\gamma}$. No entanto, muito menos atenção foi dedicada ao seu geral, o modelo *suscetível*, *infectado*, *recuperado* e *suscetível* ($SIRS$), que apresenta períodos de imunidade finitos $1/\alpha$, onde α é uma taxa de perda de imunidade. Embora o SIR ($\alpha = 0$) seja descrito com precisão por uma teoria de *transmissão de mensagem recorrente dinâmica* (do inglês, *recurrent dynamic message passing* - rDMP), uma adaptação dessa teoria ao modelo SIS ($\alpha \to \infty$) não é capaz de capturar comportamentos básicos como a ausência de limiar epidêmico λ_c no limite termodinâmico em redes com $\gamma > 3$. Uma questão em aberto é se a teoria rDMP é capaz de prever o comportamento correto do modelo $SIRS$. Nós descobrimos que epidemias com período de imunidade em topologias heterogêneas são melhor descritas pela teoria rDMP, que considera correlações no âmbito da ausência de reinfecção mútua, do que pela teoria pQMF. Por outro lado, a teoria pQMF supera a teoria rDMP em redes homogêneas sem outliers. Processos markovianos são valiosos para o estudo de modelos estocásticos, apresentando distribuição de Poisson (exponencial). No entanto, em relação a epidemias reais, os dados de recuperação são melhor ajustados pelas distribuições Gama ou Weibull. Nesta tese, também analisamos o impacto da distribuição de tempos de recuperação não markoviana na ativação epidêmica dos modelos SIS e $SIRS$, empregando-se $\eta > 1$ compartimentos de recuperação, o que leva a distribuições do tipo Gama. Descobrimos que o modelo $SIRS$ com α finito e o caso $\eta \to \infty$ em um grafo estrela leva a um tempo de atividade finito, enquanto o aumento dos compartimentos η no modelo SIS mantém o tempo de atividade aumentando exponencialmente com o tamanho da rede, conforme encontrado no modelo SIS markoviano. Simulações numéricas extensivas não mostram nenhuma alteração significativa no cenário de redes de lei de potência com $\gamma < 3$, enquanto apresentam apenas pequenas alterações para $\gamma > 3$ no que tange os padrões de ativação e localização.

Palavras-chave: Redes complexas. Fenômenos críticos. Espalhamento epidêmico. Teorias de campo-médio.

List of Abbreviations

SIS *Suscetible-infected-susceptible*

SIR *Suscetible-infected-recovered*

SIRS *Suscetible-infected-recovered-susceptible*

MF *Homogeneous Mean Field theory*

HMF *Heterogeneous Mean Field theory*

QMF *Quenched Mean Field theory*

pQMF *Pair-Quenched Mean Field theory*

MP *Message-passing theory*

rDMP *Recurrent Dynamic Message-passing theory*

UCM *Uncorrelated Configuration Model*

OGA *Optmized Gillespie Algorithm*

QS *Quasi-stationary*

RN *Random Networks*

RRN *Random Regular Network*

PL *Power-law*

ER *Erdös-Renyi model*

BA *Barabasi-Albert model*

LEV *Largest Eigenvalue*

PEV *Principal Eigenvector*

NBC Non-backtracking Centrality

EVC Eigenvector Centrality

IPR Inverse Participation Ratio

Contents

I Introduction

Epidemic outbreaks have caused severe impacts and threats during modern history. Among the most recent ones, one can recall avian influenza in Southeast Asia and Western Europe [1], Ebola in West Africa [2], Zika virus in the Americas [3] and, more recently, the COVID-19 pandemic [4, 5, 6]. Immune response plays a pivotal role as a risk parameter in the development of containment strategies in the scope of health policies. Its importance ranges from protective measures of vulnerable groups [7, 8, 9] up to the development of high efficacy vaccines and construction of optimal distribution strategies [10]. Waning immunity in epidemic models is essential to understand the long-term evolution of an infectious disease. Besides shedding light on the dynamics of spreading pathogens, the development of accurate theoretical frameworks may lead to improved forecasting.

In modeling epidemics, one usually employs compartmental models, which amount to the 18th century [11], with the seminal work of Daniel Bernoulli on the life expectancy of newborn upon immunization of a fraction of the population against smallpox (a technique known at time as *inoculation* or *variolation*) in 1766. Motivated by available data, his model is claimed to be one of the first compartmental models in history [11]. In this model, the probability of a newborn surviving takes into account the fraction of *immunes* (who are recovered after infection) and susceptibles (the ones not infected yet) who survived. In 1927 an important work of Kermack and Mckendrick introduced the widely studied *Suscetible-infected-recovered* (SIR) model, establishing a new era of epidemic modeling [12]. These early models usually rely on the assumption of *well-mixed* population (see Sec. 3.8), in which the individuals are assumed to have contact to *any* other individual of the population with the same rate. A fine-tuning of this coarse-grained assumption is achieved in the realm of *Network Theory*, popularized with the early works of Barabasi [13, 14] and Pastor-Satorras [15].

The investigation of networked systems has attracted increasing attention in the last decades due to its presence in structures of scientific and applied importance. To name just a few, we can mention contact networks of job opportunities [16, 17], rumors and diseases propagation [18, 19] as well as synchronization phenomena [20, 21]. Networks are suitable for describing complex systems, such as the *world wide web* [22], *autonomous systems* of *internet protocol* (IP) suffixes [23], yeast protein interactions (*interactomes*) [24, 25], autophagy of human pathogens identification by means of the yeast interactome [26] and the human brain mapping of structural connections [27] (human connectome), to name just a few. In this sense, Network Theory has thrived as an important tool in the description of complex systems of diverse nature.

Perfect immune response is assumed in the SIR model [28], in which susceptible individuals are infected with rate λ upon each contact with a contagious individual and

heal spontaneously with the rate μ remaining in a recovered state, in which they cannot be reinfected. In this model no active steady state exists and an epidemic threshold λ_c separates outbreaks spanning a finite fraction of the population ($\lambda > \lambda_c$) and outbreaks reaching only vanishing fractions ($\lambda < \lambda_c$). Conversely, if no immunity is conferred and an infected individual becomes susceptible again immediately after healing, the *Suscetible-infected-susceptible* (SIS) [28] epidemic model is the fundamental dynamics. In this model, a threshold λ_c separates a state in which a population presents disease prevalence with a lifespan that grows exponentially with network size ($\lambda > \lambda_c$) from a state in which the disease lifespan decays exponentially fast ($\lambda < \lambda_c$). In the case of waning immunity with an average time $1/\alpha$ after recovery, the *Suscetible-infected-recovered-susceptible* (SIRS) model [28] is a better representation of the process, also possessing an epidemic threshold λ_c separating a disease-free state from a steady state regime. However, the role of waning immunity in basic epidemic models on networks has been undervalued while being noticeably fundamental for real epidemic outbreaks.

The rigorous mathematical analysis of stochastic epidemic models in networked systems relies on solving the *Master Equation*, whose number of equations scales exponentially with network size. In this sense, solving it becomes prohibitive even computationally and some approximating scheme is necessary. In this scenario, *mean-field* theories become relevant, in which higher-order correlations are neglected, and help to obtain valuable qualitative and sometimes even quantitative insights.

The nature of the activation process in the SIS dynamics on random power-law networks involves a feedback mechanism where the epidemic activity within subextensive subgraphs is self-sustained and spreads the activity to the rest of the network [29, 30, 31]. The quenched mean-field theory (QMF) [32, 33, 34, 35, 36, 37], in which the whole network structure is explicitly considered, describes qualitatively the vanishing of the epidemic threshold in *Random Networks* (RN) presenting power-law degree distribution, $P(k) \sim k^{-\gamma}$, regardless the value of γ [32, 33]. The accuracy of such predictions can be improved by adding dynamical correlation in a pairwise level [38, 39], the *Pair-Quenched Mean Field theory* (pQMF), especially in the regime of high epidemic prevalence [40]. Shrestha et al. [41] proposed a modified version of the *Message-passing theory* (MP) developed by Karrer and Newman (2010), which describes the SIR model exactly in tree-like networks [42] for dynamic processes with an active (fluctuating) steady state in the now called *Recurrent Dynamic Message-passing theory* (rDMP) theory. However, Castellano and Pastor-Satorras [43] argued that, by construction, the backtracking mechanism absent in rDMP theory is essential to the activation of the SIS dynamics in heterogeneous networks [44, 45, 29, 30]. So, rDMP theory is not a suitable approach and is notably worse for degree exponents $\gamma > 2.5$, when the dynamics is ruled by self-sustained activation of hubs [29]. In power-law networks, standard mean-field theories for $SIRS$ predict the same epidemic threshold and critical behavior as the SIS [30, 46]. However, the waning

immunity is capable of modifying the epidemic activity in isolated hubs, implying that the activation mechanism of the SIS model, based on long-range mutual infection of hubs, is depleted [30] and the mechanism is altered. So, one central question is which mean-field approach is more accurate in describing the epidemic dynamics of the $SIRS$ model.

In random scale-free networks with degree exponent $\gamma < 5/2$ the three aforementioned models (SIR, SIS, and SIRS) behave very similarly with the epidemic threshold very well described by the QMF theory [30]. However, remarkable differences emerge for $\gamma > 5/2$ and especially for $\gamma > 3$. For example, the asymptotic epidemic threshold of the SIS model is null for any value of γ [29, 45, 47], while the threshold is finite for $\gamma > 3$ and a phase transition is observed in SIR and $SIRS$ with finite α [30]. In Chap. IV, we present a discussion based on our work published in 2022 in the *Physics Review E* (PRE) [48], where two pairwise mean-field theories, rDMP and pQMF, are compared with extensive stochastic simulations on large networks of different levels of heterogeneity. For waning immunity times longer than or comparable with the recovery time, rDMP outperforms pQMF theory on power-law networks with degree distribution $P(k) \sim k^{-\gamma}$. In particular, for $\gamma > 3$, the epidemic threshold observed in simulations is finite, in qualitative agreement with rDMP, while pQMF leads to an asymptotically null threshold. The critical epidemic prevalence for $\gamma > 3$ is localized in a finite set of vertices in the case of the pQMF theory. In contrast, the localization happens in a subextensive fraction of the network in rDMP theory. Simulations, however, indicate that localization patterns of the actual epidemic lay between the two mean-field theories, and improved theoretical approaches are necessary to understand the $SIRS$ dynamics.

It is widely known in the literature that recurrent infectious diseases often exhibit recovery time distributions that deviate from the exponential assumption typically associated with Markovian/Poisson processes, which are commonly used in epidemic compartmental models. Therefore, in Chapter V, related to our study found in Ref. [49], we address this issue by exploring a susceptible-infected-recovered-susceptible ($SI_\eta RS$) model on networks. This dynamical process features η independent infectious compartments, each governed by Markovian dynamics and resulting in Gamma-distributed recovery times. We develop an analytical theory for the epidemic lifespan on star graphs composed of a central hub with K leaves, which serve as analogs for network hubs. Our results show that the epidemic lifespan scales as a non-universal power-law $\tau_k \sim k^{\alpha/\mu\eta}$, with additional logarithmic corrections, where α^{-1} and μ^{-1} represent the mean waning immunity and recovery times, respectively. Compared to the standard SIRS dynamics (where $\eta = 1$ and the mean recovery time is unchanged), the epidemic lifespan on star graphs significantly decreases as the number of stages increases. Notably, in the limit $\eta \to \infty$, the lifespan becomes finite for star graphs. These findings are corroborated by numerical simulations that align with our approximate analytical predictions. For the SIS dynamics, numerical simulations reveal that the lifespan increases exponentially with the number

of leaves, with a non-universal rate that diminishes as the number of infectious compartments grows. We also examined the $SI_\eta RS$ dynamics on power-law networks characterized by a degree distribution $P(k) \sim k^{-\gamma}$. When $\gamma < 5/2$, where epidemic processes are governed by activation within the maximum k-core, changes in the hub's active duration do not affect the epidemic threshold or the localization pattern. Conversely, for $\gamma > 3$, where mutual activation of hubs is prevalent, localization effects are diminished, although not to the extent that they alter the threshold's scaling with network size. Thus, the activation mechanisms remain consistent with those observed under Markovian recovery assumptions.

It is worth mentioning that we also investigated the impact of low-degree nodes in the dynamics of recurrent state epidemic models, when inserted into power-law networks, with preferential attachment rules favoring hubs. We have not included this work in the present text as a matter of conciseness, although it was in the final drafting stage of the defense. For the sake of shortness, we investigated how *bridge* nodes, i.e. low-degree nodes connecting the most active parts of the network, impact the dynamics of the SIS and $SIRS$ models in heterogeneous topologies with degree distribution tail scaling as $P(k) \sim k^{-\gamma}$. We make a concise description of the preliminary results of this study in Chap. VI.

The outline of this thesis is as follows: in Chapter II, we present the basics of complex networks theory and models. Here important subjects are introduced, allowing for the description of coarse-grained metrics. In Chap. III, we discuss important mean-field theories found in literature and the activation mechanisms involved in the *absorbing state phase transition* happening in both the SIS and the $SIRS$ model. Chap. IV is devoted to our study of mean-field theories in the description of the $SIRS$ model, published in Ref. [48], while in Chap. V we study non-Markovian the $SIRS$ model on top of power-law networks, presented in Ref. [49]. Finally, our concluding remarks and prospects are summarized in Chap. VI, while 4 appendices, dealing with methodological and technical issues, complement this thesis.

II Network theory

2.1 An introduction to the chapter

In this chapter, we shall discuss important concepts in the modeling of networks for further discussion in the coming chapters. Among these concepts are coarse-grained descriptions of a graph's structure, represented by the distributions of its node's degree (connectivity), nearest neighbors' average degree and clustering. Towards the end of this chapter, centrality measures are introduced - a means of ranking nodes' importance in a dynamic process. Finally, the *Uncorrelated Configuration Model* (UCM) is presented, thus allowing for the synthesis of networks that are largely employed in theoretical considerations. For the sake of brevity, we shall not deal with all concepts in network theory in this thesis, so we refer the most interested readers to the more specialized literature [50, 51, 52, 53]

2.2 Introduction to the network theory

A *graph* or *network* may be understood, at first glance, as a collection of dots, called *vertices* or *nodes*, connected by *edges* or *links* [52]. A possible abstraction is that nodes represent agents of some dynamics, while the edges are interpreted as channels of interaction between the agents. Of course, other abstractions are possible, for example, the network of enzymes (agents) taking part in the same metabolic process (an edge) [50], to name just one example. Now, to construct our description of a graph, let us imagine that the size of this network is some positive integer N, *i.e.* the number of vertices comprising it. We can go a step further and label the nodes of our hypothetical network as $i = 1, \cdots, N$ and take a pair of such nodes, say i and j, linking them together, thus forming an edge (i, j) [52, 50]. Although there are network models which allow edges of the form (i, i) (*self-edges*) [50], we shall explicitly forbid them. Edges of this form represent *self-connections*, where i is linked to itself. To make things clearer, a simple depiction of a small graph can be seen in Fig. 2.1 (left panel).

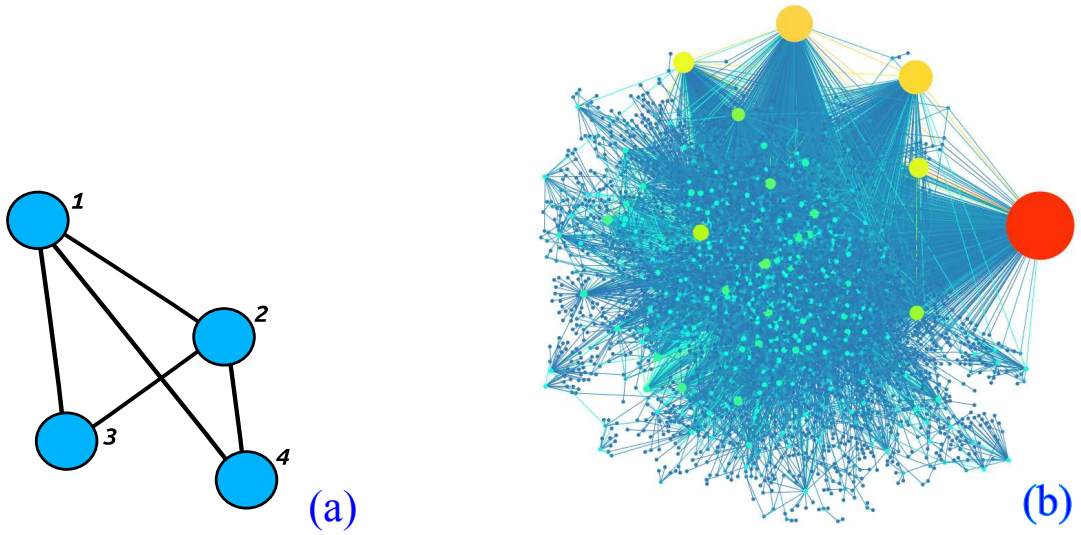

Figura 2.1 – Representations of graphs, where nodes are depicted by collections of colored circles and edges by lines. (a): Simple example of graph with $N = 4$ nodes and $L = 5$ edges. (b): network AS-Oregon, representing an autonomous system. $N = 6474$ nodes and $L = 13895$ edges. Node sizes are here represented proportionally to their connectivity degree for the sake of enhancing visualization of high-degree nodes (see Sec. 2.3.1).

The first feature found in the graph from Fig. 2.1-(a) we would like to emphasize is the lack of *multiple connections*, i.e. an edge (i, j) between a pair of nodes i and j appears only once. This absence of multiple- and self-connections allows us to categorize a network as a *simple graph*, otherwise being called a *multi-graph* (when multi-edges are present), *degenerate graph* and so on [50, 52, 51]. Another important feature of this graph is that an edge (i, j) can *always* be walked through in the reverse direction (j, i). This additional characteristic makes the graph an *undirected network*, otherwise, it is called a *directed network*.

To depict a daily example, Fig. 2.1-(a) presents a rather more intricate example of a network - this time a real-world one. It represents a simple undirected network abstraction of an *autonomous system* - a collection of internet routers managed by a single organization [54, 55]. In the following sections, we shall delve into how to extract valuable information from networks as intricate as the one depicted in Fig. 2.1-(a).

2.3 The adjacency matrix and some important metrics

In order to store information on whether a pair of nodes i and j are connected or not, we define an $N \times N$ matrix $\mathbf{A}$, whose components A_{ij} should satisfy:

$$A_{ij} = \begin{cases} 1, & \text{if i and j are connected} \\ 0, & \text{otherwise,} \end{cases} \tag{2.1}$$

where N is the network size. Directly from the adjacency matrix we can compute the *degree* k_i (also called *connectivity degree*) of a node i, a mathematical quantity that stores the number of its nearest neighbors or, put in simple words, a measure of the node's popularity [50]. Referring to the adjacency matrix, we can compute this quantity for each node by using the expression:

$$k_i = \sum_{j=1}^{N} A_{ij}. \tag{2.2}$$

As a quick example, we can apply the definition given in Eq. (2.1) to the simple graph shown in Fig. 2.1(a), so obtaining the following adjacency matrix:

$$\mathbf{A} = \begin{bmatrix} 0 & 1 & 1 & 1 \\ 1 & 0 & 1 & 1 \\ 1 & 1 & 0 & 0 \\ 1 & 1 & 0 & 0 \end{bmatrix} \tag{2.3}$$

From this follows that applying Eq. (2.3) to Eq. (2.2) yields us detailed information on the degree of each node in Fig. 2.1(a):

$$\mathbf{k} = \{3, 3, 2, 2\}. \tag{2.4}$$

As one can quickly check from simple graph in Fig. 2.1-(a), nodes 1 and 2 have both degree $k = 3$, while nodes 3 and 4 have $k = 2$.

In this section, we have just given a simple example of how one can retrieve information from the adjacency matrix. It allows researchers to obtain *any* structural information we could be interested in regarding the network under study. Among the features we can be interested in, we can mention, e.g., the state of aggregation presented by the vicinity of a typical node (for one definition of *clustering*, see Sec. 2.5) and, similarly to a node's degree of connectivity, how popular are neighbors of a typical node (see Sec. 2.4) and how distributed are the degrees between the minimum k_{min} and the maximum degree k_{max} (see Subsec. 2.3.1).

2.3.1 Node's degree and degree distributions

Let us answer this last question by forming an array of degrees $\mathbf{k} = \{k_1, k_2, \cdots, k_N\}$, as defined in Eq. (2.2). Using this information we are in place to obtain the *degree distribution* $P(k)$, defined as the probability of finding a degree-k node in the network. Since it is closely related to how often we find a node of degree k in the network, $P(k)$ can be defined as:

$$P(k) = \frac{1}{N}\sum_{i=1}^{N}\delta_{k_i,k}, \tag{2.5}$$

where $\delta_{k_i,k}$ is the *Kronecker delta function*, being 1 if $k_i = k$ and 0 otherwise. We can calculate all *moments* of the degree distribution, according to the Eq. (2.6) bellow:

$$\langle k^n \rangle = \sum_{k_{min}}^{k_{max}} k^n P(k). \tag{2.6}$$

Here, $\langle k^n \rangle$ is the $n-$th moment of the distribution, while k_{min} and k_{max} refer to the *minimum* and *maximum degree* of the network, respectively. In particular, the first and second moments of this distribution are of special interest in *mean field theories*, to be presented in Section 3.8, by relating such structural quantities to epidemic model predictions.

2.3.2 Scale-free and scale-rich networks

To further discuss the statistical point of view gathered so far, it is worth mentioning that infrastructures created by humans can frequently be represented by *Power-law* (PL) degree-distributed networks, i.e. $P(k) \sim k^{-\gamma}$ [50, 51, 56]. As theoretical models evidence, networks of this kind are formed by mechanisms that trace back to forms of *preferential attachment* in dynamically *growing* networks [57, 58], i.e. in which nodes arriving to them tend to establish connections to the most connected nodes. Among the simplest models, one could mention the combination of *linear preferential attachment* and *growth*, as in the *Barabasi-Albert model* (BA), which features $\gamma = 3$ [58]. Before moving forward to deepen our understanding of PL networks, brief considerations on graphs possessing well-bounded degree distributions, like the *Erdös-Renyi model* (ER) graph, shall pose an instructive contrast with PL networks. This model has historical importance, since it marks the foundation of what is called *Random Graph Theory* [50, 51].

This model of networks produces an ensemble of random graphs, $G(p, N)$, defined as follows. Each instance of the ensemble is a collection of N nodes, from which each pair is connected with probability p. Among its features, the degree distribution [51] is given by:

$$P(k) = \binom{N}{k} p^k (1-p)^{N-k}, \tag{2.7}$$

whose average degree and variance are $\langle k \rangle = pN$ and $\sigma^2 = \langle k \rangle (1-p)$, respectively. As we can see, with $\langle k \rangle$ fixed, the variance does not scale with N, causing typical degrees to be bounded around the average, turning $\langle k \rangle$ into an intrinsic *scale* of an ER network. The *boundedness* of typical-degree nodes in networks with this property, apart from outliers, of course, allows us to classify them as *scale-rich*. Conversely, whenever the *variance* $\sigma^2 = \langle k^2 \rangle - \langle k \rangle^2$ diverges with $N \to \infty$, the network is termed *scale-free* [50, 52, 51].

Fig. 2.2 puts examples of both classes of networks in perspective, showing the collapse of scale-rich distributions (associated with ER graphs in this case) in comparison with heavy-tailed power-law degree distributions.

In the case of power-law networks, a continuous approximation allows us to estimate $\langle k^2 \rangle$:

$$\langle k^2 \rangle = \int_{k_{min}}^{k_{max}} k^2 P(k) dk, \tag{2.8}$$

where $P(k) \sim k^{-\gamma}$. As we shall see in Sec. 2.8, when creating synthetic PL networks for simulation purposes and comparison with theoretically established results, it is desirable to impose an upper-bound on the maximum degree, such that $k_{max} \leq k_c$, where $k_c \sim N^{\frac{1}{\omega}}$, with $\omega = \max(2, \gamma - 1)$ [59, 60]. This constraint has the purpose of avoiding degree-correlations (see Sec. 2.4 and Sec. 2.8), whose absence is an important ingredient in the theoretical approaches studied in Sec. 3.8 [61, 51, 60]. Using this upper-bound in Eq. (2.8) causes $\langle k^2 \rangle$ to scale as:

$$\langle k^2 \rangle \sim \begin{cases} N^{\frac{3-\gamma}{2}}, & \text{if } \gamma < 3 \\ \ln(N), & \text{if } \gamma = 3 \\ c, & \text{if } \gamma > 3, \end{cases} \tag{2.9}$$

thus diverging in PL networks with $\gamma \leq 3$ and reaching a constant value c otherwise. Meanwhile, for any $\gamma > 2$, the average degree $\langle k \rangle$ does not scale with network size, reaching a constant value c'. As we shall see in Sec. 3.8, the way the ratio $\frac{\langle k^2 \rangle}{\langle k \rangle}$ scales with network size has deep consequences in theoretical predictions for the SIS and $SIRS$ models in networks lacking degree correlations (see Sec. 2.8 for a definition of the *Uncorrelated configuration model*) [62, 31].

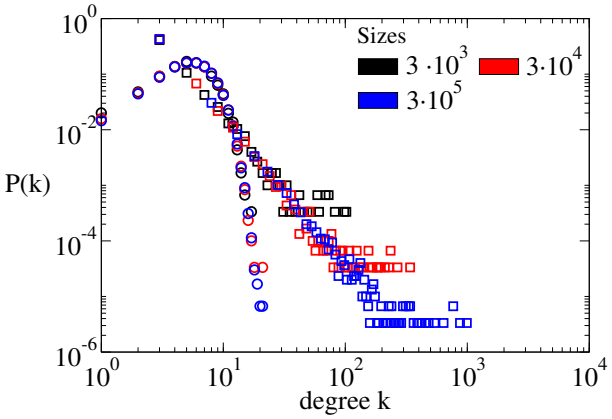

Figura 2.2 – Degree distributions of Erdös-Reyni (circles) and Power-law (squares) $P(k) \sim k^{-\gamma}$, with $k_{min} = 3$, $\gamma = 2.7$ and $k_c \sim N^{\frac{1}{2}}$. Both kinds of distribution have average degree $\langle k \rangle \sim 6$. Colors refer to the network size N.

2.4 Degree correlations

The descriptive approach presented in Subsections 2.3.1 and 2.3.2, in terms of the marginal probability $P(k)$ and its moments $\langle k^n \rangle$, could naturally be taken to the next level by considering the affinity between any pair of possible degrees in the network. As a first choice, we could seek to describe it in terms of a joint distribution $P(k,k') = \frac{E_{kk'}}{N\langle k \rangle}$ [59], related to the joint probability of finding typical nodes of degrees k and k' tied together [59, 50]. However, this function does not always deliver direct information on the affinities between the possible degrees in the network. We can accomplish this purpose more simply by means of the *average degree of nearest neighbors* κ_{nn}. This allows us to rule out the fine structure behind degree correlations associated with the joint probability, while bringing useful insights about the affinity among different degrees in the network. This quantity can be obtained intuitively, evidencing its relation to degree correlations by using:

$$\langle \kappa_{nn}(k) \rangle = \sum_{k'=k_{min}}^{k_{max}} k' P\left(k'|k\right). \tag{2.10}$$

Here $P\left(k'|k\right)$ is the conditional probability of having a node of degree k' at one side of an edge, given knowledge of having a degree-k node at the other side [50, 51].

In the absence of degree correlation, we expect $P\left(k'|k\right)$ to be independent of k and given by [50, 59, 51]:

$$P\left(k|k'\right) = k\frac{P\left(k\right)}{\langle k \rangle}. \tag{2.11}$$

Inserting this result into Eq. (2.10), gives us:

$$\kappa_{nn}^{(un)}(k') = \sum_{k=k_{min}}^{k_{max}} k^2 \frac{P\left(k\right)}{\langle k \rangle} = \frac{\langle k^2 \rangle}{\langle k \rangle}, \tag{2.12}$$

which is the ratio between the second and the first moment of $P(k)$ (see Eq. (2.6)). This kind of *degree correlation* is referred to as *neutral*, a desired signature in networked substrates object of theoretical analysis, as well shall see in Sec. 2.8 and Subsec. 3.8.3.

An overview of Eq. (2.10) may bring insightful information on the network's intrinsic structure. Alternatively to the neutral correlation case, it may be possible for some reason, indeed belonging to the network formation history [50, 22], that nodes of low degree lean toward connecting to nodes of higher degree (and vice-versa), leading to a so-called *disassortative* degree correlation. In other cases, it is also possible that nodes of a given degree may tend to connect to others in the same range of the degree spectrum, causing an *assortative* behavior. Fig. 2.3 gives some intuition of the aforementioned patterns.

Real networks can feature a mixing of correlations, rendering a more complicated picture, as exemplified in Fig. 2.3. As the reader may have also realized, the tendency of neutrality does not show up clearly in this specific case. The reason for this is that

the neutral patterns of degree correlation are much more a characteristic of *randomness* and not very often the case in real networks, in which usually networks grow over time in a self-organizing fashion [50, 51]. This happens due to the nature of their purpose, since this self-organizing tendency yields the optimization of some underlying functionality related to the network's structure. Besides that, a comparison with the neutral tendency lets us know how close or far from randomness, and with which tendency (assortatively or disassortatively), nodes of a network were leaning towards connecting to their counterparts.

To conclude, neutral degree correlation turns out to be useful for theoretical models as well. The neutral tendency in degree correlations is very useful in the study of mean-field theories, like the one described in Subsec. 3.8.2, since it allows us obtaining epidemic thresholds in closed form, thus allowing for theoretical insights. In addition to that, studies have also shown the impact of degree correlations in the dynamics and how they affect both mean-field predictions and their matching with stochastic simulation outcomes [63, 64, 65].

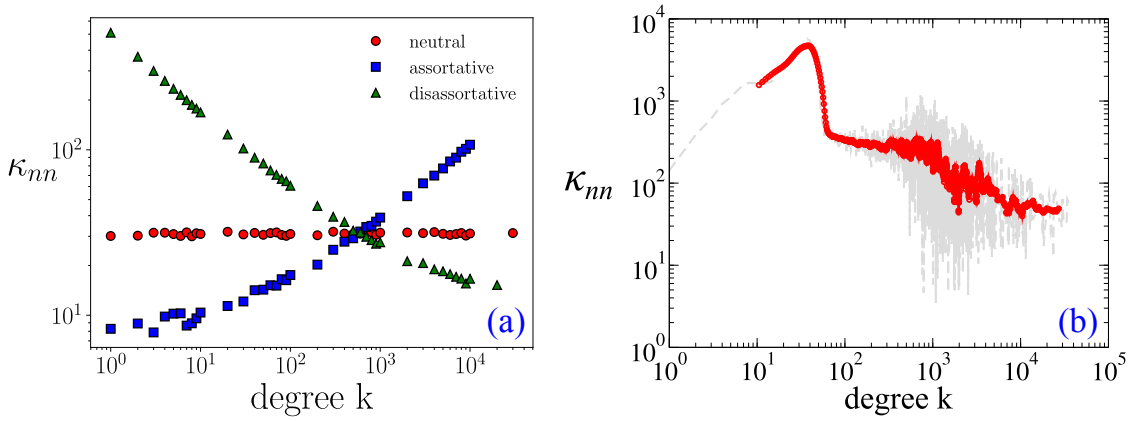

Figura 2.3 – (a): Representative behaviors of degree correlation measured by means of κ_{nn} *degree* k showing a network's neutral, assortative and dissortative character. (b): Degree correlation κ_{nn} *vs* degree k of a non-directed version of the AS-SKitter network. Grey dashed lines represent actual data, while red represents running averages.

2.5 The clustering coefficient

Still in the local scale, i.e. at the level of nodes, one metric that might interest us is not only how big a node's vicinity is, but also how much interconnected it is [51]. Put in simple words, we could first define this metric by asking ourselves: *How many of a node's acquaintances are themselves acquainted with each other?* Structurally, this has a simple interpretation, *i.e.*, the one related to how densely a graph is populated with *triangles* or, how close the referred network is to a *complete graph*, depicted in Fig. 2.4(a). In this graph, every node is connected to the others, so that the number of triangles in it is the highest, i.e. $\max(N_\Delta) = \frac{N(N-1)}{2}$. This leads us to a measure given by:

$$C^i = \frac{N_{\Delta^i}}{\max\left(N_{\Delta^i}\right)}, \tag{2.13}$$

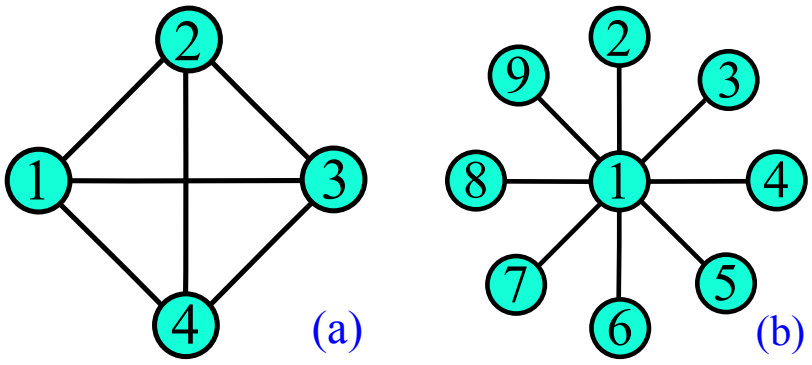

Figura 2.4 – (a): complete graph with $N = 4$ nodes. (b): star graph formed by $N = 9$ nodes. The center has degree $K = 8$, while the leaves have degree $k_l = 1$ each.

where N_{Δ^i} is actual number of *triangles* emanating from node i, while $\max\left(N_{\Delta^i}\right)$ is the maximum number of triangles if all its neighbors were connected among themselves, thus forming a complete graph [50, 51]:

$$\max\left(N_{\Delta^i}\right) = \frac{1}{2}k_i\left(k_i - 1\right), \tag{2.14}$$

where k_i is node i's degree [50]. In the simple graph shown in Fig. 2.1, nodes 1 and 2 have degree $k = 3$, with $\max\left(N_{\Delta^{1,2}}\right) = 3$, but $N_{\Delta^{1,2}} = 2$, leading to a clustering $C^{1,2} = \frac{2}{3}$, whereas nodes 3 and 4 have clustering $C^{3,4} = 1$, since their degree is $k = 2$, leading to a maximum number of triangles $\max\left(N_{\Delta^{3,4}}\right) = 1$ and effectively having this number of triangles in their neighborhood. One possible counter-example worth mentioning is the *star graph*, a structure composed of one central node of degree K linked to K nodes of degree $k_l = 1$ (also called *leaves*), as in Fig. 2.4(b). In this graph, every degree-1 node has a connection uniquely to the central node, causing $C^{star} = C^{leaves} = 0$.

2.5.1 Average clustering

Having defined how densely connected the direct neighborhood of a node is [50], it is possible to average this information throughout the whole network, thus getting:

$$\langle C\rangle = \frac{1}{N}\sum_i C^i. \tag{2.15}$$

In full analogy with the proceeding done with the nearest neighbor average degree κ_{nn} described in Sec. 2.4, we can perform this task with C^i at the degree level:

$$C(k) = \frac{1}{NP(k)}\sum_i C_i\delta_{k_i,k}, \tag{2.16}$$

where $\delta_{k_i,k}$ is 1 if $k_i = k$ and 0 otherwise.

Regarding the average clustering of *random* PL networks $P(k) \sim k^{-\gamma}$ without degree correlations (see Sec. 2.8), Fig. 2.5 shows us the scaling of this quantity for different γ exponents. As suggested by asymptotic behavior shown in Fig. 2.5, random networks

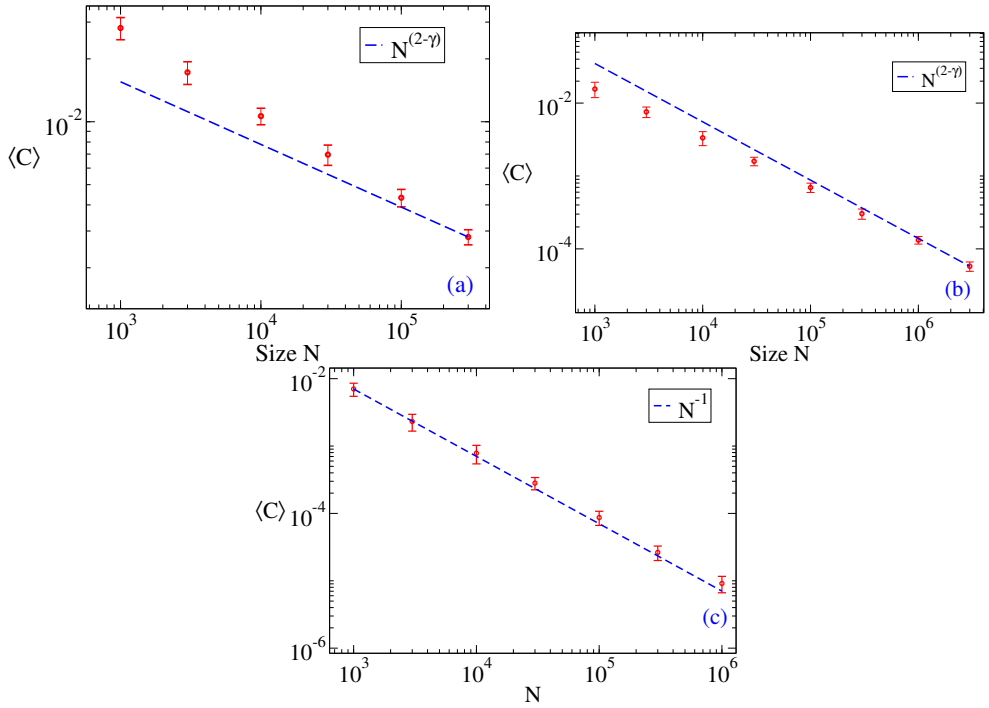

Figura 2.5 – Average clustering $\langle C \rangle$ vs size N (red circles) for UCM networks with degree distribution $P(k) \sim k^{-\gamma}$. (a) $\gamma = 2.3$, maximum degree cut-off $k_c = 2\sqrt{N}$. (b) $\gamma = 2.8$ (c) $\gamma = 3.5$, $k_{max} \leq k_c = N^{\frac{1}{\gamma}}$. blue dashed line: Expected scaling given by the Uncorrelated Configuration Model (see Sec. 2.8 - The uncorrelated configuration model (UCM)). A number equal to 10 samples was taken for each size.

(RN), in special power-law distributed graphs, present in general a vanishing average cluster coefficient. The scaling behaviors shown as dashed lines are predictions from the *Configuration Model* (briefly discussed in Sec. 2.8) [52, 51]. In the limit of $N \to \infty$, we generally expect random graphs to be locally *tree-like*, i.e., having no local loops. This assumption is assumed a necessary condition for the validity of some of the mean-field theories we shall deal with in Sec. 3.8.

2.6 Paths

Some graphs present a spatial notion of distances, for instance, 2- and 3-D lattices found in solid state physics [66], i.e. they may be thought of as being embedded in an *Euclidian Space*. Nonetheless, not all graphs will present this property, as is the case of random graphs [50, 52], which are not *a priori* embedded in a metric space. To find a substitute for the notion of spatial distance, we shall introduce first the concept of

paths along edges. Simply stated, a path is any string of links bridging two nodes in a RN. Referring to Fig. 2.6, we can state that the nodes 4 and 1 are a distance $l_{41} = 1$ apart, just like any other pair of nearest neighbors. We can extend this notion and count distances between any pair of nodes that are not direct neighbors. For example, links highlighted in red correspond to a path connecting nodes 4 and 3 through the path $(4,1) \rightarrow (1,3)$, whose path-length is $l = 2$, since there are 2 edges connecting nodes 4 and 1 through this path. Summarizing, the length of a given path l_{ij} between nodes i and j is the number of edges l comprising it [51]. If there exists a pair of nodes i and j that cannot be linked together through any finite path l_{ij}, we may refer to the graph as *disconnected*. Otherwise, the graph is referred to as *connected*.

From this definition of path, it follows quite naturally the notion of *distance* between two nodes i and j, as being the minimum path-length between $d_{ij} = \min\{l_{ij}\}$ them. In turn, an important notion following from this definition of distance is that of a network's *diameter*, as being the maximum distance $\max\{d_{ij}\}$, $\forall$ i and j in the network.

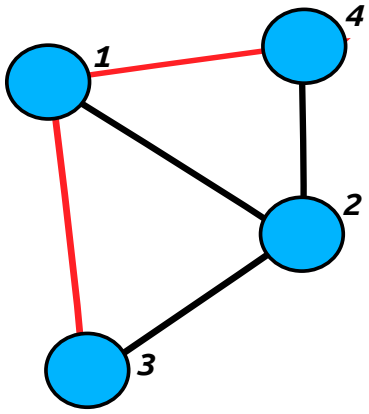

Figura 2.6 – Depiction of possible path between nodes 3 and 4 on graph presented in Fig. 2.1.

A striking difference between random graphs and lattices is how distances scale with network size. In the case of lattices, taking a simple hyper-cubic graph of dimension d as an example, we see that typical lengths L scale with the number of lattice points as $L \sim V^{\frac{1}{d}} \sim N^{\frac{1}{d}}$, since the hyper-volume is proportional to unitary cells' volume [66]. In the case of random graphs, no geometric constraint exists *a priori*, although one could intend to input spatial constraints to the model [67]. A simple reasoning leads to an approximation for the diameter l_{max} of a RN. Let us imagine a random homogeneous network, in which a typical node has degree k close to average $\langle k \rangle$, through this approach the diameter l_{max} scales as $l_{max} \sim \frac{\ln(N)}{\ln(\langle k \rangle)}$ [50, 51], which turns out to be a better approximation for the average distance $\langle l \rangle$ itself, since diameters are dominated by only a few long paths [50]. This result, in perspective with distances found in regular lattices presenting the same

number of lattice points, shows that a RN presents average distances much smaller among its nodes than a regular lattice does. This can be mathematically seen if someone checks the ratio between characteristic lengths in random graphs and lattices $\frac{\langle l^{(r)} \rangle}{\langle l^{(l)} \rangle} \sim \frac{lnN}{N^{\frac{1}{d}}}$ in the limit of $N \to \infty$. It can be seen that this limit goes to 0 for any finite value of d, regardless of how big it is, showing that average distances are always much smaller in RN. This leads to the so-called *small-world* property [68]. In other words, in just a few steps it is possible for a message sent from a given node to reach *any* other node in the network with a small number of steps, showing the network's finite character in a small number of hops. The small-world property is one reason why it does not take an infinite time for us to reach a server on the internet, geographically far apart, by typing *www...* on a browser [68]. Besides being a RN of servers and routers, the presence of large hubs (highly connected nodes) has the profound effect of shortening distances even further, thus enhancing the network's scale-free character [68]. In consequence, this leads to typical distances scaling even more slowly with network size than the one yielded by the random-graph reasoning [68].

2.7 Network centralities

So far, we have discussed some important concepts in Network Theory as degree, clustering, distances and average nearest neighbor degree. We have indeed proposed for some of these metrics, a *coarse-graining* approach by considering their average in the degree classes. However, measuring a node's importance in a network is of great interest since it can tell us who dominates the dynamics, depending on the nature of the process under study [69]. For instance, a node's degree can be regarded as the simplest centrality measure, representing the popularity of a node in a network [70].

To motivate another measure, let us take as an example data packages sent at some rate between any pair of routers on the internet [51]. Motivated by the assumption that the flux of information passing through a node i is proportional to the amount of shortest paths it lies on, we may argue that the amount of information passing through i and sent between *any* pair of routers j and k is proportional to the fraction of shortest paths connecting every pair of nodes in the network passing through i. This bears in mind a simple form of ranking, arising in the form of what is defined as *betweeness centrality* - i.e., node i's betweeness will be the *total* fraction of shortest paths between *any* pair of nodes j and k (see Sec. 2.6) traversing node i [51, 71, 70]. To name just another important measure, we mention the *closeness centrality*, which ranks a node i in the *highest* position whenever the average shortest path $\langle l_i \rangle$ from it to the rest of the network is the *lowest* - thus inversely proportional to $\langle l_i \rangle$ [18, 70].

2.7.1 Degree centrality

The simplest form of centrality we could imagine in a network could be the *degree centrality*. It relies on the assumption that a node's importance should be measured by its *popularity* or the number of contacts it has k_i. This is particularly true in the *annealed* regime, characterizing a networked system that rewires its connections over a time-scale τ_N much smaller than the scale τ_D characteristic of the dynamical process [60, 72]. Another scenario supporting the accuracy of this centrality is the one related to the analysis of dynamic processes over an ensemble of some network model. In this case, the ensemble shares only statistical measures related to the model, such as the marginal degree distribution $P(k)$ and degree correlations $P(k, k')$ [60].

2.7.2 K-core centrality

From the discussion in Subsec. 2.7.1 it is clear that the degree centrality does not take into the network structure apart from its statistical properties. A node, however, may also be important due to its position in a hierarchy of core-peripheral structure [73, 74]. Whether a given node belongs to a densely connected core, with a pronounced community structure reminiscent of a complete graph (e.g. see Fig. 2.4(a)), or the node a loosely or even dangling structure. The k-core centrality may be obtained by a pruning procedure as follows: one assigns to nodes of degree k_0 a *shell* number $k_S = k_0$, where k_0 is the lowest degree of the network. Then, these nodes are pruned and the corresponding neighbors have their vicinity updated. If the neighbors' degrees turn lower or equal to k_0, they also get the shell number k_S and are also eliminated from the network and so on. When there are no more nodes of degree $k \leq k_0$, we update the shell number $k_S \to k_S + 1$ and search for nodes of degree $k \leq k_S$, which are also assigned this shell number, eliminated and whose neighbors are also updated and possibly pruned, until there are no more nodes in the network. The highest k_S index is called the maximum k-core index K_M [74, 31]. In Fig. 2.7.2 we see an example of a simple core-periphery structure, composed by following the procedure defined in this subsection.

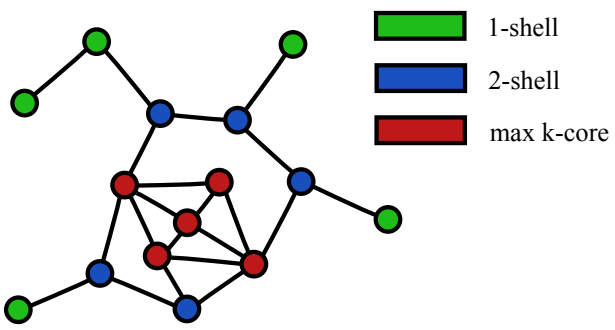

Figura 2.7 – Network presenting core-periphery structure formed by nodes with $k_S = 1$ (1-shell), $k_S = 2$ (2-shell) and K_M (k-core) indexes.

We shall see more about the influence of the k-core in the SIS and SIRS epidemic models in Sec. 3.10. Especially, PL networks with exponent $\gamma < 3$ generated by the *Uncorrelated Configuration Model* (Sec. 2.8) present a strong $k - core$ structure, whose size diverges in the thermodynamic limit ($N \to \infty$).

2.7.3 Eigenvector centrality

Eigenvector Centrality (EVC) relies on the assumption that a well-ranked node becomes more important if connected to other important nodes. So, the degree of importance x_i of a node is enhanced by the importance of its neighbors, as quantified by the equation:

$$x_i = a \sum_{j=1}^{N} A_{ij} x_j. \tag{2.17}$$

Eq. (2.17) can be easily seen as an eigenvalue equation, where x_i is an eigenvector of A_{ij}, with $a = \Lambda^{-1}$, where Λ is an eigenvalue of the adjacency matrix [51]. Since we are interested in ranking every node in the network, we need real-valued x_is. Therefore, not all eigenvectors of A_{ij} are good candidates for the task.

Nonetheless, since A_{ij}, introduced in Sec. 2.2, is irreducible (assuming it to represent a connected graph, see [75], *p.* 134), the Perron-Frobenius [75] theorem (Appendix 1.1) assures that the adjacency matrix *Largest Eigenvalue* (LEV) is positive and has a unique *principal eigenvector* (PEV), whose entries are all positive. Despite the simplicity in its definition, EV centrality has the drawback that even a node not connected to *any* important node may enhance its rank by connecting to sufficiently many *unimportant* nodes [51, 18], with this artifact usually being called *self-inflation*. This is related to a mechanism known as *back-tracking*. In literature it is reported that corrections in the EVC definition turn its usage valuable in the description of transport phenomena in porous media [76]. Furthermore, we shall see in subsequent chapters that epidemic models such as the SIS one present important feedback mechanisms for sustaining activity reminiscent of the centrality inflation mechanism just mentioned [51, 18, 77]. As a side effect, this feedback mechanism leads to important localization phenomena in dynamics ruled by highly connected spreaders [31, 78].

2.7.4 Non-backtracking centrality

In an attempt to correct the self-inflation artifact, one can define a centrality measure that takes into account the centrality of the neighborhood of a node, avoiding contributions from the node itself [79]. This avoids the back-tracking mechanism at play in the self-inflation mentioned in Subsec. 2.7.3. To mention an example, there are dynamic processes, such as *biased random walks*, in which the feedback mechanism mentioned at

the end of Subsec. 2.7.3 is prohibited by construction [80, 81], thus naturally bringing this *non-backtracking* character. Among epidemic processes whose activation mechanisms are reminiscent of this non-backtracking condition, we can mention the SIR (*susceptible, infected* and *recovered*) model [82], in which feedback of epidemic activity is intrinsically prohibited. Furthermore, we shall see in Chap. IV how it is also related to the $SIRS$ model, in which the non-backtracking condition holds only for typical time scales $\frac{1}{\alpha}$, tracing back to the period of active immune response of an agent [48, 49].

To obtain a centrality with these characteristics, we must define an eigenvalue equation in a similar way to that defined in Eq. (2.17), but this time, employing a matrix $B_{j\to i,k\to l}$ designed in such a way to explicitly avoid back-tracking paths, thus ruling out self-inflation mechanisms found in the definition based on the adjacency matrix A_{ij} [41, 83]:

$$\Lambda_B v_{j\to i} = \sum_{k\to l} B_{j\to i,k\to l} v_{k\to l}, \tag{2.18}$$

where $B_{j\to i,k\to l}$ is defined as [84]:

$$B_{j\to i,k\to l} = \begin{cases} 1, & \text{if } i = k \text{ and } j \neq k \\ 0, & \text{otherwise,} \end{cases} \tag{2.19}$$

in which $j \to i$ is a directed edge between nodes j and i, while $k \to l$ is a directed edge between nodes k and l, indicating a path of length 1 between edges $j \to i$ and $k \to l$ if they are consecutive and non-backtracking. Furthermore, Λ_B stays for the LEV of $B_{j\to i,k\to l}$, while $v_{j\to i}$ represents its PEV. Now, we can define the Non-backtracking Centrality (NBC) as:

$$x_i = \sum_j A_{ij} v_{j\to i}, \tag{2.20}$$

which can be interpreted as the sum non-backtracking *messages* arriving into node i from each neighbor j. These messages, in turn, are the result of each node j receiving them from its neighbors, excluding node i itself (in this case, node i is said in literature to be in *cavity mode*) [85].

2.8 The uncorrelated configuration model (UCM)

2.8.1 The configuration model

We have so far defined several properties of networked systems, ranging from its bare definition up to node centrality. However, very little was said about its construction from the bottom up. To fill this gap, we present in this subsection the *configuration model* (CM for short). It allows to model an ensemble of networks having N nodes following a

given degree sequence $\{k_1, k_2, \cdots, k_N\}$ [51], usually randomly generated by following some distribution. One of the hallmarks of this model is its lack of degree correlations [14, 52]. By the way, the sum of the sequence must be an even number, so that no unmatched connection is left behind, otherwise the sequence should be thrown away [50, 51]. In general, the configuration model goes as follows:

1. Define a size N for the network;
2. Establish a degree sequence by attributing to each node i a degree k_i such that $k_{min} \leq k_i \leq k_{max}$, with k_{min} being the minimum degree and $k_{max} \leq N$ the maximum degree (*e.g.*, by taking the amount N_k of degree k nodes from probability distribution $P(k)$);
3. In the next step, one appends the *stubs* (or half edges) of each node i to a list, i.e. the label i repeated as many times as the node's degree k_i;
4. Then, at each step of the iteration, two stubs i and j are selected randomly and attached, creating an edge (i, j);
5. In the sequence, the chosen stubs of i and j are removed from the list, thus remaining $k_i - 1$ and $k_j - 1$ stubs respectively;
6. Steps 4 and 5 shall be executed until no stubs are left in the list.

After finishing this algorithm, one should end up with a network containing N nodes, $N_e = \frac{1}{2}\sum_{i=1}^{N} k_i$ edges and the desired degree distribution $P(k)$.

The model may present some pitfalls that make it less interesting regarding the reproduction of real-networks basic properties [51]. For example, the model has no procedure to avoid self- and multi-edges, while the majority of real networks do not have them. On one side, avoiding undesired connections would easily fix this issue and allow us to move on and turn CM-networks into simple graphs as desired. However, on the other side, this procedure would break the ensemble's homogeneity and predictability from theoretical models [51, 50].

Consider a given degree sequence, say $\{k_1, \cdots, k_N\}$, with the number of edges satisfying the constraint $N_e = \frac{1}{2}\sum_{i=1}^{N} k_i = N\langle k\rangle$.
With a stub of a node i in hand and considering to connect it to any of k_j stubs of node j, out of $N\langle k\rangle$ stubs available in the network, our chances are:

$$p_j = \frac{k_j}{N\langle k\rangle - 1} \simeq \frac{k_j}{N\langle k\rangle}, \tag{2.21}$$

with any stub being selected homogeneously and we have taken for granted that $N\langle k\rangle \gg 1$. Let us take a look at how many connections with each other a node i and a node j would share if a stub were to be selected with probability p_j, Eq. (2.21), while stubs from other

nodes were to be selected with complementary probability $1-p_j$. Considering $N\langle k\rangle \gg 1$, the chances of node i connecting $n \leq k_j$ stubs to node j's are:

$$P(n|k_i,k_j) = \binom{k_i}{n} p_j^n \left(1-p_j\right)^{k_i-n}, \tag{2.22}$$

what gives us an expected number of connections:

$$\langle N_e^{k_i,k_j}\rangle = \frac{k_i k_j}{N\langle k\rangle}. \tag{2.23}$$

With $\frac{k_i k_j}{N\langle k\rangle} \ll 1$, for all i and $j \in \{1,\cdots,N\}$, we could certainly expect only a vanishingly small number of multiple connections between high degree nodes. However, whenever this quantity turns out to be of order $O(1)$, for some degree high enough, someone cannot ignore this fact any longer, whenever it is desirable to keep the simple graph nature of a network. Otherwise, by attempting to avoid self- and multiple-connections between high-degree nodes, disassortative correlations would unavoidably be introduced [59, 50, 51], since hubs, by attempting to link multiple times to each other, would be pushed to connect to lower degree nodes. This leads us to argue that, to preserve the simple graph nature, the quantity given by Eq. (2.23) must satisfy $\langle N_e^{k_i,k_j}\rangle \leq 1$. With this condition at our disposal, we are in place to establish a *safe* structural cut-off for the network maximum degree. This assures us a secure way to conciliate the desired network's simple graph nature with its sought degree-uncorrelated character. Setting both k_i and k_j equal to k_s leads us to:

$$k_s\left(N\right) = \sqrt{\langle k\rangle N}. \tag{2.24}$$

So, now we are able to update our Configuration Model in order to preserve the simple graph nature of a network.

1. Define the size N of the network;
2. Establish the *structural cut-off* $k_s\left(N\right) \leq \sqrt{N\langle k\rangle}$;
3. Create a degree sequence from a probability distribution $P\left(k\right)$ with the constraint that $k \leq k_s\left(N\right)$;
4. In the next step, the stubs of each node i are appended to a list, i.e. the label i is added k_i times into a list;
5. Then, at each step, two stubs i and j are randomly taken and, if it does not represent a self- nor a multiple connection, an edge (i,j) is created;
6. Subsequently, the stubs chosen in the last step are removed from the list, thus remaining k_i-1 and k_j-1 for i and j;

7. Steps 5 and 6 shall be executed until no stubs are left in the list.

Networks thus generated, although not ubiquitous in nature nor in infrastructures produced by humankind, feature complete randomness as an important ingredient for comparison with complex systems from which someone expects some sort of intrinsic ordering, possibly guiding its development. Furthermore, UCM-networks are a valuable theoretical tool, which allows one to obtain closed-form results, as we shall see in Sec. 3.8, where we deal with mean-field theories in epidemics.

2.8.2 Degree cut-offs in power-law networks

We can measure the maximum cut-off of a power-law $P(k) \sim k^{-\gamma}$ network in a simple way. Taking into account the degree distribution and enforcing the condition that we find *at most* 1 vertex of degree equal to k_c or higher, we can obtain this degree cut-off implicitly through the equation:

$$F\left(k \geq k_c\right) = N \sum_{k=k_c}^{N} A k^{-\gamma} = 1, \tag{2.25}$$

where A is a probability normalization constant, $P(k) = Ak^{-\gamma}$. In the limit of $N \gg 1$, we can approximate the discrete summation by an integral, obtaining the result:

$$k_c\left(N\right) \sim N^{\frac{1}{\gamma-1}}, \tag{2.26}$$

known as the *natural cut-off* of the network [50, 51, 52]. This happens to be the average value of the maximum degree of a power-law network, when no upper bounds are imposed [59, 60]. For a more rigorous calculation of this quantity, yielded by the statistical distribution of k_c we refer interested readers to the literature [59]. Taking into consideration the degree cut-off given by Eq. (2.26), we can see that networks with $\gamma < 3$ have an average maximum degree higher than the structural cut-off given by Eq. (2.24), since $(\gamma - 1) < 2$. This way, in order to preserve neutral degree correlations, we should impose the constraint that the maximum degree be smaller than the structural cut-off, $k_{max} \leq k_s$ (see Eq. (2.24)). Consequently, networks with $\gamma > 3$ have a k_c smaller than the structural one $k_s \sim N^{\frac{1}{2}}$. Furthermore, it is known that fluctuations around the average maximum degree $\langle k_{max} \rangle$ also diverge with network size as $N^{\frac{1}{\gamma-1}}$ [61, 86, 52], causing typical values of the maximum degree to not be well represented by the natural cut-off k_c prediction, when the structural one k_s is taken as an upper-bound [60]. Thus, to avoid such fluctuations, it is advisable to use a *rigid cut-off* $k_r \sim N^{\frac{1}{\gamma}}$ instead [60, 61]. As a matter of fact, one should take into account that the choice of degree cut-off by itself carries no actual physical meaning [61]. It is rather a facility for the sake of comparison with theoretical predictions and avoiding highly fluctuating hubs through samples [86].

2.9 Conclusions of the chapter

In this chapter, we discussed important concepts and features belonging to network modeling and description. We introduced the concept of adjacency matrix, which represents the complete footprint of a network and from which any information from it can be obtained. Statistical measures, like moments of the degree distribution, important in obtaining epidemic thresholds of mean-field theories (see Chap. III) were also introduced and briefly discussed. Approaching the end of this chapter, centrality measures were introduced to rank nodes in the network according to their importance in the epidemic process under analysis. At the end of this chapter, we could devise important aspects of the method involved in the synthesis of PL uncorrelated networks, which are employed as a 0-model for analytical approximations.

III Epidemic processes in complex networks

3.1 An introduction to this chapter

From now on, we shall develop the basic theory of *Markov processes* related to epidemic models. A process is referred to as *Markovian* when transitions between states are independent of the previous trajectory of states followed by the system up to the present state [75, 87]. The governing equations of the dynamics (see *Master Equation* in Sec. 3.2) are rarely analytically solvable, thus prompting us to employ strategies for obtaining approximate solutions, usually neglecting fluctuations and state correlations of higher orders (Sec. 3.8). They predict threshold values for infection rates above which an active state is expected and below which the number of infected agents drops exponentially fast. More sophisticated theories are even capable of predicting that huge heterogeneous networks present no epidemic threshold (Subsec. 3.8.2) for some degree of heterogeneity and, by increasing the level of description (Subsec. 3.8.3), presenting no threshold for *any* degree of heterogeneity, what has already been rigorously proven [45].

3.2 The master equation

Stochastic processes of a special kind are those in which transitions between *discrete states* [88], depend solely on the current state. Dynamics with this particular feature are referred to as *Markovian* and we can attribute them the property of being *memoryless* [75, 89].

In a system with N agents, each of them being in one of m discrete states at time t, $\sigma_i(t) \in \{1,\ 2, \cdots,\ m\}$, the global state of the system may be defined as:

$$\sigma = \{\sigma_1,\ \sigma_2,\ \ \cdots \sigma_k,\ \ \cdots,\ \sigma_N\} \tag{3.1}$$

Put simply, a node may be found in any of the m possible states.

Therefore, a state $\boldsymbol{\sigma}$, realized with probability $P^{(\boldsymbol{\sigma})}(t)$ at time t undergoes a spontaneous transition to an accessible state $\boldsymbol{\sigma'}$ with rate $W_{\boldsymbol{\sigma}\to\boldsymbol{\sigma'}}$.

Taking this into account, we may construct a *Master Equation* [52], describing the dynamics of each global state:

$$\frac{\mathrm{d}}{\mathrm{d}t}P^{(\boldsymbol{\sigma})}(t) = \sum_{\boldsymbol{\sigma'}}\left(P^{(\boldsymbol{\sigma'})}(t)W_{\boldsymbol{\sigma'}\to\boldsymbol{\sigma}} - P^{(\boldsymbol{\sigma})}(t)W_{\boldsymbol{\sigma}\to\boldsymbol{\sigma'}}\right). \tag{3.2}$$

One may be interested in the *stationary solutions* of Eq. 3.2 $\frac{\mathrm{d}}{\mathrm{d}t}P_t^{(\boldsymbol{\sigma})} = 0\ \forall\sigma$. However, an important class of systems enjoys a particular symmetry, in which the terms in parentheses

equal zero altogether, leading to $P^{(\boldsymbol{\sigma'})}(t)W_{\boldsymbol{\sigma'}\to\boldsymbol{\sigma}} = P^{(\boldsymbol{\sigma})}(t)W_{\boldsymbol{\sigma}\to\boldsymbol{\sigma'}}$, representing a zero current of probability into or out of a state $\boldsymbol{\sigma}$ [75, 90]. This is called *detailed balance*, a sufficient condition for equilibrium [91], violated by non-equilibrium systems, such as the ones possessing an *absorbing-state phase-transition*, which are of main interest in this thesis [92]. Dynamics of this kind possess *at least* one state $\tilde{\boldsymbol{\sigma}}$ from which the dynamics cannot escape once visited ($W_{\tilde{\boldsymbol{\sigma}}\to\boldsymbol{\sigma'}} = 0$) [91, 93].

3.3 The Gillespie Algorithm

The master equation can be solved exactly only for just a few cases [75, 87]. Furthermore, if we intend to employ numerical integration of Eq. (3.2), we must be aware that it takes the simultaneous solution of a set of m^N differential coupled equations, where m is the number of accessible states for each node. Therefore, we shall not attempt analytical solutions of Eq. (3.2) and employ a statistically exact method to sample solutions computationally.

For this purpose we employ the *Gillespie Algorithm* [94], in particular an optimized version developed in Ref. [94]. Let us imagine that each agent i (e.g a node) can undergo, at each time step, one of M possible spontaneous events, taking place at rate $\nu_i \in \{\nu^{(1)}, \nu^{(2)}, ..., \nu^{(M)}\}$. We can write a Master Equation related to the *Poisson process* of a single event occurring or not until time t with probabilities $P_1(t)$ and $P_0(t)$, respectively. Clearly, $P_0(t) + P_1(t) = 1$ and the master equations are:

$$\frac{d}{dt}P_0 = -\nu^{(l)}P_0 \tag{3.3}$$

and

$$\frac{d}{dt}P_1 = \nu^{(l)}P_0, \tag{3.4}$$

with $P_0(0) = 1$. Their solutions are $P_0(t) = e^{-\nu^{(l)}t}$ and $P_1(t) = 1 - e^{-\nu^{(l)}t}$. $P_0(\tau) = e^{-\nu^{(l)}\tau}$ gives the probability that no spontaneous event happens between $t \in \{t, t+\tau\}$ distribution of inter-event times τ. Since each agent transitions independently from the others, we talk about Ω independent events possibly taking place at time t. Therefore, the probability of no event taking place until time t is the product of the probability of Ω independent events:

$$P_0(t) = \prod_{l=1}^{\Omega} e^{-\nu^{(l)}t}. \tag{3.5}$$

In other words, the network state transitions to the next state at an overall rate of events $W = \sum_{l'=1}^{\Omega} \nu_{l'}$. So, with probability $\nu^{(l)}P_0(t)dt$ no event occurs until time t with probability $P_0(t) = e^{-Wt}$ and, during time $t' \in \{t, t+dt\}$, an event l occurs with probability

$\nu^{(l)}dt$. Multiplying it by $1 = \frac{W}{W}$, we have:

$$p(\text{event } l \text{ is chosen}) = \left(\frac{\nu^{(l)}}{\sum_{l'=1}^{\Omega}\nu_{l'}}\right) We^{-Wt}dt. \tag{3.6}$$

Eq. (3.6) yields a convenient means of modeling Markovian dynamical processes as follows:

1. Sort a time interval τ from distribution:

$$p(t) = We^{-Wt}. \tag{3.7}$$

   In practice, we can distribute the inter-event times in by means of $\delta t = -\frac{1}{W}\ln(u)$. Here $W = \sum_{l=1}^{\Omega}\nu^{(l)}$ is the overall rate, corresponding to all Ω independent events possibly happening at the current simulation time and u is pseudo-random number lying in the open interval $(0, 1)$ [94].

2. After choosing δt, the l-th event, happening with rate $\nu^{(l)}$, is chosen with probability $\nu^{(l)}/W$, where $W = \sum_{l'=1}^{\Omega}\nu_{l'}$.

3. Since a new transition happened, both the system state as well as the list of possible events are updated.

4. Finally, repeat from step 1 through step 3, until the evolution reaches the required time.

3.4 A brief example - the SIRS model

With the algorithm presented in Sec. 3.3, Markovian epidemic processes described through the Master Eq. (3.2) (Sec. 3.2) can be computationally modeled in large networked models [94]. Let us take as an example the *SIRS* model. Its dynamics is described by the following reaction equations at the individual level as:

$$S_i \xrightarrow{n\lambda} I_i, \quad \text{(infection)} \tag{3.8}$$

$$I_i \xrightarrow{\mu} R_i, \quad \text{(recovering)} \tag{3.9}$$

$$R_i \xrightarrow{\alpha} S_i, \quad \text{(waning of immunity)}, \tag{3.10}$$

where λ is the *infection rate* for each infectious contact of node i at the present time, n is the number of its infectious neighbors, μ is the node's *recovery rate* and α is a *rate of waning of immunity*. A node i may be found at each instant in a state $\sigma_i \in \{S, I, R\}$. By tuning the rate α, we can change the model's qualitative behavior, obtaining the SIR

model ($\alpha = 0$) and SIS ($\alpha = \infty$) [95]. In the first case, the dynamics cannot survive for long periods, inevitably falling into a disease-free state, thus having an active state only in the transient regime. In the thermodynamic limit ($N \to \infty$) there is a phase transition marked by a threshold λ_c, above which a finite fraction, i.e. a macroscopic portion of the agents, may be found in the recovered state R [96]. Meanwhile, the second case presents a prototypical dynamics possessing a phase transition to an absorbing state (in the thermodynamic limit $N \to \infty$) [91] at a threshold λ_c, above which a non-vanishing fraction of the agents is found in the infected state I [91]. With the purpose of studying such transitions, we occupy ourselves in this work with stochastic simulations and mean-field theoretical approaches in the next sections.

3.5 Quasi-stationary simulation

As mentioned in previous sections, epidemic models possess an absorbing state, which traps the dynamics once reached. Furthermore, finite systems always have the inactive state as the only stationary one. This happens since in finite systems, there is also a non-vanishing probability to an active configuration to reach the absorbing state in a finite number of steps. So, in the finite size regime one cannot properly speak of an absorbing state phase transitions. The best we can do is to sample active metastable states (long lived), when they occur. Therefore, a suitable sampling scheme must be employed. Actually, there are several schemes known in literature aimed at overcoming this problem. Under the possible schemes, we deal in this work with the *Quasi-stationary* (QS) *method* [91]. We shall not deal in deeper details over derivation of this method and refer the interested reader to the literature [91]. It consists in reviving the dynamics from a previously visited state, once it has reached the absorbing one.

Here another look into the Master Equation (3.2) is instructive. Here, we follow the notation used in [97]. Although the Master Equation (3.2) is not always exactly solvable, we can obtain some important information about the dynamics, such as the *survival probability* [91, 98] $P_S(t)$, which quantifies the probability of the dynamics being found in an active (non-absorbing) state at time t [91]. Here, we denote the set of absorbing configurations as $\{\sigma^*\}$. The survival probability is therefore defined as follows:

$$P_S(t) = \sum_{\sigma \notin \{\sigma^*\}} P(\sigma, t) = 1 - \sum_{\sigma \in \{\sigma^*\}} P(\sigma, t)\,. \tag{3.11}$$

Summing Eq. (3.11) over only active states $\sigma \notin \{\sigma^*\}$ in the Master Equation (3.2) it yields:

$$\frac{d}{dt} P_S = - \sum_{\sigma \notin \{\sigma^*\}} P(\sigma, t) \sum_{\sigma' \in \{\sigma^*\}} W_{\sigma \to \sigma'} = -W^*(t). \tag{3.12}$$

Here it was used the fact that $W_{\sigma' \to \sigma} = 0$, when $\sigma' \in \{\sigma^*\}$ and $\sigma \notin \{\sigma^*\}$, and that

$\sum_{\sigma} \rightarrow \sum_{\sigma \in \{\sigma^*\}} \cup \sum_{\sigma \notin \{\sigma^*\}}$. In Eq. (3.12) one can interpret $W^*(t)$ as the overall rate of falling into the absorbing state (or not surviving). Continuing, if we assume a *quasi-stationary* state setting in for sufficiently long times $t \gg 1$ and that a unique quasi-stationary distribution $\bar{P}(\sigma)$ exists [97] such that $P(\sigma, t) = P_S(t) P_{QS}(\sigma)$, we can rewrite Eq. (3.12) as:

$$\frac{1}{P_S}\frac{d}{dt}P_S = -\sum_{\sigma \notin \{\sigma^*\}} P_{QS}(\sigma) \sum_{\sigma' \in \{\sigma^*\}} W_{\sigma \to \sigma'} = -\bar{W}^*, \tag{3.13}$$

leading to $P_S(t) = e^{-t/\tau}$, if we assume $P_S(0) = 1$ by construction, where:

$$\tau = \frac{1}{\bar{W}^*}. \tag{3.14}$$

is the *lifespan* of the dynamics [97, 99]. Here:

$$\bar{W}^* \equiv \sum_{\sigma \notin \{\sigma^*\}} P_{QS}(\sigma) \sum_{\sigma' \in \{\sigma^*\}} W_{\sigma \to \sigma'}. \tag{3.15}$$

We shall see in the following sections that the lifespan itself can grow exponentially with size of the subgraph involved in the activation of the dynamics (when activity is localized), $\tau \sim e^{aN_{sub.}}$, or with network size (when activity is delocalized), $\tau \sim e^{aN}$ [100], where a is a positive number [91, 99].

Although we have some information about the surviving probability and its lifespan, we do not know the QS probability $\bar{P}(\sigma)$ yet. Instead of working with the usual Master Equation, we can imagine another stochastic process, with the constraint of possessing the same transitions among active configurations as the original one [99, 97]. This new stochastic process shall not posses an absorbing state by construction, if we define its pseudo Master Equation as:

$$\frac{d}{dt}\tilde{P}(\sigma, t) = \sum_{\sigma' \notin \{\sigma^*\}} \{\tilde{P}(\sigma', t) W_{\sigma' \to \sigma} - \tilde{P}(\sigma, t) W_{\sigma \to \sigma'}\} + \tilde{P}(\sigma, t) W^*(t), \tag{3.16}$$

where $W_t^* \equiv \sum_{\sigma \in \{\sigma^*\}} \sum_{\sigma' \notin \{\sigma^*\}} \tilde{P}(\sigma', t) W_{\sigma' \to \sigma}$. Eq. (3.16) represents a version of the original Master Equation in which the flux into the absorbing state $W^*(t)$ is redirected to *all* active states [99, 30] and possesses as stationary solution the same QS solution of the original Master Equation [99, 30]. It also suggests a clever simulation scheme to computationally sample the QS states, by avoiding the absorbing state, in combination with the Gillespie Algorithm described in Sec. 3.3. The method consists in reactivating a previously visited configuration, whenever the inactive state is reached. The **Standard QS Method** is performed as follows:

1. The current active configuration σ consisting of N_{inf} infected and N_R recovered nodes (or not, in the SIS limit) is stored in one of M configurations with probability

$p = \mu\delta t$, see Eq. (3.7), until the limit established for the lists in reached;

2. With probability $P_{renew} = 0.02$, one of the M configurations is randomly chosen and replaced with the current one;

3. Whenever the absorbing state is reached, one of the M configurations stored is chosen and set as the current one, which then continues the process.

3.6 Quasi-stationary quantities

To show an example in practice of the application of the QS method, let us briefly discuss *decaying simulations* [47, 61]. In this kind of simulation, one initiates the dynamics with the network under study with *every* node in the infected state. Firstly, the dynamics shall relax for a simulation time t_{relax}, so it decorrelates from the initial state. Then, for a simulation time $t_{relax} < t < t_{relax} + t_{av}$ the QS probability is computed, $P_{QS}(n) \to P_{QS}(n) + \mu\delta t$, where δt is an inter-event time drawn from the Poisson-distribution given by Eq. (3.7) and described in Sec. 3.3. As an example regarding the $SIRS$ model,

$$W_T = \mu N_{inf} + \lambda N_{SI} + \alpha N_R, \tag{3.17}$$

where N_{inf} is the number of infected nodes, N_{SI} is the number of contacts between infected and susceptible nodes and N_R is the number of recovered agents. Here, the conjugated rates μ, λ and α are the same described in Sec. 3.4. Once the QS distribution $P_{QS}(n)$ is obtained and normalized, one readily obtains the associated lifespan:

$$\tau_{LS} = \frac{1}{\mu P_{QS}(1)}, \tag{3.18}$$

as a consequence of Eq. (3.18). Fig. 3.1 shows the lifespan of star-graphs of different sizes and α values (SIRS model). One sees how the lifespan algebraically diverges with $k^{\alpha/\mu}$, in contrast to the SIS model ($\alpha \to \infty$), which diverges exponentially $\tau_k \sim e^{\lambda^2 k}$ [30].

As the next step, the moments of the QS distribution can be calculated as follows:

$$\langle \rho^l \rangle = \frac{1}{N^l} \sum_n n^l P_{QS}(n), \tag{3.19}$$

from which one defines the *infectious prevalence* or *density* $\langle \rho \rangle$ and the second moment $\langle \rho^2 \rangle$ to obtain the *modified susceptibility* χ or just susceptibility for short [47]:

$$\chi = N \frac{\langle \rho^2 \rangle - \langle \rho \rangle^2}{\langle \rho \rangle}, \tag{3.20}$$

which measures relative QS fluctuations [47]. For λ approaching the *effective epidemic threshold* $\lambda_p(N)$, χ shows a pronounced *peak* χ_p whose size depends on the system size

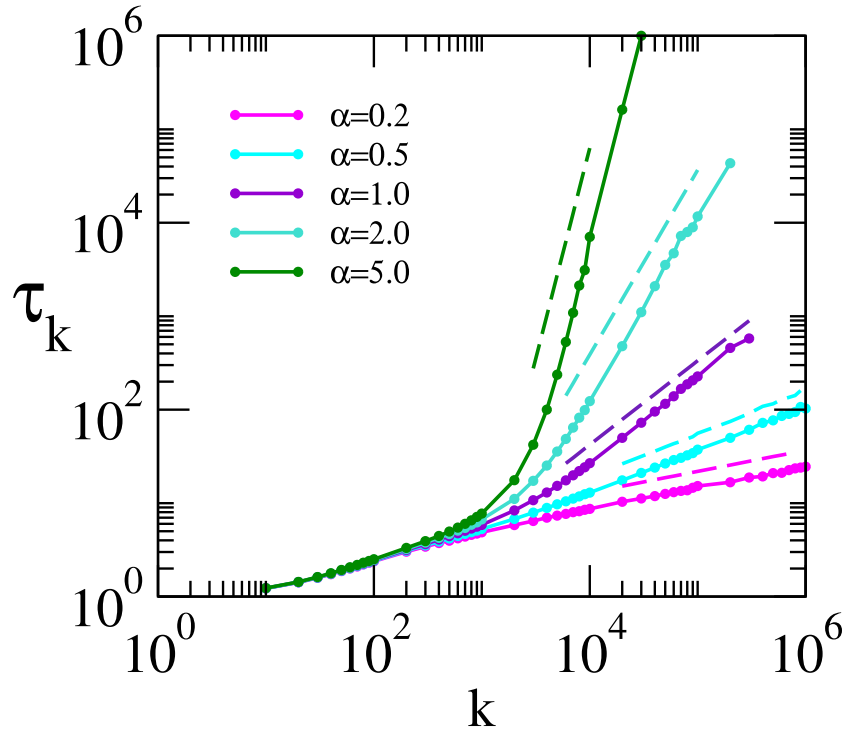

Figura 3.1 – Finite size scaling for the lifespan τ_{LS} vs star-graph size k in SIRS model with different values of α (solid lines). Dashed lines show the scaling $\tau_k \sim k^{\alpha/\mu}$, μ set to 1 without loss of generality. $\lambda = 0.05$ throughout all simulations.

N, expected to diverge in the thermodynamic limit $N \to \infty$ [47]. Fig. 3.2(a) shows the susceptibility referred behavior. Both the peak and the epidemic threshold position λ_p are emphasized (blue dotted).

3.7 Finite Size Scaling - FSS

Approaching the thermodynamic limit $N \to \infty$, in turn, the effective threshold would converge to its critical value $\lambda_p(N) \to \lambda_c$. However, regarding computational simulations, we have to overcome the fact that our resources are finite and perform a *Finite Size Scaling* (FSS) [89] in order to obtain an extrapolation to the thermodynamic limit. Fig. 3.3 shows in practice the method based on the peak of susceptibility. Here, as one sees, the peak grows with network size while its position gradually dislocates to the left, suggesting an epidemic threshold at $\lambda_c = 0$.

3.8 Mean field theories

An exact description of stochastic processes is possible by solving the set of Eqs. (3.2). As can be easily seen, the amount of micro-states accessible, as well as the number of equations, scale exponentially with the agents quantity N as m^N, where m

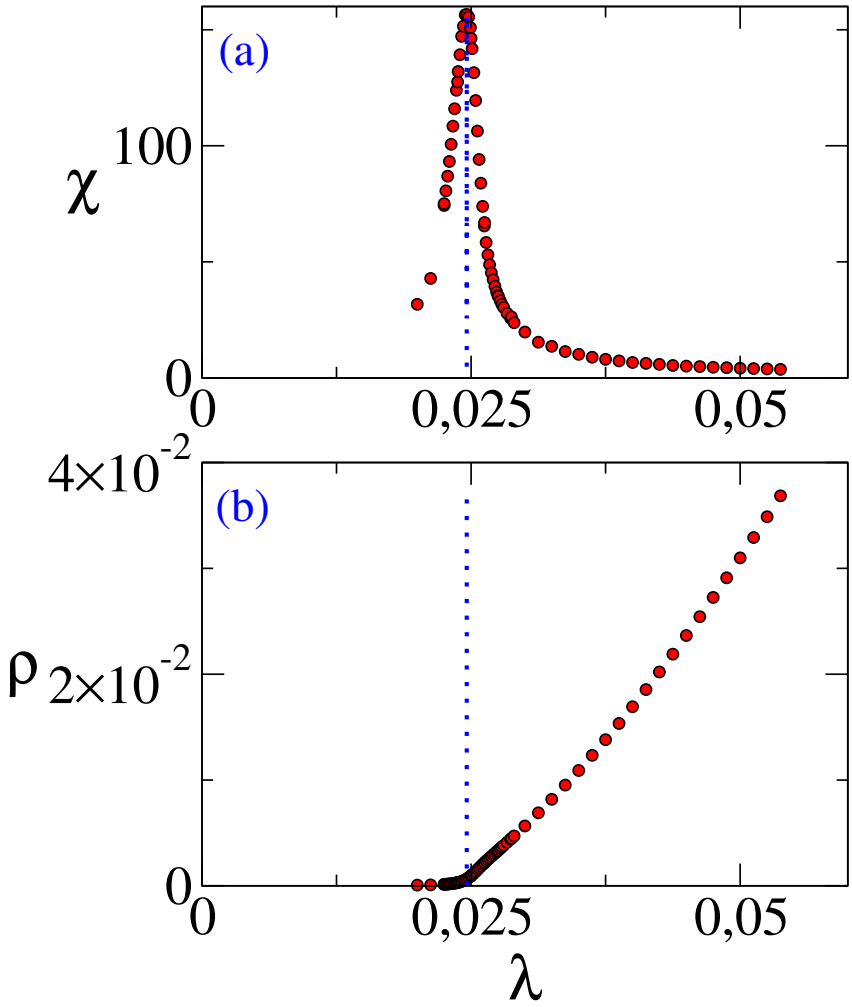

Figura 3.2 – (a): Susceptibility χ and (b): infectious prevalence ρ *vs* infection rate λ. SIS model on top of PL degree distributed network $P(k) \sim k^{-\gamma}$ with $\gamma = 2.6$. Minimum degree $k_{min} = 3$, $k_c = 2\sqrt{N}$. Size $N = 3 \times 10^5$. Dotted blue line emphasizes the peak location (a) and the epidemic threshold position (b).

is the number of states accessible at the individual level, rendering its exact solution, in general, prohibitive still for modest system sizes N [95, 101].

Besides this issue, the vast majority of networked systems found world-wide are rich in heterogeneity in the contact patterns. A combination of considerable size of the interacting components and the underlying heterogeneity is by itself capable of introducing serious difficulties in obtaining analytical as well as numerical solutions for the Master Equation [101]. Thus, the mentioned difficulties call the interested researcher for seeking simplifying approaches, keeping only the desired ingredients under investigation [95].

Although just a few models can be solved analytically, due to special assumptions like inherent symmetries, detailed balance [90] and other simplifying assumptions [101], the most of them cannot [95, 102]. Therefore, approximations and simplifying assumptions play a major role, usually represented by *mean-field* approaches and approximated schemes, such as the ones based on *dimensionality reduction* [103, 102], to name just few examples. While mean-field theories disregard inherent dynamic fluctua-

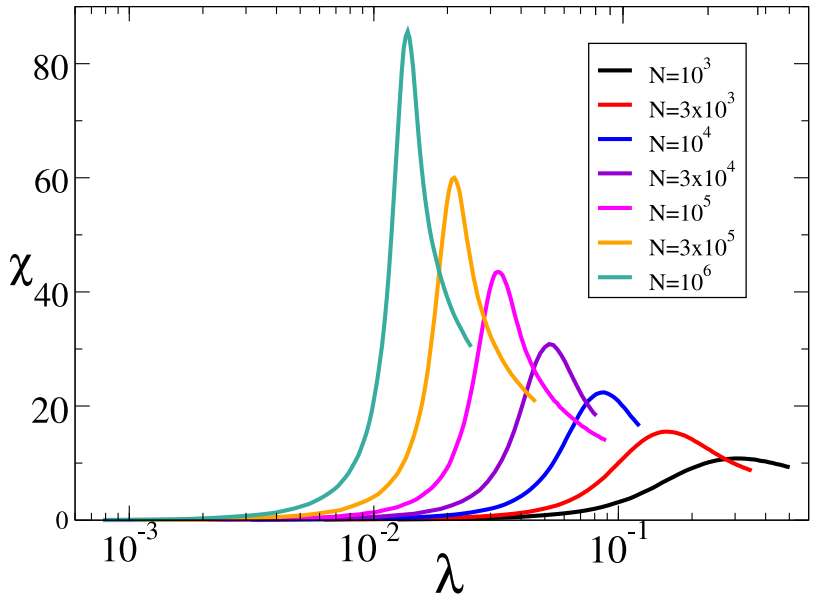

Figura 3.3 – Finite size scaling of susceptibility χ vs λ infection rate for SIRS dynamics with $\alpha = 0.10$ on top of PL degree distribute networks $P(k) \sim k^{-\gamma}$, with $\gamma = 2.3$, $k_0 = 3$ and $k_c \sim N^{\frac{1}{2}}$.

tions [38, 104, 48, 105, 106, 107], approximation schemes *do not* [102]. These, however, usually suffer under inherent artifacts, such as corrections of numerical errors caused by non-sufficient precision. Among them, it is worth to mention the possible lack of normalization of probability distributions, caused by precision issues, that, under correction may lead to even worse error propagation, causing misleading results and being usually difficult to tell from the correct ones [102]. Summarizing, although preserving only some level of the stochastic nature of the dynamics, approximation schemes feature some enhanced quantitative gain of accuracy over mean-field theories [102]. Nonetheless, such approaching schemes usually introduce artifacts that may represent sources of errors that may lead to physically inaccurate interpretations [108, 109] besides of numerical instabilities and high computational cost [102].

Although the just discussed issues may still lead someone to pursue an exact description of large systems dynamics, the need of balance between performance and computational time is not the only issue in sight. Overly intricate relations among agents states and underlying structures can be hardly interpreted and do not always bring clear insights, thus posing a major concern in the pursuing of an exact solution of the master equation [95]. At the other side, mean-field approaches are indeed based on simplifying assumptions, such as disregarding correlations and fluctuations at some level. This may cause some concern about the possible lack of *quantitatively* precise results, however some useful *qualitative* descriptions are possibly brought due to the incorporation of only the most important features of the dynamics [95].

3.8.1 Homogeneous Mean-Field Theory (MF)

As a first approach strategy, a population composed of N statistically equivalent (having approximately the same degree) agents can *be thought of* as being *mixed*, i.e., it is assumed that each agent is capable of getting in contact to any of the other agents [50, 52, 51] during the dynamic process of interest, thus characterizing a *Homogeneous Mean Field theory* (MF). Another ingredient we may investigate by the same principle is the lack of correlations between agents states [52]. These two main assumptions represent the lack of *heterogeneity* as well as *structural* and *dynamic correlations* [50]. Taking as an example the $SIRS$ model, briefly described in Sec. 3.4, we are already in place to write down a set of mean-field equations, as bellow:

$$\frac{\mathrm{d}\rho}{\mathrm{d}t} = -\mu\rho + \lambda k\rho s, \tag{3.21}$$

where ρ and s represent the fractions of infected and susceptible individuals. The first term in the right-hand side represents a *loss term*, or the rate of recovery of the infected class, being μ per individual. Meanwhile, the second term represents a *gain term*, or the total infection rate suffered by the susceptible agents, being β the infection rate per *infected-susceptible* contact. In overall, the gain part is proportional to both the fraction of infected ρ, susceptible s and the number of momentary acquaintances per agent k, along with the infection rate β.

To finish, one needs additional equations to describe the evolution of susceptible s and recovered r fractions, as bellow:

$$\frac{\mathrm{d}r}{\mathrm{d}t} = \mu\rho - \alpha r. \tag{3.22}$$

Here the first term represents a gain term, coming from the recovery of the infected population, while the second term in the right-hand side represents a loss term, coming from the *waning of immunity* of the recovered population.

Admitting a closed population (N constant) and the fact that members of the population are found either infected, recovered or susceptible, a normalization condition reads as:

$$\rho + r + s = 1, \tag{3.23}$$

thus yielding together with Eq. (3.21) and (3.22) a closed set of equations.

By setting $\alpha \to \infty$, the fixed point $r^* = 0$ is the only stable one [110] for Eq. (3.22), thus yielding the SIS model and causing Eq. 3.23 to become:

$$\rho + s = 1, \tag{3.24}$$

which has to be solved alongside Eq. (3.21). Typical example of dynamic and stationary

solutions of the mean-field SIRS (and SIS, in the limit $\alpha \to \infty$) model are shown in Fig. 3.4. Fig. 3.4(a) present some interesting qualitative remarks of the model, in which for a sufficiently high rate of infection $\lambda k > 1$, a small fraction of infectious agents ρ gets in contact with a system almost fully composed of susceptible individuals, characterized by $s \approx 1$. This causes the infection to grow exponentially fast in the early moments of the outbreak. As times goes, the rate of contact between infected and susceptible nodes $\lambda k \rho(1 - \rho - r)$ becomes smaller progressively balancing with the rate of recovery $\mu\rho$, causing the dynamics to saturate $\rho \approx \rho_\infty$ [50, 52]. In the other side, for insufficient infection rates, $\lambda k < 1$, the infected population dies out exponentially fast already in the early moments of the outbreak, ending with $\rho_\infty = 0$.

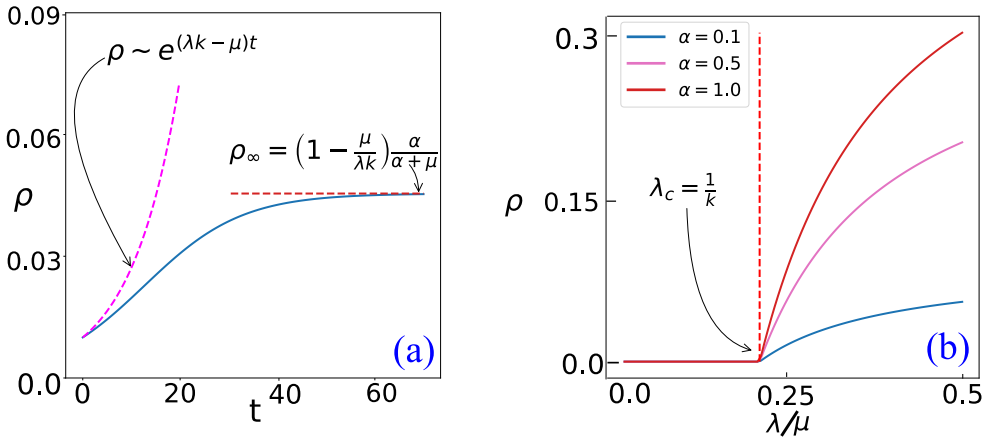

Figura 3.4 – Homogeneous approximation to the SIRS model. (a): ρ *vs* t for $\lambda > \lambda_c$, presenting a *transient* exponential regime (magenta dashed curve) and a *stationary regime* (red dashed curve). (b): Stationary curve showing ρ_∞ vs $\frac{\lambda}{\mu}$ for different α values. Red dashed vertical lines evidences the transition point between absorbing and active phase.

As seen, MF theory is capable of capturing a transition to an absorbing state and the exponential relaxation to a stationary state [111], a fact well-known in the literature. Nonetheless, the homogeneous mixing is far from being a realistic approach, since it neglects the heterogeneity of contact patterns [111] found in substrates like the internet, transport networks and interpersonal relationships, to name just a few examples [56]. This obviously calls the theory for some refinements.

3.8.2 Heterogeneous Mean-Field Theory - HMF

To fill the gap mentioned in the final remarks of Subsec. 3.8.1, the first step to be taken is to introduce the heterogeneity pattern of contacts in the theory. In a *coarse-grained* approach, we may argue that *all* nodes of degree k are dynamically equivalent, thus leading us to encapsulate the presence of the network in such a way that the agents, or nodes, are represented by their degree [111]. The network's structure enters in the

calculations at some level by means of the degree-distribution $P(k)$ and the degree-degree correlations $P(k'|k)$ [56]. This way of introducing the network structure into the theory represents the so called *Heterogeneous Mean Field theory* (HMF).

In order to write down governing differential equations, let us consider $\rho_k(t) \equiv \frac{I_k(t)}{N}$ the density of degree-k infected nodes, where I_k is the number of degree-k infected sites and N, as usually, the number of nodes in the network. Similarly, $s_k(t) \equiv \frac{S_k(t)}{N}$, where $S_k(t)$ is the number of degree-k susceptible nodes in the network at instant t and $r_k(t) \equiv \frac{R_k(t)}{N}$ represents the density of recovered nodes at instant t having degree k.

We may define the *epidemic prevalence*, or equivalently, the *global density of infectious nodes*, as:

$$\rho(t) = \sum_k P(k)\rho_k(t). \tag{3.25}$$

Similar definitions may be stated for the global density of recovered and susceptible nodes.

At both the degree and global levels we have the following normalization equations holding:

$$\rho_k(t) + r_k(t) + s_k(t) = 1, \tag{3.26}$$

and

$$\rho(t) + r(t) + s(t) = 1. \tag{3.27}$$

The latter follows directly from Eq. (3.26) multiplied by $P(k)$ and summed up over the degree k classes.

Considering the dynamic rules of the SIRS model - described in Sec. 3.4 - we are able to write down differential equations in the HMF theory, by ignoring dynamic correlations already at the pairwise level, i.e. $[A_k, B_{k'}] \sim [A_k][B_{k'}]$ [112]. Here, $[A_k, B_{k'}]$ means the expectancy of a degree-k node being in state A, while a degree-k' node is in state B [112].

We may then write down dynamical equations for $\rho_k(t)$ as follows:

$$\frac{\mathrm{d}}{\mathrm{d}t}\rho_k(t) = -\mu\rho_k(t) + \lambda k s_k(t) \sum_{k'} P(k'|k)\rho_{k'}(t). \tag{3.28}$$

The first term in Eq. (3.28) stays for recovery of degree-k nodes, while the term beside it stems from infectious contacts between degree-k and -k' nodes. Evolution of recovered nodes density $r_k(t)$ reads as follows:

$$\frac{\mathrm{d}}{\mathrm{d}t}r_k(t) = \mu\rho_k(t) - \alpha r_k(t). \tag{3.29}$$

where we may admit $\mu = 1$, without loss of generality, just setting time scales. Terms in Eq. (3.29) have analogous interpretations as those of Eq. (3.28), with αr_k representing

waning immunity of nodes.

For the sake of analytic tractability of Eq. (3.28), let us consider the case of *degree-degree uncorrelated networks*, as already discussed in Sec 2.4. Substituting $P(k'|k)$ giving by Eq. (2.11) in Eq. (3.28), we obtain:

$$\frac{\mathrm{d}}{\mathrm{d}t}\rho_k(t) = -\rho_k(t) + \lambda k\left(1-\rho_k(t)-r_k(t)\right)\Theta(\lambda,t), \tag{3.30}$$

where:

$$\Theta(\lambda,t) = \sum_{k'} k' \frac{P(k')}{\langle k\rangle}\rho_{k'}(t). \tag{3.31}$$

It is of great interest to obtaining stationary properties of the dynamics and its fixed points properties [110, 38], obtained in the limit $\lim_{t\to\infty}\frac{\mathrm{d}}{\mathrm{d}t}\rho_k(t) = 0$, from which we get:

$$\rho_k(\infty) = \frac{\lambda k\Theta(\lambda)}{1+\left(\frac{\alpha+1}{\alpha}\right)\lambda k\Theta(\lambda)}, \tag{3.32}$$

where we used $r_k(\infty) = \frac{1}{\alpha}\rho_k(\infty)$, as a result of Eq. (3.29). Applying Eq. (3.32) into Eq. (3.31), in the stationary regime, it yields:

$$\Theta(\lambda) = \sum_{k'} k'^2 \frac{P(k')\lambda\Theta(\lambda)}{\langle k\rangle\left(1+\left(\frac{\alpha+1}{\alpha}\right)\lambda k'\Theta(\lambda)\right)}. \tag{3.33}$$

Eq. (3.33) constitutes a *transcendental equation*, which we may solved numerically as well as graphically. With a simple check, one can see that $\Theta = 0$ satisfies Eq. (3.33), valid for $\lambda < \lambda_c$, still to be determined. Identifying the left and right hand sides of Eq. (3.33) as distinct functions, $F(\Theta)$ e $G(\Theta)$, respectively, non-trivial solutions can be obtained, corresponding to the intersection of $F(\Theta)$ and $G(\Theta)$ [113]. We should also note that Eqs. (3.33) and (3.32) reduce to the ones related to the SIS by making $\alpha\to\infty$, in which the term $\frac{\alpha+1}{\alpha}\to 1$.

A closer look on the behavior of $G(\Theta)$ shows us that it increases monotonically in the domain $\Theta\in[0,1]$. For non-trivial solutions to occur, it is necessary that $\frac{d}{d\Theta}G(\Theta) \geq \frac{d}{d\Theta}F(\Theta)$ for some $\Theta > 0$. This condition, together with $\frac{\alpha+1}{\alpha}\lambda k_c\Theta \ll 1$, for $\lambda \gtrsim \lambda_c$, allows us to determine the value of λ_c, for which a steady active state starts to establish [114, 113], leading to:

$$\lambda_c^{HMF} = \frac{\langle k\rangle}{\langle k^2\rangle}, \tag{3.34}$$

We should note that Eq. (3.34) is identical to the threshold obtained for the SIS model ($\alpha\to\infty$) [18]. This may counter-intuitive but, let us recall that HMF theory yields the exact description in the *annealed network* limit [94] [1], in which both structural and

[1] This is the limit of dynamic networks in which connections rewire within time scales much shorter

dynamic correlations are absent. In this regime, it is reasonable to expect that near the epidemic threshold, the amount of infectious sites is so small and rewiring of connections so quick, that an infectious node will barely encounter recovered nodes that hinder the disease spreading. Thus, near criticality, new infections occur just like in the SIS model. Inserting the values of $\langle k^2 \rangle$ from Eq. (2.9) into Eq. 3.34 leads us to the following behavior:

$$\lambda_c^{HMF} \sim \begin{cases} N^{\frac{\gamma-3}{2}}, & \text{if } \gamma < 3, \\ (\ln N)^{-1}, & \text{if } \gamma = 3, \\ \text{cte.}, & \text{if } \gamma > 3, \end{cases} \tag{3.35}$$

which says us that for $\gamma \leq 3$, the epidemic threshold λ_c^{HMF} vanishes and stays finite for $\gamma > 3$ [111]. This astonishing result states that HMF theory forecasts an active state in the thermodynamic limit for *any* disease on top of PL networks with $\gamma < 3$. This, however is accompanied either by finite size effects that suppress the extent of an outbreak above the effective threshold $\lambda_c(N)$ or, in the thermodynamic limit, by critical exponent $\beta = \frac{1}{3-\gamma}$, related to the prevalence $\rho \sim \lambda^\beta$ (see Ref. [15] for a thorough derivation of β), which, for being greater than 1 in the regime $2 < \gamma < 3$, leads to vanishingly small fractions of infected nodes close to the threshold. At $\gamma = 3$, the prevalence is exponentially small around the epidemic threshold $\lambda_c = 0$ [15].

3.8.3 The QMF theory (quenched mean-field theory)

HMF theory takes the network structure only statistically as seen in Sec. 3.8.2. Nonetheless, one can go further and make a theory in which the *actual* network structure is considered by means of the adjacency matrix A_{ij} [38], while still neglecting dynamical correlations which reads as:

$$\frac{\mathrm{d}}{\mathrm{d}t}\rho_i = -\rho_i + \lambda\,(1 - \rho_i - r_i)\sum_{j=1}^{N} A_{ij}\rho_j, \tag{3.36}$$

where we also used the normalization condition $\rho_i + r_i + s_i = 1$. Together with Eq.:

$$\frac{\mathrm{d}}{\mathrm{d}t}r_i = \rho_i - \alpha r_i, \tag{3.37}$$

we have a closed set of equations in ρ_i and r_i only.

3.8.4 QMF theory's threshold

A combination of Eqs. (3.36) and (3.37) in the stationary state ($\frac{d\rho_i}{dt} = \frac{dr_i}{dt} = 0$) yields:

than the typical times in which the pathogen spreads between neighbors.

$$\rho_i = \lambda \frac{\sum_{j=1}^{N} A_{ij}\rho_j}{1 + \lambda\left(1 + \frac{1}{\alpha}\right)\sum_{j=1}^{N} A_{ij}\rho_j}. \tag{3.38}$$

It follows that $\rho_i = 0$ is a trivial solution, which should loose stability as soon as the infection rate is equal or greater than a certain threshold $\lambda \geq \lambda_c$. Sufficiently close and above this threshold, we expect $\rho_i \ll 1$, so that we can perform a QS approximation, as described in App. C.

Proceeding with a linear stability analysis around the trivial fixed point $\rho_i^* = 0$, described in App. C, we obtain a linear system:

$$\frac{\mathrm{d}}{\mathrm{d}t}\rho_i = \sum_{j=1}^{N} J_{ij}\rho_j, \tag{3.39}$$

where the Jacobian matrix possesses the form:

$$J_{ij} = \lambda A_{ij} - \delta_{ij}. \tag{3.40}$$

The trivial solution of Eq. (3.39), ρ_i^*, is stable when all Jacobian's eigenvalues are smaller than zero (see App. C for more details). However, when its LEV is null, the fixed point looses stability. In this regard, we can obtain an epidemic threshold:

$$\lambda_c^{QMF} = \frac{1}{\Lambda^{(1)}}, \tag{3.41}$$

where $\Lambda^{(1)}$ is the largest eigenvalue of A_{ij}. For $\lambda - \lambda_c^{QMF} > 0$ the system is predicted to have a non vanishing prevalence $\rho \equiv \frac{\sum_i I_i}{N} > 0$. From Ref. [62], it is demonstrated that, for PL uncorrelated networks, the adjacency matrix LEV scales as:

$$\Lambda^M \sim \begin{cases} \frac{\langle k^2\rangle}{\langle k\rangle}, & \text{if } \gamma < \frac{5}{2} \\ \sqrt{k_c}, & \text{if } \gamma > \frac{5}{2}, \end{cases} \tag{3.42}$$

thus leading the epidemic threshold to have the scaling form:

$$\lambda_c^{QMF} \sim \begin{cases} \frac{\langle k\rangle}{\langle k^2\rangle}, & \text{if } \gamma < \frac{5}{2} \\ \frac{1}{\sqrt{k_c}}, & \text{if } \gamma > \frac{5}{2}. \end{cases} \tag{3.43}$$

Eq. (3.43) foresees a vanishing threshold $\lambda_c^{QMF} \to 0$ for *any* γ, at odds with results of HMF theory through Eq. (3.34). While the degree based theory predicts a null threshold only on top of PL networks with $\gamma < 3$, QMF theory forecasts a vanishing threshold for any γ in the thermodynamic limit, as long as k_c diverges.

3.8.5 The rDMP theory (recurrent dynamic message-passing)

The SIRS (and SIS) epidemic threshold under *Quenched Mean Field theory* (QMF) theory is dominated by the spectral properties of the adjacency matrix's largest eigenvalue and principal eigenvector [115]. As pointed out in Subsec. 2.7.3 and further discussed in Sec. 3.9, A_{ij}'s PEV may present inflation of a few nodes' component and related centrality due to effect mentioned in Subsec. 2.7.3 [51, 115, 78].

In the case of the SIR model ($\alpha \to 0$), a general theory, embedding generic inter-event time distributions demonstrated exact in tree-like networks (average clustering $\langle C_i \rangle \to 0$) and rendering an upper limit otherwise, in a scheme known as *Message-Passing* - MP [42] formalism. The theory deals with a set of self-consistent integral equations in the quantity $H^{i \leftarrow j}(t)$, accounting for the probability that node j does not infected its neighbor i until time t plus the probability of that j received the disease from its other neighbors too late to infect i in time [42]. The SIR model is one of the simplest epidemic model without active state, but possessing a transition to state in which outbreaks reach a finite fraction of the network [82, 42]. It has been demonstrated to have interesting counterparts in the bond-percolation model [82] and even recently in the modeling of stimulated emission of photons in lasers [116]. Seeking to extend a similar approach to epidemic models with active steady states, like the SIS one, Shrestha *et.al.* developed an approach preserving the non-reinfection condition present in the theory of Karrer and Newman [42], reminiscent of correlations intrinsic to the SIR model. However, in Shrestha's theory the purpose of this condition is aimed at ruling out artifacts present in the QMF theory [41] mentioned in Subsec. 2.7.3. The rDMP equations may be written as:

$$\frac{\mathrm{d}}{\mathrm{d}t}\rho_i = -\rho_i + \lambda s_i \sum_{j=1}^{N} A_{ji}\rho_{j\to i}, \tag{3.44}$$

where $\rho_{j\to i}$ is the probability that node j can transmit an infection (or a *message*) received from its neighbors except i, which is referred to be in the cavity mode [41]. In turn, messages $\rho_{j\to i}$ evolve following:

$$\frac{\mathrm{d}}{\mathrm{d}t}\rho_{j\to i} = -\rho_{j\to i} + \lambda s_j \sum_{k=1}^{N} \left(A_{kj} - \delta_{ki}\right)\rho_{k\to j}, \tag{3.45}$$

and to finish, the probability of i being found recovered at time t, $r_i(t)$, evolves as:

$$\frac{\mathrm{d}}{\mathrm{d}t}r_i = \rho_i - \alpha r_i, \tag{3.46}$$

which, together with the normalization condition represented by $\rho_i + r_i + s_i = 1$, yields a closed set of equations.

Linear stability analysis around the fixed point $\rho_i^* = \rho_{j\to i}^* = r_i^* = 0, s_i^* = 1$ allows

us to write:

$$\frac{\mathrm{d}}{\mathrm{d}t}\rho_{j\to i} = -\mu\rho_{j\to i} + \lambda\sum_{k=1}^{N}\left(A_{kj} - \delta_{ki}\right)\rho_{k\to j} \tag{3.47}$$

$$\frac{\mathrm{d}}{\mathrm{d}t}\rho_{i} = -\mu\rho_{i} + \lambda\sum_{j=1}^{N}A_{ji}\rho_{j\to i}, \tag{3.48}$$

where an index manipulation allows us to write down:

$$\frac{\mathrm{d}}{\mathrm{d}t}\rho_{j\to i} = \sum_{k,l}A_{kl}\left[\lambda\left(1-\delta_{ki}\right)\delta_{jl} - \delta_{kj}\delta_{li}\right]\rho_{k\to l}. \tag{3.49}$$

In Eq. (3.49), we may identify the Jacobian:

$$L_{(j\to i),(k\to l)} = \lambda B_{(j\to i),(k\to l)} - \delta_{jk}\delta_{il}, \tag{3.50}$$

where

$$B_{(j\to i),(k\to l)} = A_{kl}\left(1-\delta_{ki}\right)\delta_{jl} \tag{3.51}$$

is the *Hashimoto Matrix* [41, 79], presented in Subsec. 2.7.4. In Eq. (3.51) has a simple interpretation: it is 1 if ($k\to l, j\to i$ is a non-backtracking path formed by two links ($l = j$ and $k \neq i$) and 0 otherwise (including backtracking paths $k = i$). Another interpretation is also possible, in which $B_{(j\to i),(k\to l)}$ represents the adjacency matrix of a *directed graph* in which nodes in the original graph are replaced by links, which are connected if they are contiguous and non-backtracking [41].

Assuming an irreducible Hashimoto matrix [117, 118, 119] [2], from the Perron-Frobenius theorem we can thus assure its PEV to have only positive entries, and a positive LEV [51]. From this fact, the fixed point looses stability when the Jacobian's LEV, defined in Eq. (3.50), is null, what is equivalent to:

$$\lambda_c = \frac{1}{\Lambda_H^M}. \tag{3.52}$$

Here, Λ_H^M is the LEV of the Hashimoto matrix. With that said, let us recall from Ref. [41] that the SIRS model presents the same epidemic threshold as the SIS in the rDMP theory. In general, one cannot find the LEV analytically, thus having to resource to numerical methods. In this work, we employed the *power method* [120] to achieve this goal. Obtaining the LEV from Eq. (3.51) turns out to be computationally costly, see App. 1.2. This is due to the Hashimoto having $\langle k\rangle N \times \langle k\rangle N$ entries, where $\langle k\rangle$ represents the network's average degree and N is its size. Fortunately, one can compute spectral measures of a $2N \times 2N$ matrix, whose principal eigenvector is related to a PEV related to

[2] i.e. not reducible to the form $\left(\begin{smallmatrix}\hat{X} & \hat{Y}\\ \hat{0} & \hat{Z}\end{smallmatrix}\right)$ by any permutation of indexes, where $\hat{X}$ and $\hat{Y}$ are square, while $\hat{Z}$ and $\hat{0}$ are rectangular matrices, with the addition that $\hat{0}$ is a *null matrix* [75, 117]

the Non-backtracking's PEV. Actually, the first N components of the *Ihara-Bass Matrix* (*IBM*) [79] relate to Hashimoto Matrix by $x_i = \sum_{j=1}^{N} v_{j\to i}$, which has N components instead of $\langle k\rangle N$, where $\langle k\rangle = \frac{1}{N}\sum_{i,j}^{N} A_{ij}$. The matrix Ihara-Bass Matrix is defined as follows:

$$\mathbf{M} = \begin{bmatrix} \mathbf{A} & \mathbf{I}-\mathbf{D} \\ \mathbf{I} & \mathbf{0} \end{bmatrix}. \tag{3.53}$$

In Eq. (3.53), we have $\mathbf{A}$ representing the network's adjacency matrix, while $\mathbf{I}$ represents the $N \times N$ identity, $\mathbf{D} = \delta_{ij}k_i$, with nodes k_i degrees as diagonal entries and $\mathbf{0}$ the $N \times N$ null matrix. From Ihara-Bass determinant formula [79], we can obtain the LEV from the Non-backtracking matrix. In its compact form, the largest eigenvalue of the Hashimoto Matrix is given by [79]:

$$\Lambda_H^M = \frac{\sum_{i,j} A_{ij} v_{j\to i}\,(k_i - 1)}{\sum_{i,j} A_{ij} v_{j\to i}}, \tag{3.54}$$

which, by means of $x_i = \sum_{j=1}^{N} v_{j\to i}$ results in:

$$\Lambda_H^M = \frac{\sum_i x_i\,(k_i - 1)}{\sum_i x_i}. \tag{3.55}$$

This formula represents a useful convergence criteria when utilizing iterative methods to calculate the principal eigenvector of the Ihara-Bass matrix. Another useful expression is obtained in Ref. [79] for UCM networks, in which $v_{j\to i}$ is approximated by:

$$v_{j\to i} \approx k_j - 1, \tag{3.56}$$

which is specially accurate for power-law degree-distributed UCM networks with $\gamma < 3$ [79]. Just like HMF theory, $rDMP$ theory also presents a finite transition threshold in PL networks with $\gamma > 3$ [79].

3.9 Localization

In QMF, which neglects dynamical correlations, while allowing structural ones, the Jacobian LEV together with the *Principal Eigenvector* (PEV) alone dominate critical ($\lambda \gtrsim \lambda_c$) properties if there is a large difference, or *spectral gap*, between $\Lambda^{(1)}$ and $\Lambda^{(2)}$, i.e. the LEV and the second LEV respectively [115], see App. C for more details. Thus, the QMF dynamics stays dominated by its PEV $v_i\left(\Lambda^{(1)}\right)$. Spectral localization can be measured by the Inverse Participation Ratio (IPR), given by:

$$Y_4 = \sum_{i=1}^{N} {v_i}^4, \tag{3.57}$$

assuming that $\sum_{i=1}^{N} v_i^2 = 1$. Corresponding to delocalization, $v_i \sim \frac{1}{\sqrt{N}}$, we have $Y_4 \sim N^{-1}$. This will be the case, for instance, for the adjacency matrix of a *Random Regular*

Network (RRN) (and other homogeneous graphs, lacking outliers), in which the degree distribution is $P(k) = \delta_{k,k'}$ and connections are made randomly. The extreme opposite is the case of *localization*, where just a few components scale as $v_i \sim O(1)$, leading to $Y_4 \sim O(1)$, indicating that only a finite fraction of components of v_i contribute for the bulk of Y_4 [115]. The intermediate case happens when $Y_4 \sim N^{-\beta}$, where $0 < \beta < 1$. This case indicates localization in a sub-extensive graph. In other words, a graph whose size diverges in the thermodynamic limit, but whose ratio relative to the network size goes to zero [121]. Uncorrelated PL networks with $\gamma < \frac{5}{2}$ have a PEV whose components are known to be proportional to the corresponding node degree $v_i \sim k_i$, thus leading to $Y_4 \sim N^{(-\frac{3-\gamma}{2})}$[122]. We should recall that in this regime of networks, the LEV scales as $\frac{\langle k^2\rangle}{\langle k\rangle}$ [123], corresponding to the network subgraph whose LEV dominates [121, 122]. A transition to localized state is predicted to take over when the outlier degree exceeds a certain value, $K > \langle k\rangle\,(\langle k\rangle + 1)$ [83].

Similar reasoning also applies to the NB centrality, with v_i given by $v_i = \sum_{i=1}^{N} A_{ij} v_{j\to i}$. We should recall that this centrality was introduced as a means to avoid self-inflation of outliers [79], but it may still present localization in extreme cases, e.g. for an integrated hub whose degree K satisfies $K \gg (N/\langle k\rangle)^{\frac{1}{2}}$ [79]. Other cases are also reported in Ref. [79].

3.10 Activation mechanisms in the SIS and SIRS models

The SIS ($\alpha \to \infty$) model is one of the simplest epidemic models possessing a transition from an absorbing state to an active state in the thermodynamic limit [94, 111], differently from the SIR ($\alpha = 0$) model, that possesses only transient active states, but transition in which outbreaks span a non-vanishing fraction of a population [82, 74]. In the latter, reinfections are prohibited, while in the former mutual recurrent infections are in the heart of mechanisms sustaining activity [31].

Studies on the role played by structural heterogeneity in PL distributed networks allowed to grasp the importance of hubs in sustaining long term epidemics. A degree-k infectious hub and its vicinity mutually reinfect each other at a rate λ per contact, leading them to possess an expected lifespan $\tau_{k,\lambda} \sim e^{\lambda^2 k}$, see Ref. [30] for more details. In its turn, small world networks present distances between high degree nodes [124, 125, 30], the expected required time for two hubs of degrees k and k' to transmit an infection to each other scales as $\tau^{inf}_{kk'} \sim \left(\frac{N\langle k\rangle}{kk'}\right)^{b(\bar{\lambda})}$, with $b(\bar{\lambda}) \sim \left(\ln\left(\frac{\langle k^2\rangle}{\langle k\rangle} - 1\right)\right)^{-1}$. Here one sees again the effects of the network's heterogeneity coming into play. In both the SIS and SIRS model, extensive numerical simulations show good agreement of the actual mutual infection time realized in PL networks with the aforementioned scaling [30, 29]. Let us recall that the $\gamma < 3$ regime presents diverging degree distribution second moments, thus leading to an infection time $\tau^{inf}_{kk'} \sim O(1)$, while in the complementary $\gamma > 3$ case it scales algebraically.

In the SIS model one sees, for any γ value, a scenario dominated by the most connected spreaders, either in the k-core (see Subsec. 2.7.2) or by the communication among distant hubs, due to exponentially growing lifetimes. In the SIRS model, however, $\tau_k \sim k^{\frac{\alpha}{\mu}}$, leads to a hub communication scenario only in networks with $\frac{5}{2} < \gamma < 3$. By requiring $\tau_k^{rec} \gg \tau_{kk'}^{inf}$ on top of networks with $\gamma > 3$, we would then require $\frac{\alpha}{\mu} > a \ln\left(1 + \frac{\mu}{\lambda}\right)$, where $a \sim O(1)$. Here we clearly see that $\lambda_c(N) \to 0$ in the thermodynamic limit violates the inequality for finite α. So, a decaying of $\lambda_c(N)$ is only possible in finite-size regimes [30], then entering a regime in which it saturates to a finite $\lambda_c(\infty)$ in the thermodynamic limit, triggered by a collective action, not by hubs mutual reinfection [30].

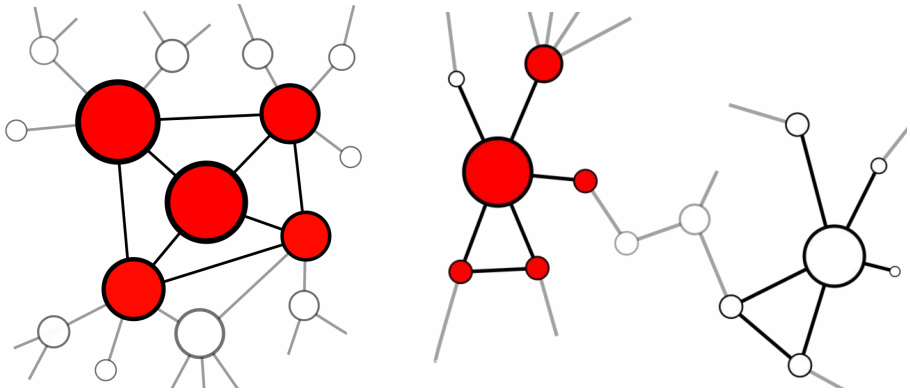

Figura 3.5 – Representation of a dense active k-core (left) and an active sending infection to an inactive hub (right). Active nodes are represented in *red*, while inactive nodes are represented in *white*. Fig. from author, Ref. [126].

We shall discuss our generalization of this phenomenological theory of hub mutual reinfection at distance [49] in Sec. 5.2, in which we develop the lifespan scaling for the SIS and SIRS models with overall non-Markovian infectious times.

3.11 Conclusions of the chapter

In this chapter we outline the main theories employed throughout this work. Mean-field approaches have as common place predicting an effective (usually size dependent) transition to an active state, at the cost of neglecting fluctuations. In addition to that, theories taking heterogeneity into account feature vanishing epidemic thresholds in the asymptotic limit, when PL distributed networks with $\gamma \leq 3$ come into play. However QMF theory presents a null epidemic threshold even in the complementary case of $\gamma > 3$. We shall see in Chap. IV, that adding pairwise correlations to QMF theory keeps this feature [38, 48].

IV Comparison of theoretical approaches in the SIRS model

Related publication:

Comparison of theoretical approaches for epidemic processes with waning immunity in complex networks [48]

José Carlos M. Silva, Diogo H. Silva, Francisco A. Rodrigues, Sílvio C. Ferreira

Physics Review E **106** (2022)

In this chapter we discuss and study the role of waning immunity in epidemic models, in perspective with the accuracy of theoretical frameworks, aiming to an improved forecast. Despite its natural relevance for applications, the $SIRS$ dynamics has attracted much less attention than its SIR and SIS limits and an efficient theoretical approximation for $SIRS$ dynamics on networks remains an open question. In this chapter, the role of immunity is investigated using intermediate values of the waning immunity rate α. We compared extensive stochastic simulations with rDMP and PQMF theories, establishing which theory performs better. In the case of power-law networks, the rDMP theory correctly predicts the epidemic threshold behavior (vanishing or not) at the limit of asymptotically large networks, while the PQMF theory is ruled by localization on a finite set of vertices which leads to a vanishing threshold for $\gamma > 3$, in contrast with stochastic simulations that indicate a finite threshold. However, we also report evidence that the rDMP theory underestimates while PQMF overestimates the epidemic localization leading, respectively, to upper and lower bounds for the epidemic thresholds of the actual $SIRS$ dynamics. Our results indicate that an improved theoretical approach is necessary to accurately describe the critical behavior of the $SIRS$ dynamics on networks. The remainder of this paper is organized as follows. In Sec. 4.1, the theoretical approaches for the SIRS model are presented. The epidemic thresholds obtained with stochastic simulations are compared with the theoretical predictions for different complex networks in Sec. 4.2. Finally, in Sec. 4.3, we present our conclusions and prospects. Two appendices with technical details of the work complement the paper.

4.1 Theoretical approaches for the SIRS model on networks

4.1.1 The pQMF theory (*pair quenched mean-field*) theory

As an improvement over the QMF theory, Sec. 3.8.3, which takes into account the network structure only, but neglects dynamic correlations, we shall now introduce them at the level of pairs [38] to investigate how much of improvement correlations can bring to the

description in the mean-field framework. We shall analyze the pQMF approach in different levels of heterogeneity, together with results found in the literature for homogeneous networks in both the SIS and SIRS models [38, 127]. Our direct purpose now is to describe the evolution of the probability of finding a node i in states I, R and S, with the transitions among theses states being described by the reaction Eqs. (3.8), (3.9) and (3.10).

As in the QMF theory, in the pQMF one, the network structure is encompassed in the theory, but in contrast, dynamical correlations are included in the pairwise level. A pQMF was developed for the SIS model in Ref. [38]. In this work, we shall extend it to the SIRS model. A similar notation shall be used, with a couple of extensions. A node i's state has its state represented by a variable σ_i, which takes the values 0, for susceptible, 1, when infected, or 2, when recovered. We shall define variables to represent marginal probabilities of finding node i in each of the above states: $s_i = [0_i]$, $\rho_i = [1_i]$, $r_i = [2_i]$. We shall also define joint probabilities for a pair (i, j) of nodes being in the possible states $[\sigma_i, \sigma_j]$. For the sake of shortness and following Ref. [38], we define $\phi_{ij} = [0_i, 1_j]$, $\overline{\phi}_{ij} = [1_i, 0_j]$, $\psi_{ij} = [1_i, 1_j]$ and $\omega_{ij} = [0_i, 0_j]$, as in the SIS model. Now we add pairwise states relevant to the SIRS model: $\theta_{ij} = [2_i, 1_j]$, $\chi_{ij} = [2_i, 0_j]$, $\upsilon_{ij} = [2_i, 2_j]$, $\overline{\theta}_{ij} = [1_i, 2_j]$, $\overline{\chi}_{ij} = [0_i, 2_j]$. As constraints of the model, we write the following closure relations, which tie together marginal and joint probabilities:

$$\begin{aligned} s_i &= \omega_{ij} + \overline{\chi}_{ij} + \phi_{ij}, \\ \rho_i &= \psi_{ij} + \overline{\phi}_{ij} + \overline{\theta}_{ij}, \\ r_i &= \upsilon_{ij} + \theta_{ij} + \chi_{ij}. \end{aligned} \tag{4.1}$$

Now, we write gain-loss equations that define the temporal evolution of the probability of a node i being infected and recovered:

$$\frac{d\rho_i}{dt} = -\mu\rho_i + \lambda \sum_j A_{ij}\phi_{ij}, \tag{4.2}$$

and

$$\frac{dr_i}{dt} = -\alpha r_i + \mu\rho_i, \tag{4.3}$$

respectively. The first term (loss) in Eq. (4.2) represents recovery of an infected node, while the second term states for infection (gain). Similarly, the first term of (4.3) represents waning of immunity (loss), while the second term represents recovery (gain). In Eq. (4.2), the network structure is represented by the adjacency matrix, given by $A_{ij} = 1$ whenever i and j are connected and $A_{ij} = 0$, otherwise. For the sake of normalization, a node i is found susceptible with probability $s_i = 1 - \rho_i - r_i$. Deaths and births are not considered in our model [38]. We recover QMF theory if consider neighbors states to be

independent, $\phi_{ij} \approx s_i \rho_i$, as follows:

$$\frac{d\rho_i}{dt} = -\mu\rho_i + \lambda s_i \sum_j A_{ij}\rho_j. \tag{4.4}$$

With this remark made, we come back to the development of Eqs. (4.2) and (4.3), which cannot be solved yet, since we still do not have equations for the joint probability ϕ_{ij} of connected nodes ($A_{ij} = 1$) being together in the infected and susceptible states. To accomplish this task, we write:

$$\begin{aligned}\frac{d\phi_{ij}}{dt} &= -(\mu+\lambda)\phi_{ij} + \alpha\theta_{ij} + \lambda\sum_{l\neq i}[0_i, 0_j, 1_l]A_{lj} \\ &\quad -\lambda\sum_{l\neq j}[1_l, 0_i, 1_j]A_{li}.\end{aligned} \tag{4.5}$$

Similarly to the interpretations of Eqs. (4.2) and (4.3), terms of Eq. (4.5) represent loss and gain from state ϕ_{ij}. The first contribution (loss) states for both internal infection $j \to i$, with rate λ, and recovery of the infectious node j, with rate μ. The second term (gain) accounts for spontaneous waning of immunity of node i, with neighbor j in the infected state. The last two terms account for the infection of node j by a neighbor $l \neq i$, with i also susceptible, and infection of node i by an infected neighbor $l \neq j$, while j is already infected. We can write down equations involving the other states:

$$\frac{d\theta_{ij}}{dt} = \mu\psi_{ij} - (\alpha+\mu)\theta_{ij} + \lambda\sum_{l\neq i}[2_i, 0_j, 1_l]A_{lj}, \tag{4.6}$$

$$\frac{d\chi_{ij}}{dt} = \mu\overline{\phi}_{ij} - \alpha\chi_{ij} + \alpha\upsilon_{ij} - \lambda\sum_{l\neq i}[2_i, 0_j, 1_l]A_{lj}. \tag{4.7}$$

Worth noting that the dynamical equations for $\overline{\phi}_{ij} = \phi_{ji}$, $\overline{\chi}_{ij} = \chi_{ji}$, and $\overline{\theta}_{ij} = \theta_{ji}$ are easily obtained if one switches i and j in Eqs. (4.5), (4.6) and (4.7). To finish, equations for the remaining ω_{ij}, ψ_{ij} and υ_{ij} are yielded from the ones already obtained by evoking the closure relations found in Eqs. (4.1). If we do not stop here, the hierarchy of equations will scale up the number of relations even further. So, we need a pair approximation to close the system [128]. So, we use the approximation [38]:

$$[A_iB_jC_k] \approx \frac{[A_iB_j][B_jC_k]}{[B_j]}. \tag{4.8}$$

Now we obtain a closed set of equations, by gathering Eqs. (4.1), (4.2) and (4.3) [48] together with:

$$\begin{aligned}\frac{d\phi_{ij}}{dt} &= -(\mu+\lambda)\phi_{ij} + \alpha\theta_{ij} + \lambda\sum_{l\neq i}\frac{\omega_{ij}\phi_{jl}}{s_j}A_{lj} \\ &\quad -\lambda\sum_{l\neq j}\frac{\phi_{ij}\phi_{il}}{s_i}A_{li},\end{aligned} \tag{4.9}$$

$$\frac{d\theta_{ij}}{dt} = \mu\psi_{ij} - (\alpha+\mu)\theta_{ij} + \lambda\sum_{l\neq i}\frac{\chi_{ij}\phi_{jl}}{s_j}A_{lj}, \tag{4.10}$$

and

$$\frac{d\chi_{ij}}{dt} = \mu\bar{\phi}_{ij} - \alpha\chi_{ij} + \alpha\upsilon_{ij} - \lambda\sum_{l\neq i}\frac{\chi_{ij}\phi_{jl}}{s_j}. \tag{4.11}$$

4.1.2 Perturbative analysis of pQMF theory

From Eqs. (4.2), (4.3), (4.9), (4.10) and (4.11), we can identify the trivial fixed point represented by $\rho*_i = r*_i = 0$, $\phi*_{ij} = \psi*_{ij} = \theta*_{ij} = \chi*_{ij} = \eta*_{ij} = 0$ and $s*_i = \omega*_{ij} = 1$. Recall that η_{ij} and ψ_{ij} can be solved for the other variables by means of the closure relations (4.1) [48].

Now we can state that, for values of λ below a certain value λ_c, this fixed point is stable [38, 48, 61], while for $\lambda > \lambda_c$, this assumption no longer holds, with non-trivial stable fixed points taking over. We shall investigate this condition thoroughly by means of linear stability analysis.

Assuming that for values of the control parameter $\lambda \gtrsim \lambda_c$, with λ_c still to be determined, $\rho_i \ll 1$ holds true for long times. Consequently, other variables related to infected and recovered must also be equally small (r_i, ψ_{ij}, ϕ_{ij}, ...). As a consequence, $s_i \approx \omega_{ij} \approx 1$. Applying these assumptions to the dynamic Eqs. (4.2), (4.3), (4.9), (4.11) and (4.10), together with algebraic manipulations we are in place to obtain the approximation:

$$\phi_{ij} \approx \Upsilon\rho_j - \Xi\rho_i, \tag{4.12}$$

where the epidemic transition rates are grouped as:

$$\Upsilon(\mu,\lambda,\alpha) = \frac{2\mu(\mu+\lambda+\alpha)+\lambda\alpha}{2\lambda(\mu+\alpha)+2\mu(\mu+\lambda+\alpha)} \tag{4.13}$$

and

$$\Xi(\mu,\lambda,\alpha) = \frac{\lambda(\alpha+2\mu)}{2\lambda(\alpha+\mu)+2\mu(\mu+\lambda+\alpha)}. \tag{4.14}$$

Now, employing a quasi-static approximation, i.e., assuming that for $t \gg 1$ $\frac{d}{dt}\rho_i \simeq 1$, we can insert Eq.(4.12) into Eq. (4.2), thus obtaining a linear equation, whose Jacobian

matrix is given by:

$$L_{ij} = -\left[\mu + \lambda k_j \Xi(\mu, \lambda, \alpha)\right] \delta_{ij} + \lambda \Upsilon(\mu, \lambda, \alpha) A_{ij}. \tag{4.15}$$

Here, δ_{ij} states for the Kronecker delta, taking value 1 when $i = j$ and 0 otherwise. Proceeding with a linear stability analysis, the trivial fixed point becomes unstable and an active steady state ($\rho > 0$) emerges, as long as the LEV of L_{ij} is null. This condition enables obtaining the *effective* epidemic threshold $\lambda_C(N, \alpha)$ under pQMF theory. Moreover, one can obtain the SIS Jacobian, obtained in Ref. [38], from Eq. (4.15) by taking the limit $\alpha \to \infty$.

We shall now analyze some special graphs in order to understand the predictions yielded by Eqs. (4.15).

4.1.2.1 pQMF theory of the *star graph*

We shall now apply Eq. (4.15) to a star graph, which is defined as a center node $l = 0$ connected to K_0 leaves, labeled $m = 1, 2, 3...K_0$, and possessing degree $k_m = 1$. The connections in this graph are represented in the adjacency as $A_{0m} = 1$ (star connected to each one of the K_0 leaves), $A_{m0} = 1$ (each leaf connected to the star) and $A_{mm'} = 0$ (no connection among the leaves). To obtain the Jacobian LEV, we apply the just defined adjacency matrix A_{ij} to Eq. (4.15) and solve the corresponding eigenvalue problem. We constraint the LEV found to be null, from which we obtain the epidemic threshold, implicitly defined through the relation:

$$\left(\frac{\lambda_c}{\mu}\right)^2 N[\Xi_c^2 - \Upsilon_c^2] + \frac{\lambda_c}{\mu}\Xi_c(K+1) + 1 = 0, \tag{4.16}$$

from which one recognizes Ξ_c and Υ_c as given by Eqs (4.14) and (4.13) at $\lambda = \lambda_c$. Inserting their values, in terms of the epidemic parameters, into Eq. (4.16) and applying the asymptotic limit $K \gg 1$, one obtains:

$$\frac{\lambda_c}{\mu} \simeq \sqrt{\frac{2\,(\alpha + \mu)}{\alpha K}} \tag{4.17}$$

By making $\alpha \gg \mu$, we recover the expression found in Ref. [38] for the SIS model: $\lambda_c/\mu \simeq \sqrt{2/K}$. Another interesting limit is found when $\alpha \ll \mu$, thus yielding the epidemic threshold:

$$\frac{\lambda_c}{\mu} \simeq \sqrt{\frac{2\mu}{\alpha K}}. \tag{4.18}$$

Summarizing, the pQMF theory predicts the epidemic threshold to vanish, regardless of how small the waning immunity rate α, as long as it is non-zero. Although appealing, this result disagrees with the stochastic theory presented in Ref. [30] and rigorous analysis of Refs. [129, 130], which point out for an epidemic lifespan increasing

algebraically with the graph size $\tau_k \sim k^{\alpha/\mu}$ instead of exponentially. Extensive numerical simulations found in Ref. [49] also support this conclusion.

4.1.2.2 pQMF predictions for RR networks

RR networks represent the most homogeneous case of degree distributions, in which all nodes present the same degree m, i.e. $P(k) = \delta_{k,m}$, with connections made randomly. By direct checking $v_i = 1$ as an eigenvector of Eq. (4.15), we end up with the eigenvalue:

$$\Lambda = (\mu + \lambda m \Xi) + \lambda m \Upsilon. \tag{4.19}$$

Perron-Frobenius theorem (see App. 1.1) allows us to assert that the ansatz solution $\mathbf{v} = \mathbf{1}$ is the Jacobian's PEV, since each of $v_i > 0$ and A_{ij} is an irreducible non-negative matrix (strongly connected graph). The epidemic threshold is obtained when $\Lambda = 0$:

$$\lambda_c = \frac{\mu(\mu + \alpha)}{(m-1)(\mu + \alpha) - \mu}, \tag{4.20}$$

in agreement with the homogeneous pair approximation for SIRS dynamics found in Ref. [127]. Epidemic thresholds for the SIS and SIR models are obtained by applying the limits $\alpha \gg \mu$ and $\alpha \ll \mu$, respectively, thus yielding $\lambda_c^{\mathrm{SIS}} = \mu/(m-1)$ [38] and $\lambda_c^{\mathrm{SIR}} = \mu/(m-2)$ [82].

4.1.3 The rDMP theory

In the rDMP approach [41], an infectious node that was infected by a given neighbor can not reinfect him or herself, which can be encoded by a *message* variable $\rho_{j\to i}$ defined as the probability that an infectious node j was infected by any of its neighbors except node i, such that node j can infect i, but cannot infect the node which transmitted the contagion to j. Assuming a mean-field hypothesis that neglects nearest-neighbor dynamical correlations, this variable evolves as [41]:

$$\frac{d\rho_{j\to i}}{dt} = -\mu\rho_{j\to i} + \lambda s_j \sum_{k\neq i} \rho_{k\to j} A_{jk}. \tag{4.21}$$

The remaining compartments of the SIRS dynamics are given by [41]:

$$\frac{d\rho_i}{dt} = -\mu\rho_i + \lambda s_i \sum_j \rho_{j\to i}, \tag{4.22}$$

$$\frac{dr_i}{dt} = -\alpha r_i + \mu\rho_i, \tag{4.23}$$

and $s_i + r_i + \rho_i = 1$. Performing again a quasi-static approximation with $\frac{dr_i}{dt} \approx 0$ and linearizing the rDMP equations around the absorbing state $\rho^*_{j\to i} = 0 = \rho^*_j$, we obtain the

Jacobian matrix

$$J_{j\to i,k\to l} = -\mu\delta_{kj}\delta_{il} + \lambda B_{j\to i,k\to l} \tag{4.24}$$

in which,

$$B_{j\to i,k\to l} = \delta_{jl}(1-\delta_{ik}) \tag{4.25}$$

is the non-backtracking or Hashimoto matrix [131, 132]. The epidemic threshold is then given by the inverse of the LEV of the Hashimoto matrix [41].

4.1.3.1 Particular case: Star graph

Exploiting the definition of a message from j to i, $\rho_{j\to i}$, if $j > 0$ is a leaf, it would be infected only by the center such that $\rho_{j\to 0} = 0$. Thus, Eq. (4.21) with $j = 0$ becomes

$$\frac{d\rho_{0\to i}}{dt} = -\mu\rho_{0\to i} + \lambda s_0 \sum_{k=i}^{K} \rho_{k\to 0} = -\mu\rho_{0\to i}, \tag{4.26}$$

implying in exponential decay with time, independently of infection rate and that rDMP does not predict an active phase for the SIRS model in a star graph as well as it does not for the SIS dynamics, in odds with both the algebraic and exponential increases of SIRS [30, 129] and SIS [29, 45] models, respectively.

4.1.3.2 Particular case: RR networks

For homogeneous networks we have that $\rho_{j\to i} = \eta$ and Eq. (4.21) becomes

$$\frac{d\eta}{dt} = -\mu\eta + \lambda s(m-1)\eta, \tag{4.27}$$

that provides the epidemic threshold

$$\lambda_c = \frac{\mu}{m-1} \tag{4.28}$$

and corresponds to the same result of the SIS model and, within the rDMP approach, is independent of the rate of waning immunity.

4.2 Theory versus simulation

To compare the performance of theoretical frameworks, we performed stochastic simulations of the SIRS model following the Gillespie algorithm described in App. B. We deal with absorbing state using the QS method [98, 133] explained in Appendix B. The epidemic threshold is determined using the infection rate corresponding to the largest value of the dynamical susceptibility defined as $\chi = N(\langle\rho^2\rangle - \langle\rho\rangle^2)/\langle\rho\rangle$ [47], as discussed in Sec. 3.6, where the averages are computed in the QS regime (see Sec. 3.5). We investigate

the rate of waning immunity $\alpha \leq \mu$, which corresponds to a time of conferred immunity longer than that of infectiousness.

Considering star graphs, we have shown that PQMF theory predicts an active state while rDMP does not. Indeed, a stochastic approximation and numerical simulations for SIRS dynamics on a star of size $k+1$ leads to an algebraic increase of the epidemic lifespan given by $\tau_k \sim k^{\alpha/\mu}$ [134] in contrast with the exponential law $\tau_k \sim \exp(-\lambda^2 k/\mu^2)$ of the SIS dynamics [29]. However, this metastable activity in star graphs can introduce localization effects on hubs within the networks. Recalling Sec. 3.9, localization can be investigated by computing the scaling of the inverse participation ratio (IPR) associated with the PEV of the Jacobian corresponding to the mean-field theory under study. The relevant Jacobians in this work are the adjacency matrix A_{ij} for QMF [115], Hashimoto matrix $B_{j\to,k\to l}$ for rDMP [79] and Eq. (4.15) for PQMF [39]. If $\{v_j^{(1)}\}$ are the N_c components of the normalized PEV, the IPR is defined as [115]:

$$Y_4 = \sum_{j=1}^{N_c} \left[v_j^{(1)}\right]^4. \tag{4.29}$$

Also in Sec. 3.9, we discussed the expected scaling of the IPR. The localization analysis debated there can be extended to stochastic simulations by means of the normalized activity vector (NAV) $\{v_i\}$ [78] defined in terms of the probability that a node is active (infected) ρ_i as:

$$v_i = \frac{\rho_i}{\sqrt{\sum_{j=1}^{N} \rho_j^2}}, \tag{4.30}$$

and the corresponding IPR can be calculated by replacing the PEV with the NAV components in Eq. (4.29).

4.2.1 RR networks without and with an outlier

We start with RR networks since, in principle, these networks present no relevant localization effects. In the thermodynamic limit, the epidemic threshold converges to a finite value as predicted by all theoretical frameworks, for all values of α studied. The PQMF theory significantly outperforms both QMF and rDMP in determining the epidemic threshold in comparison with stochastic simulations, as shown in Fig. 4.1 for $\alpha/\mu = 0.2$. This result holds for other values of α/μ. The partial reckoning of dynamical correlation in rDMP leads to an improvement of the QMF theory, but still substantially below the accuracy of the PQMF theory. The results shown in Fig. 4.1 correspond to a degree $m = 6$. The relative accuracy of all theories is reduced for lower degrees, and the relative improvement of the PQMF with respect to the other theories is increased.

We tackle the effects of localization by introducing a single hub with fixed degree $k = 10^3$ in an RR network where all the remaining $N - 1$ nodes have degree $m = 6$. In the SIS model two activation processes, expressed as a double peak at susceptibility

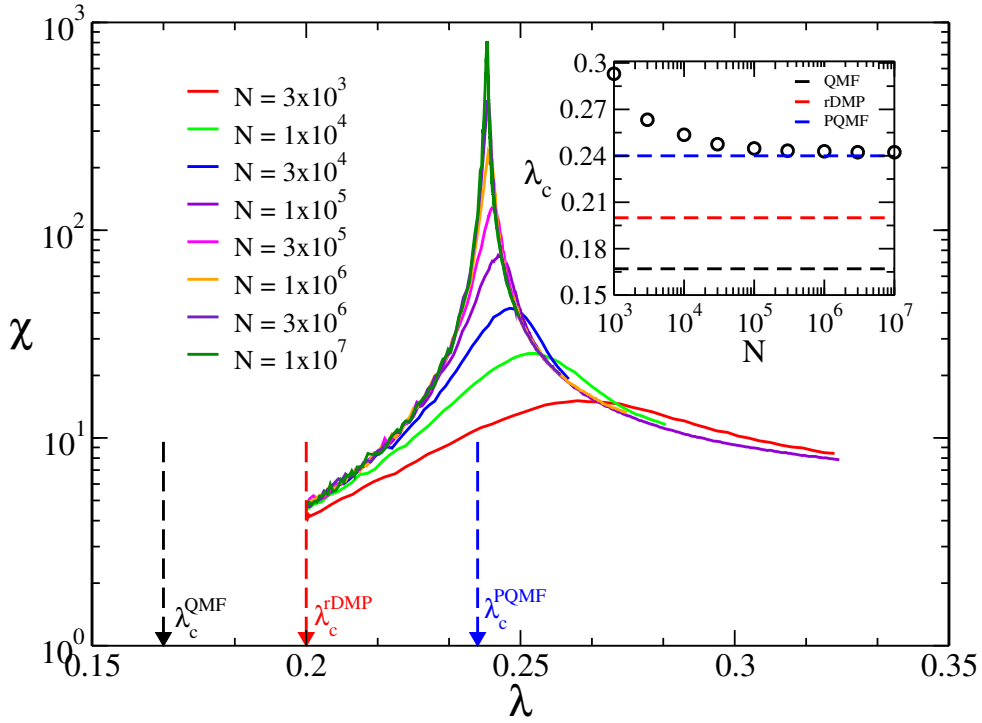

Figura 4.1 – Susceptibility as a function of λ for RR networks with $m = 6$ and different sizes indicated in the legend. Black, red, and blue dashed arrows correspond to QMF, rDMP, and PQMF predictions of the epidemic threshold, respectively. Inset compares the epidemic threshold as a function of the network size in simulations (symbols) and mean-field theories (dashed lines)

curves [47], take place: one belonging to the subgraph composed of the hub, plus its nearest neighbors, and another belonging to the rest of the network, coinciding with the epidemic threshold of the pure RR network [78]. The multiple activations are not detected in quasistationary simulations of the SIRS dynamics with $\alpha/\mu \leq 1$. The top panels of Fig. 4.2 present the estimated epidemic thresholds as functions of the network size for three values of α/μ considering QS simulation, PQMF, and rDMP mean-field theories. The corresponding thresholds for a pure RR network are also presented. Since the hub size is fixed, epidemic thresholds of QS simulations converge to the value obtained in the pure RR network in the thermodynamic limit. However, localization remains relevant in finite-size systems, altering the convergence to the asymptotic limit: While the pure RR presents a monotonic decay towards the asymptotic value, the presence of the hub lowers the threshold and inverts the finite-size dependence. In contrast with the pure RR networks shown in Fig. 4.1, the PQMF theory deviates significantly from the simulation outcomes, the more for the higher rate of waning immunity, thus being outperformed by rDMP.

The localization associated with the mean-field theories and simulations characterized with the IPR of the Jacobians PEV and NAV at the threshold, respectively, are shown in Figs. 4.2(d,e,f). The PQMF theory presents a finite IPR due to the localization in the hub, while the NAV obtained in simulation becomes delocalized as the network

size increases. Notice, however, that the IPR decays slower with size than predicted by the Jacobian of PEV (Hashimoto matrix) in the rDMP theory, being differences more evident for larger α, showing that the actual stochastic dynamics is more localized than that of the rDMP. Indeed, the PEV of the Hashimoto matrix for the RR network with an integrated hub is localized only if $K \gg (N/\langle n \rangle)^{1/2}$ [135].

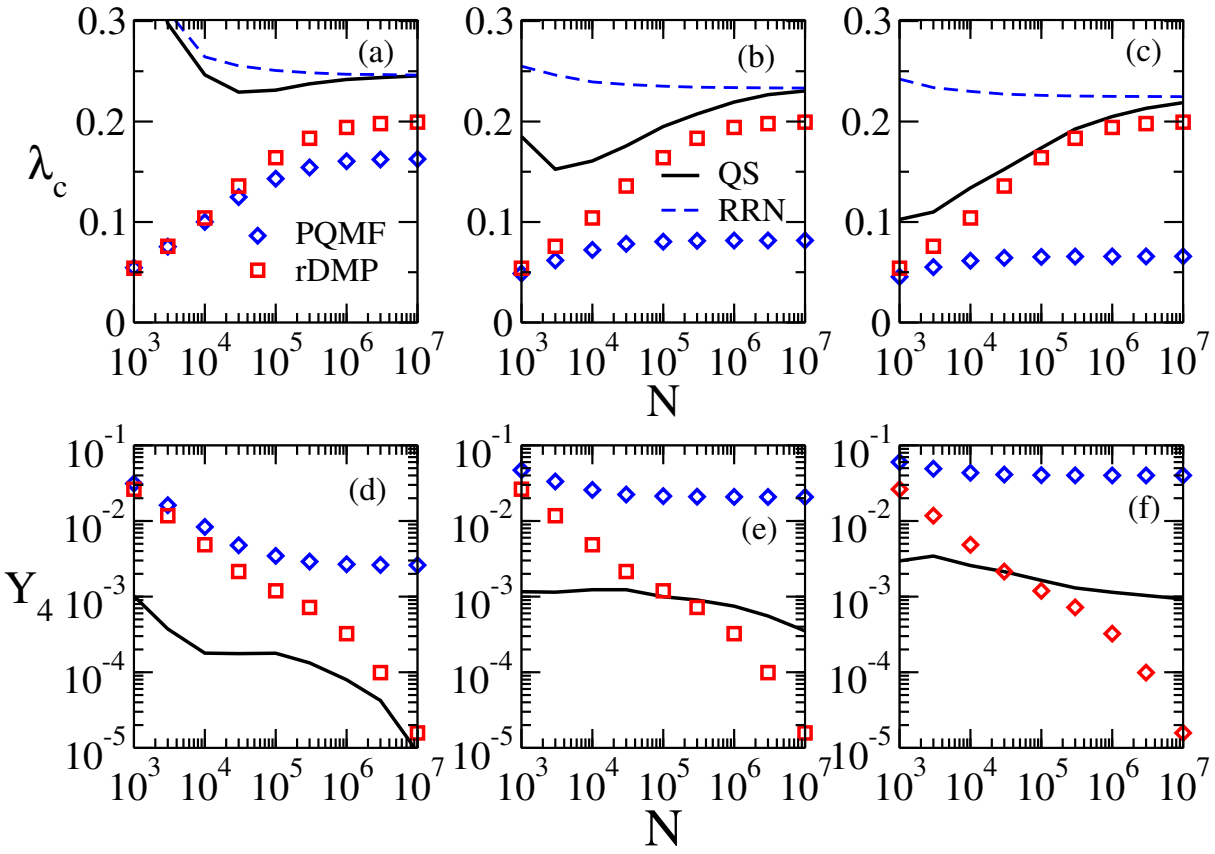

Figura 4.2 – (a,b,c) Epidemic threshold and (d,e,f) IPR as functions of the network size for the mean-field theories and simulations of the SIRS model with (a,d) $\alpha/\mu = 0.1$, (b,e) 0.5 and (c,f) 1.0. The system is an RR network with $m = 6$ plus a single vertex of fixed size $k = 10^3$. The threshold for a pure RR network is also shown for the sake of comparison.

4.2.2 Power-law networks

We investigated SIRS dynamics on synthetic uncorrelated networks presenting a power-law degree distribution, $P(k) \sim k^{-\gamma}$, generated through the UCM model [136] with a structural cutoff $k_c = 2\sqrt{N}$. The threshold and IPR analyses for power-law networks with $\gamma < 5/2$ are presented in Fig. 4.3. For all investigated values of α, the same behavior is observed: the epidemic threshold goes to zero in simulations as well as PQMF and rDMP theories, the last two being indistinguishable from each other in the presented scales. Simulations asymptotically agree with mean-field theories, being the convergence faster for higher waning of immunity rates. The localization analyses indicate the agreement between simulations and mean-field theories, whose IPR scales consistently

with an epidemic localization in the maximum K-core, as conjectured for SIRS dynamics in this range of degree exponent γ [30]. The maximum K-core is a strongly connected subgraph [137] obtained by means of a K-core decomposition, discussed in Sec. 2.7.2. Thus, our results for SIRS support that the outbreak is triggered as does the SIS dynamics for $\gamma < 2/5$ [31].

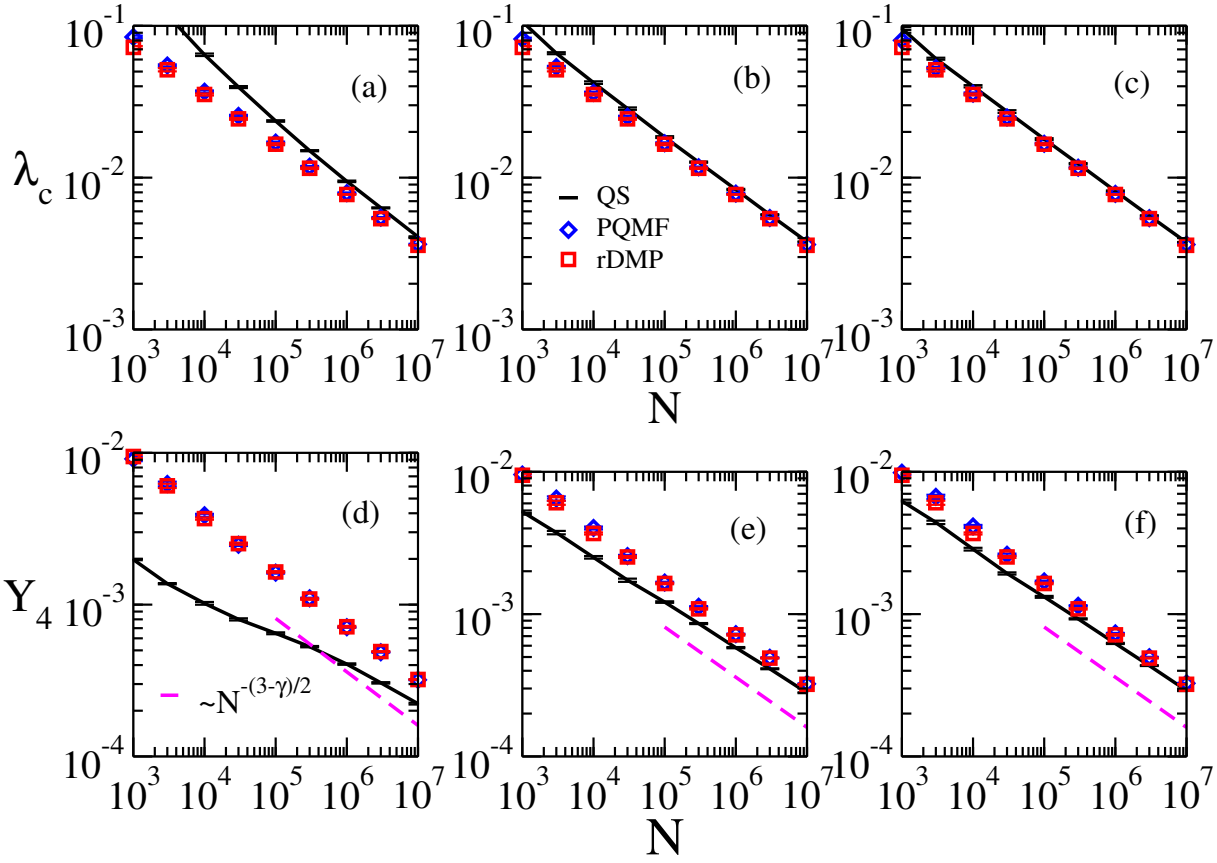

Figura 4.3 – (a,b,c) Epidemic threshold and (d,e,f) IPR as functions of the network size for the SIRS dynamics on UCM networks with $\gamma = 2.3$ using (a,d) $\alpha/\mu = 0.1$, (b,e) 0.5 and (c,f) 1.0. Stochastic simulations (black line) are compared to PQMF (blue diamonds) and rDMP (red squares). The dashed line is a guide to eyes indicating the scaling $Y_4 \sim N^{(3-\gamma)/2}$, expected for IPR of vector localized in maximum K-core [121].

For $\gamma > 5/2$, the PEV of the PQMFs Jacobian is localized in the largest hub and its neighbors [39], as does the adjacency matrix [121], differently from the Hashimoto matrix whose PEV $v_i \sim \sum_j A_{ij}(k_j - 1)$ [135] leads to a different type of localization. In both cases the respective LEVs diverge for $5/2 < \gamma < 3$, but following different scaling laws. When $\gamma > 3$, the LEV of the PQMFs Jacobian still diverges in the thermodynamic limit [38] and remains finite for the Hashimoto matrix [135]. Thus, rDMP and PQMF theories predict, respectively, finite and null epidemic thresholds for $\gamma > 3$. For this reason, we analyze the case $\gamma = 3.5$ where differences are more noticeable.

The finite-size scaling of the epidemic threshold of stochastic simulations depends on the rate of waning of immunity while the asymptotic threshold decreases only slightly

with α, as shown at the top panels of Fig. 4.4. In the range of network sizes investigated (up to $N = 10^7$), the epidemic threshold seems to converge to a finite value, which is qualitatively described by rDMP theory. The PEV associated with the PQMFs Jacobian matrix is strongly localized in some nodes represented by an asymptotically finite IPR, the stronger for larger α. Conversely, the PEV of the Hashimoto matrix does not depend on α, being localized in a subextensive fraction of nodes manifested as a scaling law $Y_4 \sim N^{-a}$, with $a < 1$. Stochastic simulations present a localization pattern that depends on α, becoming slightly more localized as the immunity time $1/\alpha$ decreases. The PQMF is clearly outperformed by the rDMP theory. However, simulations indicate that rDMP theory yields an epidemic activity less localized than the actual simulations and overestimate the asymptotic epidemic threshold, more evident for larger α.

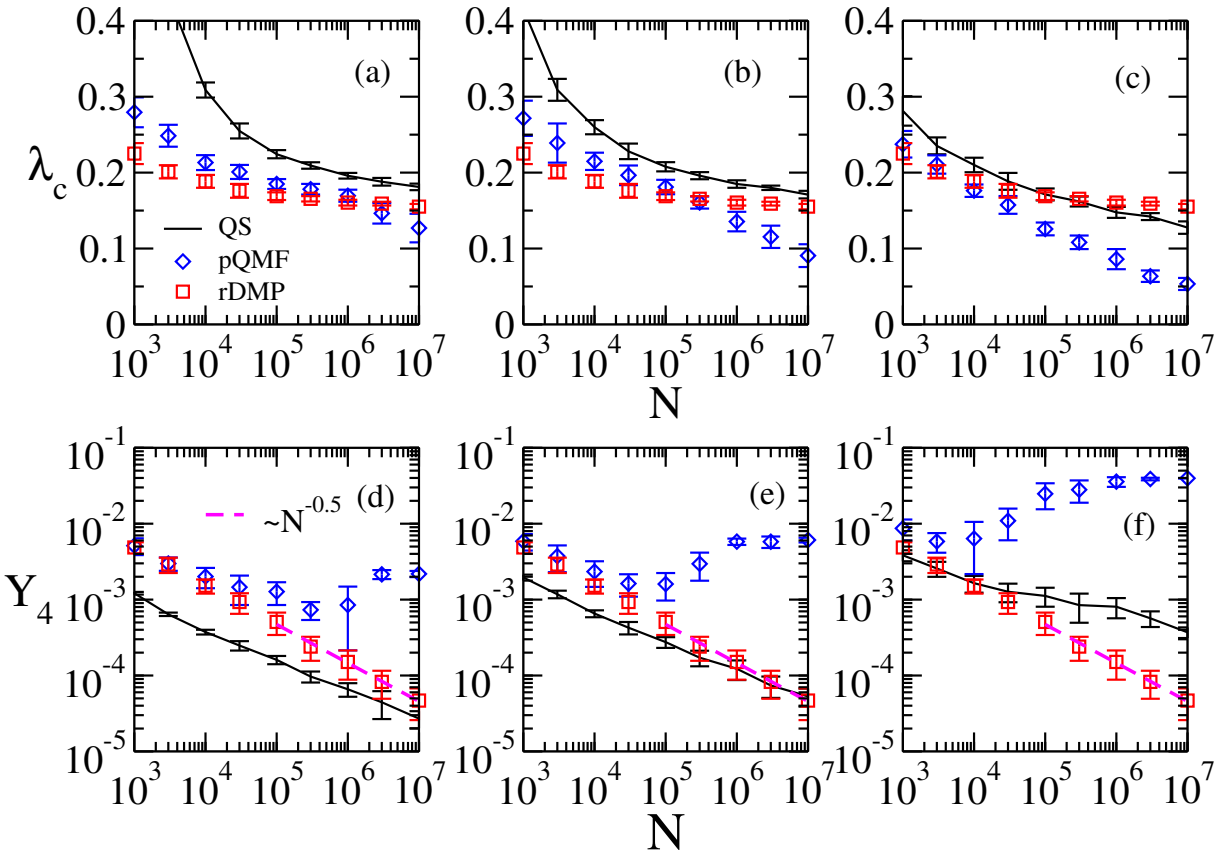

Figura 4.4 – (a,b,c) Epidemic threshold and (d,e,f) IPR as functions of the network size for a SIRS dynamics on UCM networks with $\gamma = 3.5$ using (a,d) $\alpha = 0.1$, (b,e) 0.5, and (c,f) 1.0. Stochastic simulations (black line) are compared to PQMF (blue diamonds) and rDMP (red squares).

4.3 Conclusions

In some aspects, the $SIRS$ presents similarities to the SIS model (existence of an active steady state and universality class in regular lattices [138, 127]), while others resemble the SIR dynamics (the finite epidemic threshold for degree exponent $\gamma > 3$ and activation mechanism in complex networks [30]). The present chapter investigated the SIRS model within two theoretical frameworks, namely rDMP or PQMF theories, and stochastic simulations. Both theories present pairwise correlations, while rDMP does not permit backtracking reinfection, while PQMF does. We tackle the problem of which mean-field theory more accurately reproduces the epidemic threshold and epidemic localization patterns of the SIRS dynamics on different types of complex networks. Homogeneous degree distributed networks, with no relevant localization present, presented a better performance of pQMF over rDMP theory. The introduction of a single node of a large degree, not scaling with network size, however, promotes strong localization effects, with PQMF performance becoming worse. On star graphs, the rDMP for SIRS dynamics predicts a finite epidemic lifespan for stars of any size, at odds with PQMF theory, which predicts an exponentially long lifespan. The algebraic increase with the star size reported in Ref. [30] is not predicted by any of both theories, showing that they either under or overestimate, respectively, the localization of the epidemic activity around hubs in the networks, with stochastic simulations on power-law networks confirming this conjecture. A finite epidemic threshold can be observed in simulations of the SIRS dynamics on networks with $\gamma > 3$, in qualitative agreement with rDMP theory and contrasting with the vanishing epidemic predicted by the pQMF theory. Localization analysis, however, also hints that rDMP theory underestimates the actual epidemic localization observed in simulations, which occur in a subextensive fraction of the network asymptotically much smaller than the subset corresponding to the localization of the PEV of the Hashimoto matrix predicted by the rDMP theory.

Our results call for a modification of the rDMP theory, lifting the strict prohibition of backtracking reinfection. This aims to be in consonance with the occurrence of non-backtracking only in typical periods $\tau \sim 1/\mu + 1/\alpha$, reckoning to the combination of infection plus immunity periods, for predicting with higher accuracy both the localization and the epidemic thresholds of SIRS dynamics in networks.

V Consequences of multiple infectious stages in recurrent epidemic models

Related publication:

Consequences of non-Markovian healing processes on epidemic models with recurrent infection on networks [49]

José Carlos M. Silva, Diogo H. Silva, Francisco A. Rodrigues, Sílvio C. Ferreira

New Journal of Physics **27** (2025)

In this chapter, we investigate the $SIRS$ epidemic model with η statistically identical infectious stages, hereafter called $SI_\eta RS$, on star graphs composed of a center and k leaves, mimicking isolated hubs in networks. We employed a modified version of discrete-time dynamics for $SIRS$ on star graphs proposed by Ferreira et al. [30] (see also Boguñá et al. [29] for the theory of the SIS model). We derived an approximate analytical expression for the epidemic lifespan, considering an average healing time of $1/\mu$ and a small infection rate $\lambda \ll \mu$. The analytical expression yields an epidemic lifetime $\langle \tau_k \rangle \sim k^{\frac{\alpha}{\eta\mu}}$ for finite α, along with logarithmic corrections. In particular, for finite α and $\eta \to \infty$ (i.e., a deterministic recovery period), this lifetime is finite. Stochastic simulations in which a hub is modeled as an isolated star graph support the analytical result for finite α, but the theory does not capture the dependence with η in the limit of instantaneous waning immunity, which corresponds to the SIS model. We also investigated the transition from an epidemic-free to an endemic state of the $SI_\eta RS$ model on different networks. Despite the remarkable differences in the epidemic lifespan of isolated hubs as the number of infectious states increases, stochastic simulations on power-law networks with sizes up to 10^7 nodes lead only to a reduction in epidemic localization and a displacement of the epidemic threshold for $\gamma > 3$, with no significant difference observed for scale-free networks with $\gamma < 3$. For the case of random regular (RR) networks with $P(k) = \delta_{k,6}$, a reduction in the epidemic threshold is reported. Therefore, the alterations in the activity lifespan on isolated hubs for non-Markovian dynamics are not sufficient to change the activation mechanisms of the Markovian $SIRS$ dynamics on networks. The remainder of this chapter is organized as follows. In Sec. 5.1, the model is described, highlighting some consequences of the η stages on the recovery time distribution. In Sec. 4.1, the average lifetime feedback mechanism and the hub's mutual infection time are analytically determined, grounded in the theoretical framework of Refs. [139, 29, 30], and compared with (statistically exact) stochastic simulations. The critical $SI_\eta RS$ dynamics is investigated on power-law networks using stochastic simulations in Sec. 5.3, while our conclusions and prospects are summarized in Sec. 5.4. Three appendices with simulation and analytical

technical details complement the chapter.

5.1 The $SI_\eta RS$ Model

The $SI_\eta RS$ model is an extension of the usual $SIRS$, incorporating η sequential infectious stages I_1, I_2, ..., I_η, as shown in Fig. 5.1(a). An infected individual goes through each stage before recovery, whose transition rates between any pair j and $j+1$ (for $j < \eta$) are assumed time-independent and given by μ_j. The transition from $j = \eta$ to the recovered state R occurs at rate μ_η. An agent in the infective states $j = 1, \ldots, \eta$ transmits the disease to a susceptible contact at constant rates $\lambda_1, \ldots, \lambda_\eta$, respectively, as depicted in Fig. 5.1(b). Once infected, a node starts in stage $\eta = 1$. A recovered individual returns to the susceptible state at rate α, as shown in Fig. 5.1(c). For the sake of simplicity, we will consider the same infection and recovery rates for all stages: $\lambda_j = \lambda$ and $\mu_j = \mu\eta$. This choice is suitable for comparing different values of the number of infectious compartments, as the average recovery time is given by $\langle\tau\rangle = 1/\mu$, irrespective of η. The $SI_\eta RS$ dynamics includes the particular cases of $SI_\eta R$ and $SI_\eta S$ models with η infectious stages when $\alpha \to 0$ and $\alpha \to \infty$, respectively.

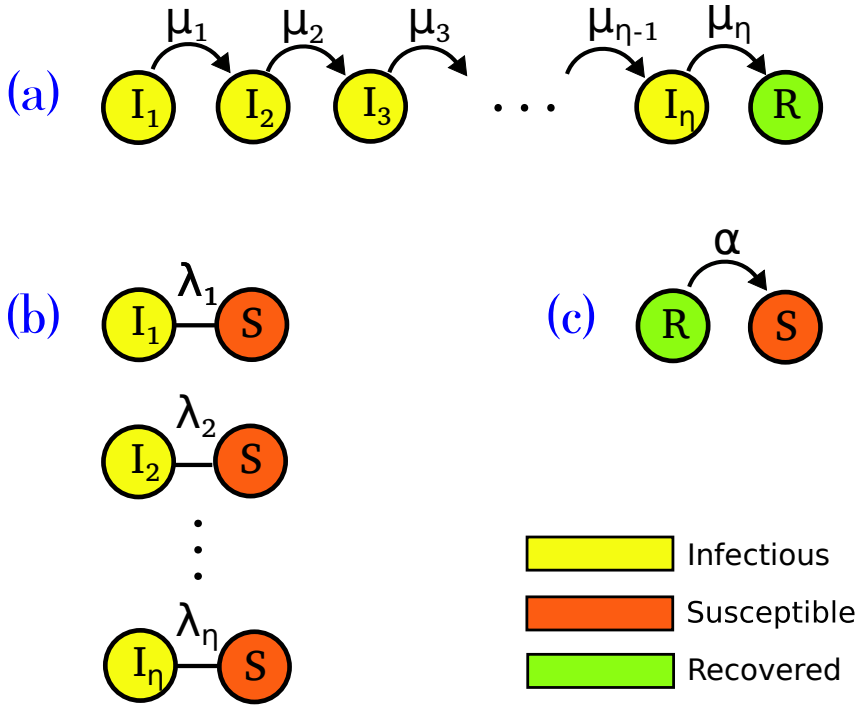

Figura 5.1 – Schematic representation of (a) infectious state evolution until the recovering state, (b) transmission processes of the disease, and (c) waning of immunity returning to the susceptible state in $SI_\eta RS$ epidemic model with η compartments.

The total infectious time is given by the sum of identical and independent exponentially distributed transition times between subsequent infectious states, which in turn are given by $\psi(t_j) = \eta\mu \exp(-\eta\mu t_j)$. It can be shown that it leads to a Gamma

distribution for the total recovery time:

$$\tau = \sum_{j=1}^{\eta} t_j, \tag{5.1}$$

given by [140, 141]:

$$\psi_{\text{rec}}(\tau) = \frac{(\eta\mu)^{\eta}}{(\eta-1)!}\tau^{\eta-1}e^{-\eta\mu\tau}. \tag{5.2}$$

If the infectious state passes through an increasing number of stages, the distribution approaches a Dirac delta function centered at $\tau = \langle\tau\rangle = 1/\mu$, as shown in Fig. 5.2(a) for $\eta = 1, 2, 5, 10$, and 50. The probability of being infected up to time τ since infection is given by:

$$P_{\text{inf}}(\tau) = 1 - \int_0^{\tau} \psi_{\text{rec}}(\tau')d\tau', \tag{5.3}$$

which converges to a Heaviside step function as $\eta \to \infty$ [142]; see Fig. 5.2(b). Empirical data on household recovered periods of whooping cough are better fit by a Gamma-distributed function, Eq. (5.2), than by an exponential one [143].

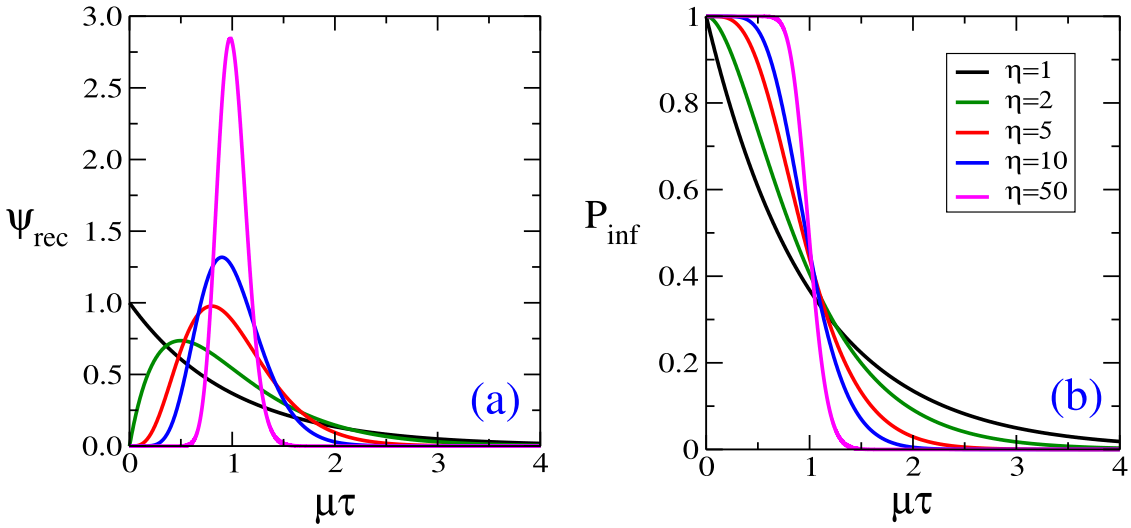

Figura 5.2 – (a) Distribution of recovering period (ψ_{rec}) and (b) probability of remaining infected (P_{inf}) until a time τ for healing processes with η stages.

5.2 $SI_{\eta}RS$ dynamics on star graphs

The transition from a disease-free state to an endemic phase can be triggered by different activation mechanisms depending on the network structure, which is related to the degree exponent in RN [31, 29, 30].

Different activation mechanisms can be involved in the onset of the endemic phase, which highly depend on structures possibly found in the network. Depending on the network's heterogeneity degree, also dependent on the network exponent γ, either a den-

sely connected sub-graph (see Subsec. 2.7.2), star-graphs (Sec. 2.5) in the thermodynamic limit. Furthermore, in the finite size regime, a competition between both structures takes place [31, 121].

The regime of $\gamma > 3$ is characterized by low heterogeneity and ruled by rare structural disorders represented by the hubs, which are involved in the activation mechanism discussed in Sec. 3.10. Let us recall that their meta-stable activity is determinant for the epidemic lifespan of the whole network [139, 29, 30] and is ruled by feedback between the center (hub) and its leaves (neighbors), leading to an algebraic lifespan in the hub degree for the $SIRS$ and exponential in the SIS model, while the reinfection mechanism between hubs always scales algebraically. The hub infects several of its leaves, which can in turn reinfect the hub by chance, even at low infection rates per edge. In the case of infectious activity long enough, the star can activate other hubs far from the source, thus characterizing a long-range mutual infection mechanism at play (see Sec. 3.10).

5.2.1 Epidemic lifespan

To analyze the implications of multiple infectious stages, we consider the $SI_\eta RS$ dynamics on star graphs. They consist of a center connected to k neighboring nodes, or leaves (see Sec 2.5 for a brief discussion of its properties). This structure serves as a prototype for network hubs (large degree nodes), capturing the local feedback mechanisms between hubs and their neighbors that are crucial for sustaining epidemics [31, 61], as already discussed in Sec. 3.10.

The epidemic lifetime of a star graph for $SI_\eta RS$ models is estimated in an adaptation of the theory found in Ref. [30]. It is performed by considering discrete-time dynamics where each time step has the following sequence:

1. At $t = 0$, the center is infected in the stage $j = 1$ and the k leaves are susceptible.

2. By time $t = t_1 = 1/\mu$, the center is recovered, while n_1 leaves are infected (in stage $j = 1$) according to a binomial distribution:

$$P_1(n_1|k) = \binom{k}{n_1} p_1^{n_1} (1 - p_1)^{k-n_1}, \tag{5.4}$$

where p_1 is the probability that the center infects a susceptible neighbor before healing. It is computed as the complementary probability that the individual passes through all η compartments without healing, which is given by:

$$p_1 = 1 - \prod_{j=1}^{\eta} \left[\frac{\mu_j}{\lambda_j + \mu_j} \right]. \tag{5.5}$$

This is due to the fact that the progression between compartments $j \to j + 1$ and infections are independent Poisson processes with rates μ_j and λ_j, respectively. For

the case of interest $\mu_j = \eta\mu$ and $\lambda_j = \lambda$, so Eq. (5.5) becomes

$$p_1 = 1 - \left[\frac{\mu\eta}{\lambda + \mu\eta}\right]^{\eta}. \tag{5.6}$$

In Eq. (5.6), the limit cases $\eta = 1$ (Markovian healing time) and $\eta = \infty$ (deterministic healing time) are $p_1 = \lambda/(\lambda+\mu)$ and $p_1 = 1 - \exp(-\lambda/\mu)$, respectively. Both cases have $p_1 \approx \lambda/\mu$ in the limit of interest $\lambda \ll \mu$.

3. At $t = t_1 + t_2$, the center loses its immunity and becomes susceptible again, i.e. after an interval t_2 distributed by $\rho_2 = \alpha \exp(-\alpha t_2)$. After this interval, only n_2 leaves remain infected with probability:

$$P_2(n_2|n_1) = \binom{n_1}{n_2} p_2^{n_2}(1-p_2)^{n_1-n_2}, \tag{5.7}$$

where $p_2 = P_{\text{inf}}(t_2)$ is given by Eqs. (5.3) and (5.2).

4. At time $t = t_1 + t_2 + t_3$ all leaves become synchronously susceptible, with the center reinfected in the process. The state of the star thus returns to the initial configuration, described in item 1. Here, $t_3 = 1/\mu$. This event happens with probability:

$$q(n_2) = 1 - (1-p_1)^{n_2}, \tag{5.8}$$

i.e., the probability that at least one leaf tried to infect the center. Otherwise, the dynamic ends with probability $1 - q(n_2)$.

Therefore, the epidemic process to remains active for an interval $t = t_1 + t_2 + t_3 = 2/\mu + t_2$ with a probability given by:

$$\begin{aligned} Q_k(t_2) &= \sum_{n_1=1}^{k} \sum_{n_2=1}^{n_1} P_1(n_1|k) P_2(n_2|n_1) q(n_2) \\ &= 1 - [1 - p_1^2 p_2]^k, \end{aligned} \tag{5.9}$$

where Eqs. (5.4) and (5.7), as well as algebraic manipulations using Newton's binomial formula were employed. Taking the average of $Q_k(t_2)$ over t_2 gives the probability of the epidemic activity surviving the sequence of steps 1 to 4, given by:

$$\bar{Q}_k = 1 - \alpha \int_0^{\infty} e^{-\alpha t_2}(1 - p_1^2 p_2)^k dt_2. \tag{5.10}$$

Now, we are in position to estimate the number of steps n_s that the dynamics remains active, being distributed by:

$$P_s(n_s) = (\bar{Q}_k)^{n_s - 1}(1 - \bar{Q}_k). \tag{5.11}$$

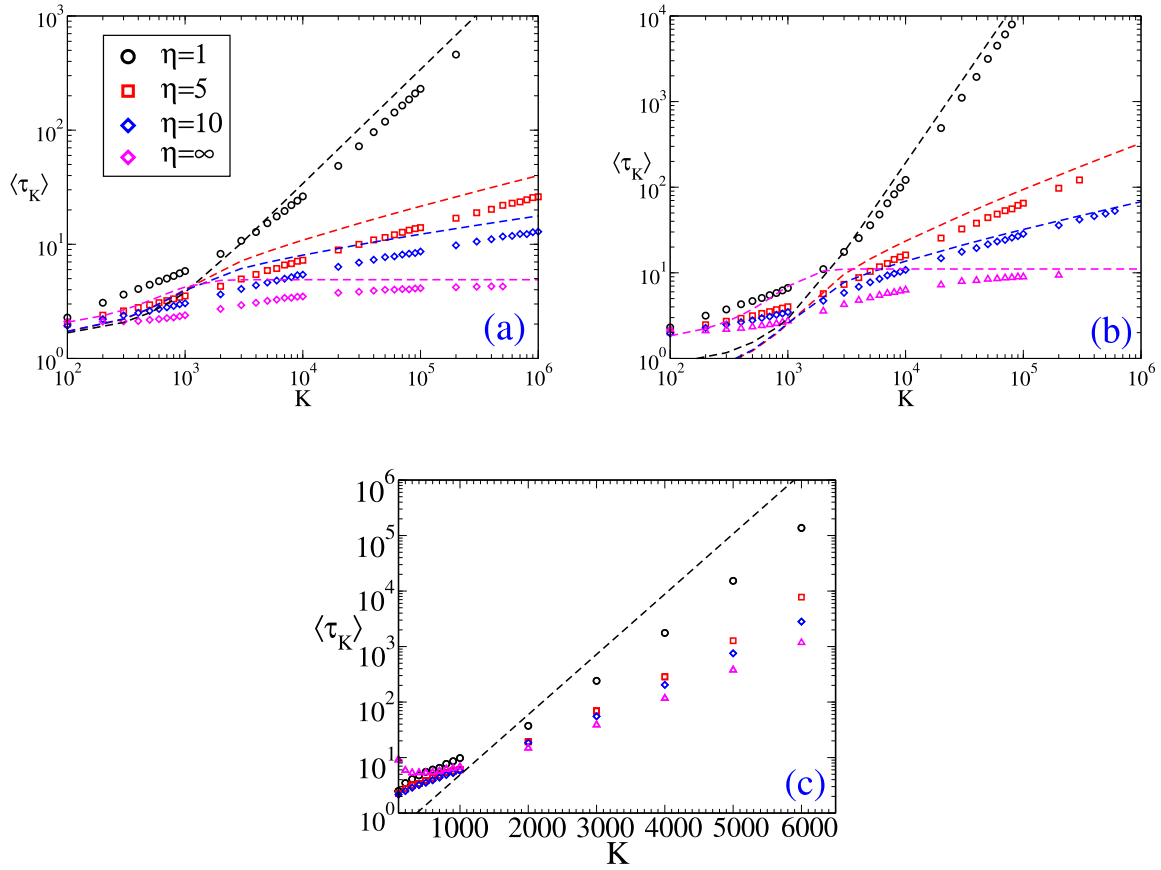

Figura 5.3 – Epidemic lifespan $\langle\tau_k\rangle$ as function of the star graph size k, for different number of infectious stages $\eta = 1$, $\eta = 5$, $\eta = 10$, and $\eta = \infty$ (deterministic recovering time). The parameters of the dynamics are $\lambda = 0.05$, $\mu = 1$, (a) $\alpha = 1$, (b) $\alpha = 2$ and (c) $\alpha = \infty$ (SIS). Symbols are simulations while dashed lines correspond to Eqs. (5.12) and (5.17) for finite and infinite η, respectively.

Eq. (5.11) is the probability that the dynamics survives $n_s - 1$ times in sequence and finally dies out right after. So the activity lifetime of a hub and its k nearest neighbors, $\langle\tau_k\rangle$ assumes the form:

$$\begin{aligned}
\langle\tau_k\rangle &= \tau \sum_{n_s=1}^{\infty} n_s P_s(n_s) \\
&= \tau(1-\bar{Q}_k) \sum_{n_s=1}^{\infty} n_s (\bar{Q}_k)^{n_s-1} \\
&= \tau(1-\bar{Q}_k) \frac{d}{d\bar{Q}_k}(1-\bar{Q}_k)^{-1} \\
&= \frac{\tau}{1-\bar{Q}_k}
\end{aligned} \tag{5.12}$$

in which, $\tau = t_1 + \langle t_2\rangle + t_3 = 2/\mu + 1/\alpha$ is the average duration of a cycle. To determine the epidemic lifespan $\langle\tau_k\rangle$ is necessary to evaluate the integral given by Eq. (5.10). For a finite number of stages η, the asymptotic limit can be computed by applying the saddle-point

method (see Appendix 4.2), resulting in:

$$\langle \tau_k \rangle \sim (kp_1^2)^{\frac{\alpha}{\eta\mu}} \left(\ln \left(kp_1^2 \right) \right)^{\frac{\eta-1}{\eta}\frac{\alpha}{\mu}} \tag{5.13}$$

in the limit of large k. In particular, when $\eta = 1$, Eq. (5.13) corresponds to the result of Ref. [30] for the Markovian $SIRS$ dynamics, where $\langle \tau_k \rangle \sim k^{\alpha/\mu}$.

In the limit of $\eta \to \infty$, the saddle-point method cannot be applied to evaluate Eq. (5.10). In this limit, the healing processes becomes deterministic, i.e., its distribution yields:

$$\psi_{\text{rec}}(\tau) = \delta(\tau - 1/\mu), \tag{5.14}$$

where $\delta(\tau - 1/\mu)$ is a *Dirac delta function* centered at $1/\mu$. In this case, the probability of being infected until time t_2, $p_2 = P(t_2)$, becomes a step function:

$$p_2 = \begin{cases} 1, & \text{if } \ t_2 < 1/\mu \\ 0, & \text{if } \ t_2 > 1/\mu. \end{cases} \tag{5.15}$$

By inserting Eq. (5.15) into (5.10), one obtains:

$$\begin{aligned} 1 - \bar{Q}_k =& \alpha \int_0^{1/\mu} e^{-\alpha t_2} e^{-p_1^2 k} dt_2 + \alpha \int_{1/\mu}^{\infty} e^{-\alpha t_2} dt_2 \\ =& e^{-p_1^2 k} \left(1 - e^{-\alpha/\mu} \right) + e^{-\alpha/\mu}, \end{aligned} \tag{5.16}$$

where we have used $(1-p_1^2)^k \approx \exp(-kp_1^2)$ valid for $p_1 \ll 1$. Now, substituting Eq. (5.16) in Eq. (5.12) we obtain

$$\langle \tau_k \rangle = \frac{\tau}{e^{-kp_1^2} \left(1 - e^{-\alpha/\mu} \right) + e^{-\alpha/\mu}}, \tag{5.17}$$

which assumes the constant value $\langle \tau_k \rangle = \tau \exp(\alpha/\mu)$ for $k \to \infty$ and α/μ finite.

The theoretical predictions obtained by numerical integration of Eq. (5.10) and the analytical expression given by Eq. (5.17) are in very good agreement with continuous-time stochastic simulations (see Sec. 3.3 for the general framework and App. 4.1 for a specific approach) on a star graph for large k and distinct values of η, as Figs. 5.3(a) and (b) show. A prefactor poses the only difference between both approaches, which is not a relevant matter since analytical results rely on approximated discrete-time dynamics.

The limit case $\alpha \to \infty$, corresponding to the SIS dynamics, can be directly obtained using $\lim_{\alpha\to\infty} \alpha \exp(-\alpha t) = \delta(t)$ in Eq. (5.10):

$$\begin{aligned} 1 - Q_k &= \int_0^{\infty} \delta(t_2)(1 - p_1^2 p_2) dt_2 \\ &= (1 - p_1^2)^k \simeq e^{-k\frac{\lambda^2}{\mu^2}}, \end{aligned} \tag{5.18}$$

where the last approximation is valid $\lambda/\mu \ll 1$ where $p_1 \approx \lambda/\mu$. So, in the SIS dynamics,

the analytical average lifetime is independent of η and given by:

$$\langle \tau_k \rangle \approx \frac{2}{\mu} e^{k\frac{\lambda^2}{\mu^2}},$$

in agreement with the Markovian SIS result of Ref. [29]. Simulations agree with the exponential increase in the star graph size. However, the exponential's slope varies slightly with η as can be seen in Fig. 5.3(c). Thus, the feedback activation mechanism of Markovian SIS dynamics on star graphs [29] is not significantly altered by the Gamma distribution of the recovering period and one expects that the activation mechanism by hubs in power-law networks is not significantly altered. Indeed, this result is in agreement with Ref. [144], in which, at a mean-field level, the epidemic threshold is independent of the recovery time distribution once the healing times are exponentially distributed.

5.2.2 Mutual infection time

We have so far discussed the *local* activation mechanism, responsible for a star's metastable activity. Another important mechanism where this metastability has a key role is the long-range mutual infection of hubs, which is driven by fluctuations [139, 29, 30]. To estimate the average time $\langle \tau_{kk'} \rangle$ for infections in a hub of degree k to reach another hub of degree k', we analyze a path of length d, as discussed in Sec. 2.6, connecting a source of degree k and a target of degree k' (see figure 5.4). For the sake of simplicity, we assume that the source does not recover, thus representing an upper bound for the actual probability of long-range infection. The probability that a node in the path infects its neighbor before recovering is given by Eq. (5.6). Thus, an infection starting at the source reaches the target with probability p_1^{d-1}, which corresponds to an effective infection rate given by λp_1^{d-1}.

Random uncorrelated networks (see Sec. 2.8) with N nodes present an average distance between nodes of degree k and k' given by [145]:

$$d = 1 + \frac{\ln(N\langle k \rangle / kk')}{\ln \kappa}, \tag{5.19}$$

in which,

$$\kappa = \frac{\langle k^2 \rangle - \langle k \rangle}{\langle k \rangle}. \tag{5.20}$$

Here, $\langle k^2 \rangle$ and $\langle k \rangle$ are the second and the first moment of the degree distribution, defined in Subsec. 2.3.1. Therefore, the estimated average time required for the source to activate the target is given by:

$$\langle \tau_{kk'} \rangle = \frac{1}{\lambda p_1^{d-1}} = \frac{1}{\lambda} \left(\frac{N\langle k \rangle}{kk'} \right)^{b(\lambda,\eta)}, \tag{5.21}$$

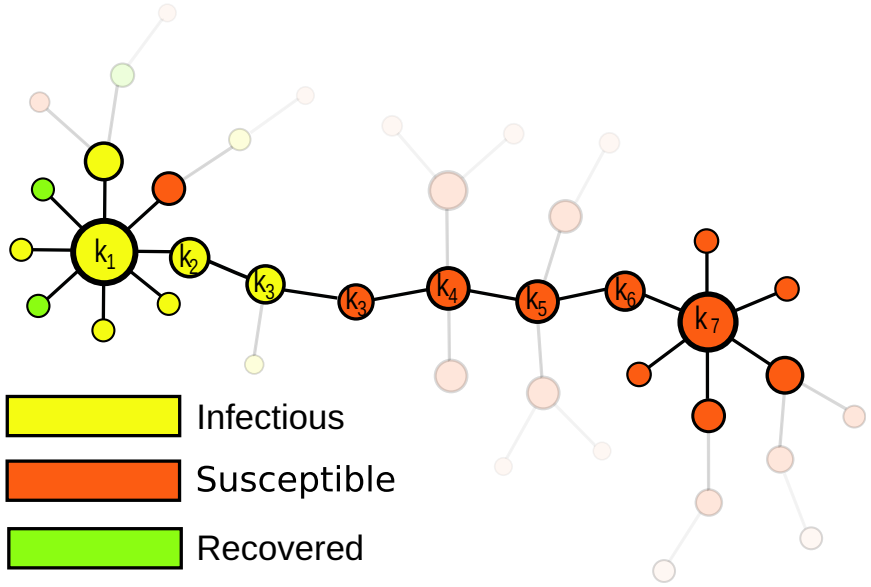

Figura 5.4 – An illustrative case of communication between hubs. The infection starts at the center of the left hub of degree k_1 (source) and travels through this path to reach the right hub of degree k_7 (target). The shaded nodes represent other connections that are not relevant for the infection propagation.

where the exponent $b(\lambda, \eta)$ is given by:

$$b(\lambda, \eta) = -\frac{\ln p_1}{\ln \kappa} \geq 0. \tag{5.22}$$

Since, in a network, there are other paths linking hubs, $\langle \tau_{kk'} \rangle$ is an upper bound to mutual infection time. This expression is essentially the same derived for Markovian SIS and $SIRS$ dynamics in Refs. [29, 30] with the only difference of using the modified p_1. Since in the limit of low infection $\lambda/\mu \ll 1$, $p_1 = \lambda/\mu$ independently of η, we have that the result is indeed equivalent to Refs. [29, 30].

5.3 $SI_\eta RS$ dynamics on networks.

The analytical results for the epidemic lifetime and mutual infection time indicate that alterations in relation to Markovian spreading may occur in the dynamics since the epidemic lifetime on hubs is modified by the number of infectious stages η, while the mutual long-range infection time is not. To analyze these possible effects, we consider uncorrelated networks with a power-law degree distribution, $P(k) \sim k^{-\gamma}$, generated with the uncorrelated configuration model (UCM), discussed in Sec. 2.8, where an upper cutoff $k_c \sim \sqrt{N}$ is used to ensure the absence of degree correlations in simple graphs without self- and multiple-connections. The most connected node of the network will have an average degree $\langle k_{\max} \rangle \sim N^{1/2}$ for $\gamma < 3$ and $\langle k_{\max} \rangle \sim N^{1/(\gamma-1)}$ for $\gamma \geq 3$ [59]. Finally, the

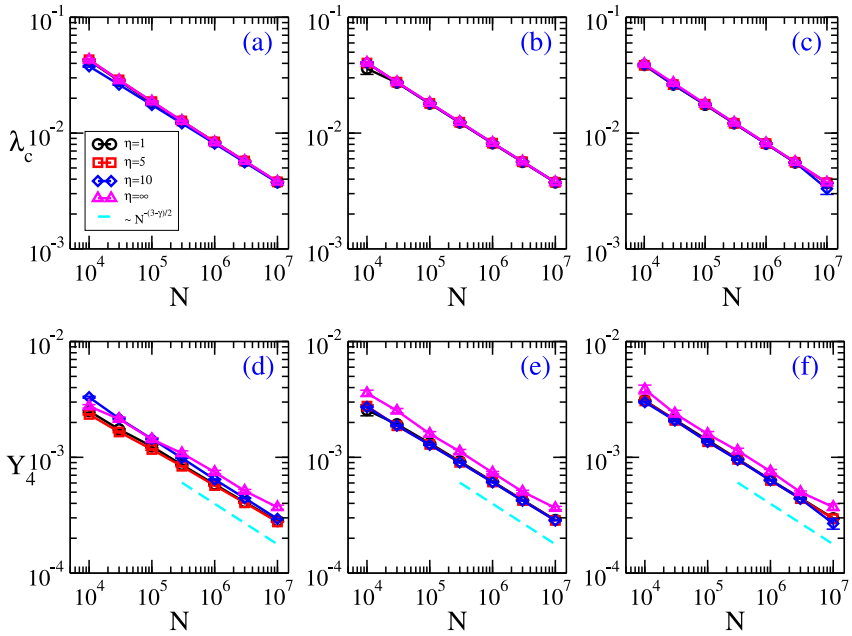

Figura 5.5 – Epidemic threshold (top) and IPR of activity (bottom) as a function of network size for (a,d) $\alpha = 0.5$, (b,e) $\alpha = 1$, and (c,f) $\alpha = 2$ and different numbers of stages η. The dashed lines are power-law decays $Y_4 \sim N^{(3-\gamma)/2}$ corresponding to a maximum k-core localization. The simulations were run on power-law networks with $\gamma = 2.3$, $k_{\min} = 3$ and $k_c = 2\sqrt{N}$.

scaling of κ, Eq. (5.20), is given by:

$$\kappa \sim \begin{cases} k_{\max}^{(3-\gamma)/2} \sim N^{(3-\gamma)/2} & , \quad \gamma < 3 \\ \text{const} & , \quad \gamma \geq 3. \end{cases} \tag{5.23}$$

By inserting Eq. (5.23) into Eq. (5.22), we obtain $b(\lambda, \eta) \to 0$, and $\langle \tau_{kk'} \rangle$ increases slower than algebraically for $\gamma < 3$ in the limit of large network size, regardless of η. Thus, Eq. (5.13), which holds for finite η, implies that $\langle \tau_k \rangle > \langle \tau_{kk'} \rangle$. This means that an epidemic spreading starting in a hub would remain active long enough to communicate the disease to other hubs, thereby triggering an outbreak, i.e., mutually establishing a domain of activity larger than their local domains of infectious activity [146, 29, 30].

To explicitly check the effect of the multiple infection stages, we ran stochastic simulations (see App. 4.1) of $SI_\eta RS$ dynamics on UCM networks with $\gamma = 2.3$. For this exponent, the Markovian dynamics is activated by a densely connected core composed of hubs, as identified by an innermost component of k-core decomposition (see Subsec. 2.7.2), the maximum k-core [137, 31]. We also analyzed the dynamical susceptibility [47], defined as $\chi = N\left(\langle \rho^2 \rangle - \langle \rho \rangle^2\right) / \langle \rho \rangle$, as a function of the infection rate λ. As discussed in Sec. 3.6, for systems undergoing a transition to absorbing states in complex networks, the position of the principal peak in these curves is an estimate of the epidemic threshold [47, 61].

The case $\gamma = 2.3$ does not yield any appreciable effect on the threshold for the investigated network sizes (up to 10^7) and values of α adopted when infectious stages

are introduced, as top panels of Fig. 5.5 shows. This shows that the same activation mechanism triggered in the maximum k-core, as in the SIS model [31, 74], seems to be at work irrespective of η. To validate this hypothesis, we evaluated a normalized activity vector ϕ_i, introduced in Ref. [78] and presented in this chapter in Sec. 4.2, which is given in terms of the probability ρ_i that node i is infected in the quasistationary state (see Appendix 4.1): $\phi_i \propto \rho_i$ and $\sum_i \phi_i^2 = 1$. We compute the inverse partition ratio (IPR) [115], defined as $Y_4 = \sum_i \phi_i^4$. Regardless of η, we observed $Y_4 \sim N^{-(3-\gamma)/2}$ for all α/μ considered, as shown in the bottom of Fig. 5.5. This scaling is associated with the maximum k-core localization [121]. Note that a finite lifetime of hubs in the case $\eta = \infty$ is not able to alter the scenario.

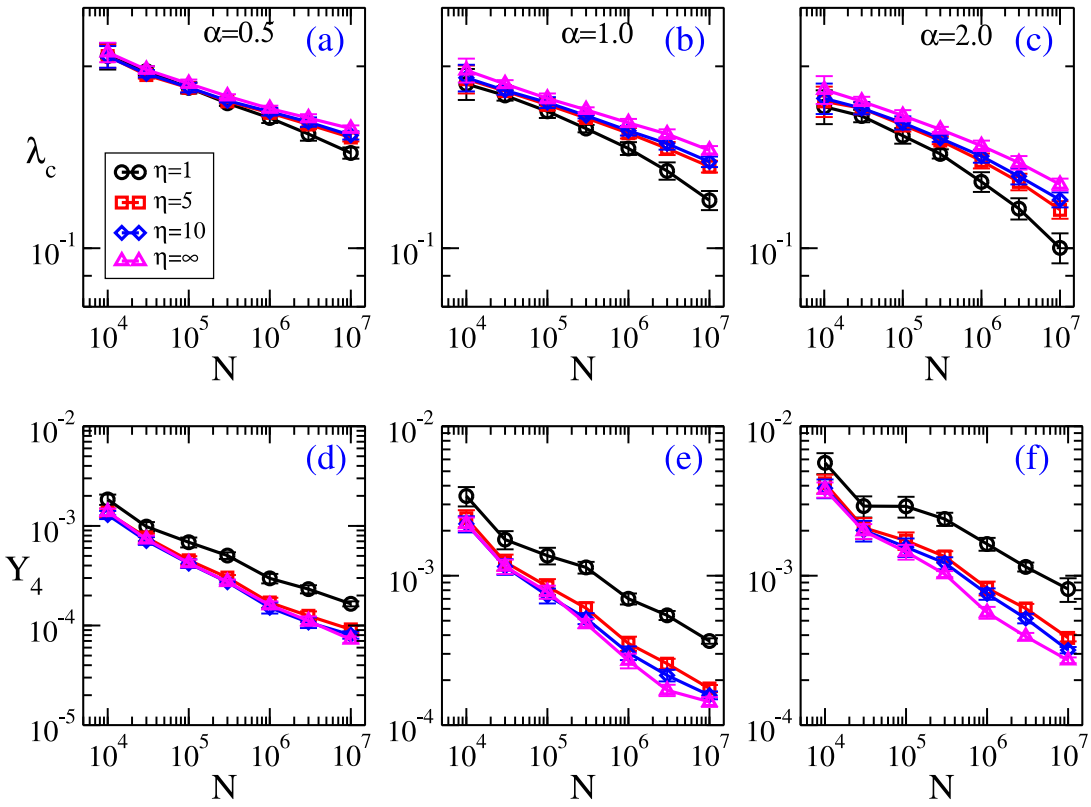

Figura 5.6 – Epidemic thresholds (top) and IPR of activity (bottom) as functions of network size for (a,d) $\alpha = 0.5$, (b,e) $\alpha = 1$, and (c,f) $\alpha = 2$ for a different number of infectious stages η. The simulations were run on power-law networks with $\gamma = 3.5$, $k_{\min} = 3$ and natural upper cutoff.

For $\gamma > 3$, a long-range mutual activation of hubs may be present in place of the maximum k-core activation, as in the case of Markovian SIS [29]. However, this mechanism does not rule the epidemic activation of the Markovian $SIRS$ dynamics, which instead happens collectively, involving an extensive part of the network [30]. Since the epidemic lifespan on star graphs decreases with η, the hubs have shorter-lived activity for $\eta > 1$ compared to the Markovian case $\eta = 1$, while the scaling with network size of mutual infection time is independent of η. Therefore, the collective activation where $\langle \tau_{kk'} \rangle \gg \langle \tau_k \rangle$ remains valid. Figure 5.6 presents the analysis of the $SI_\eta RS$ dynamics for

$\gamma = 3.5$. For $\alpha \leq 0.5$, the epidemic threshold is only slightly altered with respect to the Markovian $SIRS$, as shown in Fig. 5.6(a). The impact of non-Markovian dynamics on the epidemic threshold becomes more evident as α increases, as illustrated in Figs. 5.6(b) and (c), where we observe an increase in the epidemic threshold with η. This is consistent with the analysis of epidemic lifetime on star graphs since a shorter activity duration on hubs implies slower epidemic spreading. In particular, when $\eta \to \infty$, from Eq. (5.17) and Eq. (5.21), we find that $\langle \tau_{kk'} \rangle \gg 1$, while $\langle \tau_k \rangle$ remains finite for $\lambda/\mu \ll 1$. Figure 5.6, however, does not indicate the limit of threshold saturation as a function of size. Indeed, as in the Markovian case [30], this regime is observable, for the investigated values of α, only for exceedingly large sizes, much larger than those that can currently be simulated. The saturation can be seen for smaller values of α, but in this regime, the effects of multiple stages are very small, as in the case of $\gamma = 2.3$ shown in Fig. 5.5.

In the SIS model ($\alpha \to \infty$), the existence of hubs can trigger multiple peaks in the susceptibility curves, indicating the activation of different parts of the networks [61, 47]. Figure 5.7 confirms the existence of multiple peaks in the susceptibility curves for all values of η studied in networks with $\gamma > 3$ and the presence of outliers in the degree distribution, as shown in Fig. 5.7(b). The observable effect is the slight shift of the curves and peaks compared to the Markovian case $\eta = 1$, implying that the localization pattern holds regardless of η. This result aligns with the effects of the number of stages on the epidemic lifetime shown in Sec. 5.2.1, supporting the resilience of the long-range hub mutual activation mechanisms.

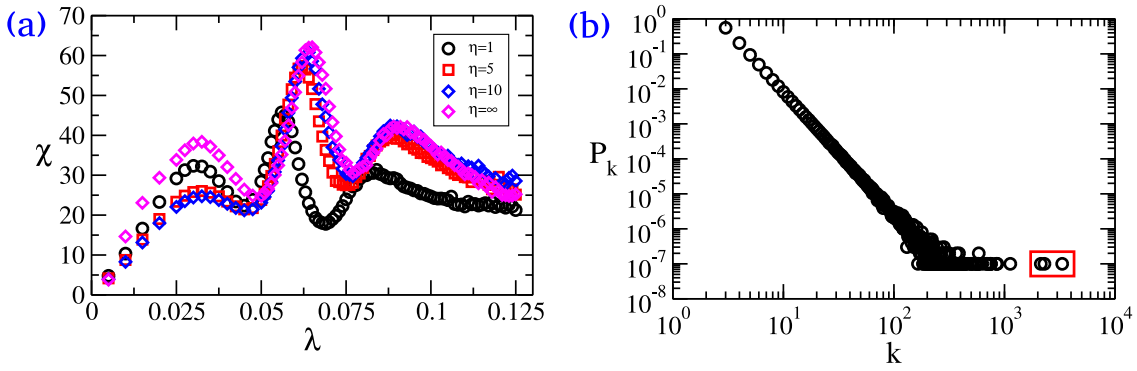

Figura 5.7 – (a) Susceptibility as a function of the infection rate for different number of infectious stages. Simulations were run in a network with degree distribution shown in (b). The red square highlights the outliers of this network. The other parameters are $N = 10^7$, $\gamma = 3.5$, $k_{\min} = 3$, and natural upper cutoff.

We conclude the results section by considering RRNs, where each node has the same degree k and edges among them are formed randomly without self- and multiple connections. A homogeneous mean-field theory to compute the epidemic threshold of the SI_ηRS on RRNs is developed in Appendix 4.3. Multiple stages do not alter the epidemic threshold in a mean-field approach, given by $\lambda_c/\mu = 1/k$, irrespective of the number of stages η. This result is consistent with the non-Markovian SIS model [147, 148].

However, in stochastic simulations, the introduction of several infectious stages shifts the epidemic threshold to lower values. Incorporating dynamical correlations into the mean-field approach can enhance the precision of the theoretical framework, as seen in the Markovian case [48].

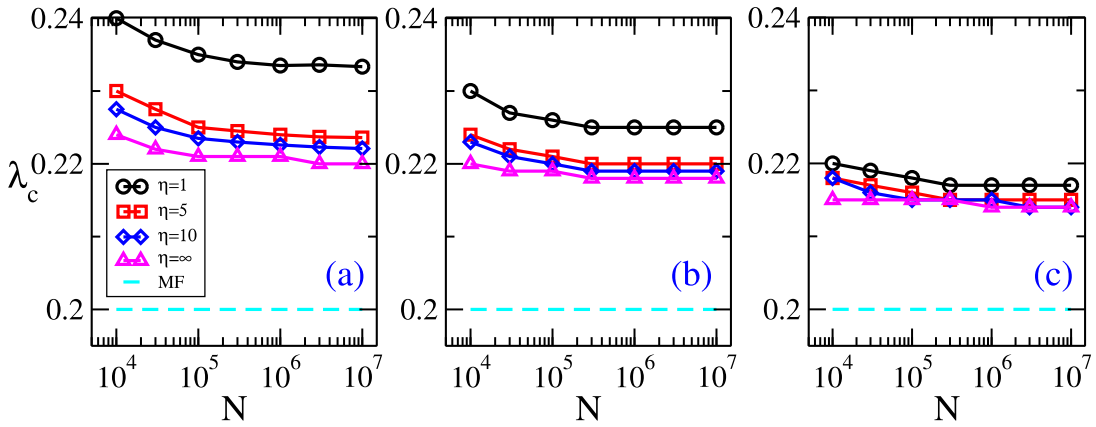

Figura 5.8 – Epidemic threshold as a function of the network size for RR networks with $k = 6$ and a different number of infectious states η. The cyan dashed line corresponds to mean-field prediction. We waning immunity rates are (a) $\alpha = 0.5$, (b) $\alpha = 1$, and (c) $\alpha = 2$.

5.4 Conclusions

In this chapter we investigated the role of non-Markovian recovery times in the $SIRS$ epidemic model, considering $j = 1, \ldots, \eta$ infectious stages that evolve sequentially from j to $j + 1$ towards the recovered state R with rate $\mu_j = \eta\mu$, for $1 \leq j \leq \eta$, implying in a recovery time that follows a Gamma distribution [141] with the same average time as the Markovian $SIRS$ model. At the center of our study were the activation mechanisms sustaining the endemic phase. For this purpose, the lifespan of star graphs of size $k+1$, which mimic the sparsely distributed hubs in the network and serve as a proxy for determining whether the activation mechanism is governed by the mutual activation of sparsely distributed hubs or by a densely connected set of hubs determined by the maximum k-core [137] of the network.

An approximated analytical calculation based on discrete-time dynamics predicts that the non-Markovicity of the recovery processes drastically alters the $SIRS$ dynamics on star graphs, strongly reducing the average epidemic lifespan compared to the Markovian case. Indeed, the larger the number of infectious stages η, the lower the scaling of the epidemic lifespan with the star graph size, while the mutual long-range infection among hubs remains essentially unaltered. In particular, the limit $\eta \to \infty$, which corresponds to a deterministic recovery time, leads to a finite epidemic lifespan even in the limit of infinite star graph size. Stochastic simulations for different values of the waning immunity

rate α support analytical results. However, for the SIS limit, the lifespan still increases exponentially with the graph size, in consonance with the Markovian case.

The activity lifespan of hubs on the epidemic spreading on networks was investigated by means of stochastic simulations on large RN with PL degree distributions in the regimes of $\gamma = 2.3$, characterized by a maximum k-core activation [31, 30, 121], and $\gamma = 3.5$, where k-core structure is not present [137]. In the former, the epidemic localization pattern and, consequently, the epidemic threshold is unaltered by multiple infectious stages in consonance with mean-field analysis for non-Markovian SIS on networks [148]. In the latter, a shift in the epidemic threshold towards values bigger than the Markovian ones and a reduction of the epidemic localization are observed, but not sufficient to change the qualitative conclusions reported previously for the Markovian $SIRS$ [30, 48], at least for the range of networks size attainable in this study.

In a nutshell, although the non-Markovian nature of the process, characterized by the multiple infectious stages, significantly alters the lifespan of localized epidemic activity, it is not relevant to the nature of the activation processes ruling recurrent infection dynamics on the whole networks. As prospects of the present chapter, we can consider the effects of viral-load [149] and multiple stages in the recovering compartment [150].

VI Concluding remarks and future contributions

Networks have become an indispensable tool in understanding complex systems, ranging from the yeast protein-protein interaction (yeast interactome), and the mapping of human brain connections (human brain connectome) all the way up to the worldwide web. Beyond a purely descriptive approach (see Chap. II), the study of these systems usually aims to unveil the relationship between their intrinsic function and statistical metrics, their robustness under failure of randomly affected agents, and so on. Apart from the structural investigation, other dynamic events may be of interest, notably spreading phenomena. Among them, we can mention rumors and pathogens in the network of human contact and computer viruses throughout router networks. The increasing computational power witnessed in the last decades, allied to the growing importance of networked human-crafted structures (apart from their growth itself) has called for a corresponding increase in the interest in the study of both network theory as well as the corresponding dynamic process on top of them. Processes involving epidemic spreading are usually related to absorbing state phase transitions, described in Chap. III. How prone a networked population is to the pervading of a life-threatening pathogen and how large the corresponding outbreaks are expected to be are surely a matter of actual concern, calling for meticulous forecasting.

The development of theoretical frameworks capable of reproducing epidemic models with accuracy is crucial to the progress of forecasting and controlling epidemic outbreaks. Basic models such as SIS and SIR present different natures of epidemic activation and are better suited to different theoretical approaches. Waning immunity with the rate α, where a recovered individual becomes susceptible again after an average time $1/\alpha$, introduces the generalized SIRS dynamics, which interpolates between SIR ($\alpha \to 0$) and SIS ($\alpha \to \infty$) epidemic models. As pointed out in Chap. IV some aspects of SIRS dynamics are similar to the SIS model, regarding the existence of an active steady state, while in other aspects it resembles the SIR dynamics, in which a finite epidemic threshold for degree exponent $\gamma > 3$ is present. So, the mean-field theory that better describes the SIRS dynamics is not completely ascertained. In this thesis, we investigated the $SIRS$ model within both rDMP and PQMF theories, together with stochastic simulations. Both approaches present different ways of taking pairwise correlations into account, with rDMP not allowing for backtracking reinfection, while PQMF does permit, together with other kinds of pairwise correlations. In homogeneous topologies lacking relevant localization, PQMF theory outperforms rDMP. However, by introducing an immersed single node of a large, but size-independent degree, the promotion of strong localization effects could be

witnessed, with the depletion of PQMF performance. Regarding star graphs, the rDMP predicts a finite epidemic lifespan for any network size, with PQMF theory predicting an exponential one, at odds with the correct algebraically increasing lifespan, reported in Ref. [30]. This shall be taken as an indication that both theories under or overestimate, respectively, the localization of the epidemic activity around hubs in the networks. Simulation of the SIRS dynamics on networks with power-law degree distribution confirms this conjecture. Indeed, a finite epidemic threshold observed in simulations of the SIRS dynamics on networks with degree exponent $\gamma > 3$ is in qualitative agreement with the rDMP theory and contrasts with the vanishing epidemic threshold obtained with the PQMF theory. By means of localization analysis, we observe that rDMP underestimates the actual epidemic localization observed in simulations. This strongly points out the necessity of an enhanced version of the rDMP theory.

Despite the simplicity brought by the Markovian assumption in the investigation of spreading phenomena in complex networks, represented by exponentially distributed (Poisson) inter-event times, data on actual epidemic recovery periods are not well fitted by Poissonian distributions, being better described by Weibull or Gamma distributed recovery times. Regarding the investigation presented in Chap. V, we studied the impact of non-Markovian recovery times, considering a healing period formed by η infectious stages progressively evolving to the recovered state R with rate μ_j, where $1 \leq j \leq \eta$. For the sake of simplicity, $\mu_1 = \mu_2 = \cdots = \mu_j = \cdots = \mu_\eta = \eta\mu$, leading to a Gamma distribution with average time equal to the Markovian one in the SIRS model. Since we were interested in the activation mechanisms triggering the endemic phase, we investigated the epidemic dynamics on star graphs of size $K+1$, an important entity in the activation mechanisms governed by the mutual reinfection of distant hubs. An analytical calculation based on discrete-time dynamics allowed us to predict that the non-Markovian character of the recovery processes profoundly changes the SIRS dynamics on star graphs, strongly reducing the average epidemic lifespan in comparison to the Markovian case. In addition to that, in the limit of $\eta \to \infty$, the epidemic lifespan does not scale with the star graph size, with the mutual long-range infection among hubs remaining unaltered. Analytical results for the epidemic lifespan are supported by stochastic simulations for different values of the waning immunity rate α. In the SIS limit ($\alpha \to \infty$) in contrast, the lifespan still increases exponentially with the star size, akin to the Markovian case, with stochastic simulation also supporting this scenario. In order to evaluate impacts of the activity lifespan of hubs on the epidemic spreading on complex networks, we conducted extensive stochastic simulations on power-law networks in two regimes: $\gamma = 2.3$, characterized by a maximum k-core activation [31, 30, 121] and $\gamma = 3.5$, where k-core structure is not present [137]. In the former case, the epidemic localization is unaltered by multiple infectious stages in consonance with mean-field analysis for non-Markovian SIS on networks [148]. In consequence, so does the epidemic threshold. The regime $\gamma = 3.5$ presents a shift in the

epidemic threshold towards smaller values, accompanied by a reduction of the epidemic localization. The intensity of the shift, however, shows that the non-Markovian recovery times are not sufficient to change the Markovian SIRS scenario [30, 48], at least for the range of network sizes attainable in this work.

In Chap. IV, we were able to show that the rDMP theory, albeit not suitably describing the correct scaling of the SIS model in network topologies with $\gamma > \frac{5}{2}$, represents a better approach to the SIRS model in the same network regimes. In particular, this approach performs better than the pQMF theory in correctly predicting a non-vanishing epidemic threshold and a qualitatively correct localization pattern for finite immune periods $1/\alpha$ in the regime of $\gamma > 3$. Our data point out, however, that rDMP theory is not sensible to the waning of immunity rate α in the transition. So, as future work, we propose a modified approach capable of softening the strong prohibition of backtracking reinfection in order to predict more accurately the localization pattern and thus the epidemic threshold of SIRS dynamics in networks. In simple words, although the non-Markovian character investigated by means of multiple infectious stages in Chap. V alter significantly the lifespan of localized epidemic activity, it is not relevant to the activation processes ruling recurrent infection dynamics on the whole networks. This supports the robustness of the Markovian framework in the qualitative and approximate description of epidemic processes in networked systems, although it falls short in describing the lifespan of isolated hubs subjected to non-Markovian recovery times. As a natural sequence of this work, we intend to investigate the effects of viral-loads [149] and non-Markovian immunity periods [150]. We have found evidence that this last one can have profound impacts on the dynamics of the SIRS model with $\alpha > 1$ and non-Markovian distributed immune times (characterized by a number of compartments ϕ), see Fig. 6.1. Also, the behavior we found in isolated hubs under non-Markovian recovery times may dramatically impact the activity relaxation times of rare regions below the endemic threshold, calling for a new study on the Griffiths phenomenon in non-Markovian dynamics.

To conclude, we also investigated the role of low-degree nodes strategically introduced in the network in macroscopic amounts and linked to hubs. This work was not included in the present text for the sake of conciseness but it is in the final writing stage. In summary, we investigated the impacts of bridge nodes (low-degree nodes connecting different parts of the network) in the SIS and $SIRS$ models on top of power-law networks, $P(k) \sim k^{-\gamma}$. We found that the SIS model is sensibly affected due to the linking bridges to the original power-law network (referred to as *core*) with a preferential attachment rule, $\Pi(k_{(core)}) \sim k^{a}_{(core)}$ with $a = 2$. This leads to an increase of localization and consequent quantitative change of scaling of the effective threshold $\lambda_c(N)$ in networks with $\gamma > \frac{5}{2}$. This is in consonance with the hub activation picture, while the regime of $\gamma < \frac{5}{2}$ showed robustness in the finite size scaling measured. To scrutinize between the pure lifespan enhancement due to augmenting the hubs' degrees and possible communication

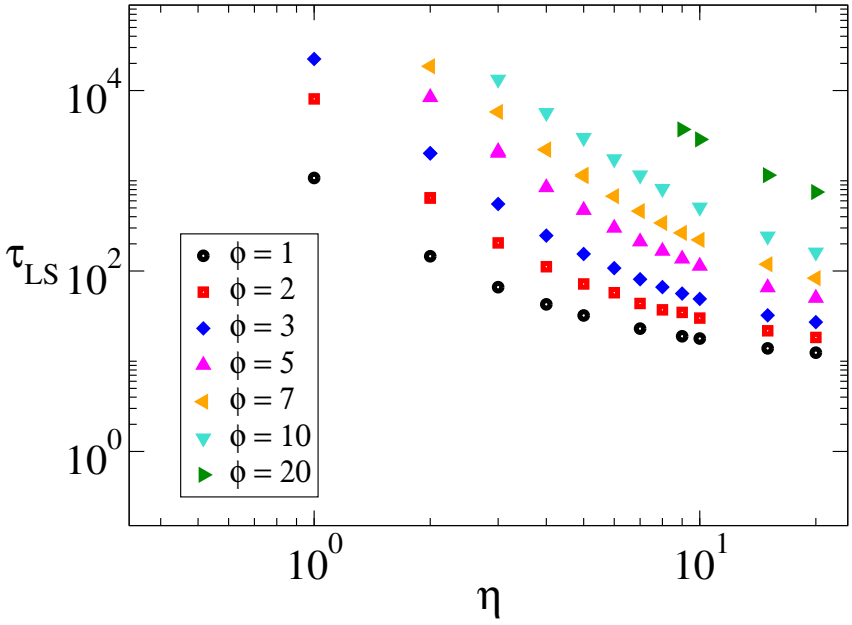

Figura 6.1 – Lifespan of SIRS model with $\alpha = 2.0$, together with a varying number of recovery stages η (horizontal axes), and a different number of waning immunity stages ϕ on a star with fixed size ($N = 3 \times 10^4$).

between core nodes promoted by bridges, we substituted each of their stubs by degree 1 (leaves), thus preserving the hubs' degrees, as Fig. 6.2 shows. This allowed us to confirm the communication role played by bridges in this regime of power-law networks. In the $SIRS$ case, a more interesting picture emerged, in which we could witness the change of activation mechanism by adding bridges. As discussed in Sec. 3.10, the $SIRS$ model presents an activation in the regime $\gamma > 3$ that is only globally possible, represented by a non-vanishing threshold $\lambda_c > 0$, in contrast to the SIS case, which is activated by mutual hub communication at distance and presents a vanishing threshold $\lambda_c = 0$ in the thermodynamic limit. We found evidence that, in agreement with the theory presented by Ferreira et al. (2016), adding bridges with preferential attachment $\Pi(k_{(core)}) \sim k^2_{(core)}$ leads to a profound change in the activation picture of the $SIRS$ model for $\gamma > 3.5$. This change is marked by an emergent localized activation among a finite group of hubs, interconnected by bridges of length 2, leading to a vanishing epidemic threshold $\lambda_c = 0$ in the thermodynamic limit.

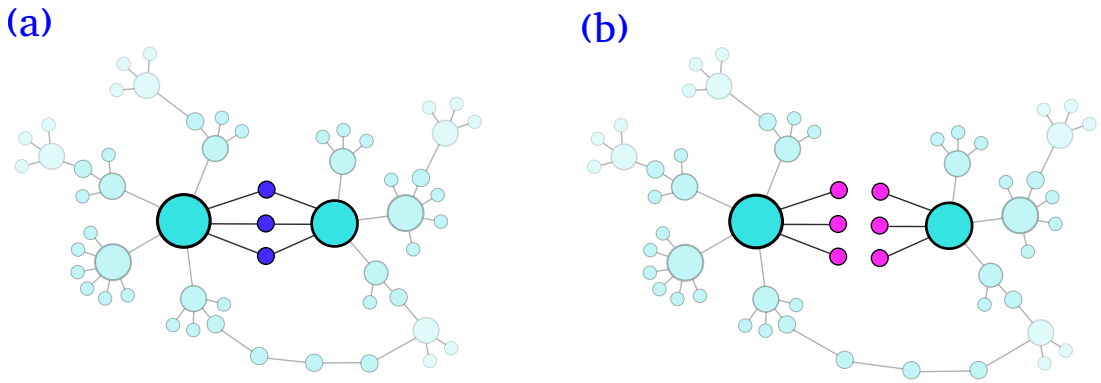

Figura 6.2 – (a): hubs (cyan) mutually communicating via bridges (in dark blue). (b): creation of leaves (magenta) for each stub of a bridge connected to a core node.

List of Appendices

Appendix A – Spectral methods

In this Appendix, we introduce some important spectral concepts and methods used throughout this thesis. The Perron-Frobenius theorem for instance is very important in determining the existence of a positive leading eigenvector of irreducible matrices (to be defined in Sec. 1.1). In addition to this, we define the *power method* in Sec. 1.2, used to obtain the largest eigenvalue and the leading eigenvector of a matrix.

1.1 Perron-Frobenius theorem

We may be interested in an $N \times N$ non-negative matrix A_{ij}, i.e. $A_{ij} \geq 0$ [120]. Besides that, we may also be interested in an irreducible matrix, i.e. the ones such that $\left(A^l\right)_{ij} > 0$ for any i and $j \leq N$ and some integer l [75].

A matrix possessing these features has some interesting properties. For instance, its largest eigenvalue Λ_1 is positive and unique, such that $\Lambda_1 > |\Lambda_2| \geq |\Lambda_3| \cdot \cdot\cdot$. Its associated eigenvector also has only positive entries [51, 151], as long as the associated graph in connected [151], i.e., there always exists a path l_{ij} between any i and j belonging to the graph. In the unconnected case, the Perron-Frobenius theorem is somehow still valid, however only in each of the network's connected components [51, 120, 151].

Suppose that we multiply a vector $\mathbf{v}_0$ by a non-negative matrix $\mathbf{A}$, i.e. $A_{ij} \geq 0$. If we multiply $\mathbf{v}_0$ by $\mathbf{A}$ l times, we end up with:

$$\mathbf{v}_l = \mathbf{A}^l v_0. \tag{1.1}$$

By expanding $\mathbf{v}_0$ in terms of $\mathbf{A}$'s eigenvectors $\mathbf{a}_i$ as $\mathbf{v}_0 = \sum_{i=1}^{N} c_i \mathbf{a}_i$, we have:

$$\mathbf{v}_l = \Lambda_1^l \sum_{i=1}^{N} c_i \left(\frac{\Lambda_i}{\Lambda_1}\right)^l \mathbf{a}_i, \tag{1.2}$$

where Λ_i are eigenvalues of $\mathbf{A}$ and Λ_1 is its largest eigenvalue. As long as $|\frac{\Lambda_i}{\Lambda_1}| < 1$ for any $i > 1$, after enough l multiplications, all terms in the right-hand side of Eq. (1.2) decay exponentially but $\Lambda_1^l c_1 \mathbf{a}_1$. In other words, the leading eigenvector a_1, associated to the largest eigenvalue Λ_1 dominates. If we take $\mathbf{v}_0$ to be non-negative, with $\mathbf{A}$ being non-negative, it implies that $\mathbf{a}_1$ must have all elements non-negative as well [51]. As a consequence, Λ_1 also has to be positive [51].

However, the non-negative character of the matrix is not enough to guarantee the uniqueness of $\mathbf{a}_1$, which may be associated with a degenerate eigenvalue Λ_1. The irreducible character mentioned at the beginning of this section is the sufficient condition leading to the uniqueness of the leading eigenvector $\mathbf{a}_1$.

1.2 Matrix diagonalization

Usually in network theory as well as in epidemic modeling, one needs to obtain the largest eigenvalue (LEV) and the principal eigenvector of a $N \times N$ matrix $\mathbf{C}$. To achieve this, we usually employ a simple approach called the *Power Method* [120], whose reason for this name will become clear in a few lines. It consists of recursively multiplying a matrix $\mathbf{C}$ by an initial guess $\mathbf{w}^{(0)}$, with the restriction that $|\mathbf{w}^{(0)}| = 1$, as follows:

$$w_i^{(1)} = \sum_{j=1}^{N} C_{ij} w_j^{(0)}, \tag{1.3}$$

where $w_i^{(0)}$ is the i-th component of vector $\mathbf{w}^{(0)}$. We shall perform this task several times:

$$w_i^{(l)} = \sum_{j=1}^{N} C_{ij} \tilde{w}_j^{(l-1)}, \tag{1.4}$$

always normalizing the outcome $\mathbf{w}^{(l)}$ to 1, i.e. $\tilde{\mathbf{w}}^{(l)} = \frac{\mathbf{w}^{(l)}}{|\mathbf{w}^{(l)}|}$. Let us linearly expand $\tilde{w}_j^{(l-1)}$ in the eigen-basis of C_{ij}, $\{v_i^{(1)}, v_i^{(2)}, ..., v_i^{(N)}\}$, with $v_i^{(l)}$ satisfying $\Lambda^{(l)} v_i^{(l)} = \sum_{j=1}^{N} C_{ij} v_j^{(l)}$. Therefore, applying $\tilde{w}_i^{(l-1)} = \sum_{k=1}^{N} c_k^{(l-1)} v_i^{(k)}$ to Eq. (1.4) one obtains:

$$\begin{aligned} w_i^{(l)} &= \sum_{k=1}^{N} c_k^{(l-1)} \sum_{j=1}^{N} C_{ij} v_j^{(k)} \\ &= \sum_{k=1}^{N} c_k^{(l-1)} \Lambda^{(k)} v_i^{(k)}. \end{aligned} \tag{1.5}$$

where the spectrum of $\mathbf{C}$ is organized in such a way that $\{|\Lambda^{(1)}| > |\Lambda^{(2)}|, ..., |\Lambda^{(N-1)}| > |\Lambda^{(N)}|\}$.

$$\begin{aligned} w_i^{(l)} &= \sum_{k=1}^{N} c_k^{(0)} \sum_{j=1}^{N} C_{ij} v_j^{(k)} \\ &= \sum_{k=1}^{N} c_k^{(0)} \left(\Lambda^{(k)}\right)^l v_i^{(k)} \\ &= \left(\Lambda^{(1)}\right)^l \sum_{k=1}^{N} c_k^{(0)} \left(\frac{\Lambda^{(k)}}{\Lambda^{(1)}}\right)^l v_i^{(k)}, \end{aligned} \tag{1.6}$$

If $\Lambda^{(1)}$ is the *only* largest eigenvalue of $\mathbf{C}$, as assumed, with a sufficiently large l, $\tilde{w}_i$ will converge to:

$$\tilde{w}_i \approx \left(\Lambda^{(1)}\right)^l c_1 v_i^{(1)}. \tag{1.7}$$

Let us recall that, in order to avoid overflow in the matrix multiplication, i.e., that the memory allocated for a variable is not sufficient for large numbers, we need to normalize the vector resulting from each matrix multiplication.

Appendix B – Stochastic simulation of the SIRS model

2.1 The Gillespie algorithm

We performed stochastic simulations of the SIRS model using an *Optmized Gillespie Algorithm* (OGA) [94]. Let us define the number of recovered N_{rec} and infected N_{inf} nodes as well as the total number of edges emanating from the latter, N_{SI}. At each time step, with probability

$$P_{\text{I}\to\text{R}} = \frac{\mu N_{\text{inf}}}{W_T}, \tag{2.1}$$

an infected node is chosen at random and recovered. Here, $W_T = \mu N_{\text{inf}} + \lambda N_{\text{SI}} + \alpha N_{\text{rec}}$ and can be understood as the *total* or *global rate of events*. With probability

$$P_{\text{R}\to\text{S}} = \frac{\alpha N_{\text{rec}}}{W_T}, \tag{2.2}$$

a recovered node is chosen at random and becomes susceptible. Finally, with probability

$$P_{\text{I}\to\text{S}} = \frac{\lambda N_{\text{SI}}}{W_T}, \tag{2.3}$$

an infected node i is selected with probability proportional to its degree k_i. Then, a neighbor of i is chosen at random and becomes infected if it is susceptible; otherwise, the simulation goes to the next step without changing the configuration. Finally, time is incremented by

$$\delta t = -\frac{\ln u}{W_T}, \tag{2.4}$$

where u is a pseudo-random number uniformly distributed in the interval $(0, 1)$.

2.2 The quasi-stationary method

Since a finite system always falls into the absorbing state whenever simulations run for a time long enough [133], we need to perform some procedure to keep the sampling of the true stationary state. With this in mind, we use a scheme known as the standard quasi-stationary method [133, 134, 98]. Put simply, it consists of bringing the dynamics after it falls into the absorbing, or inactive state. After a relaxation time t_{relax}, quasi-stationary distributions are computed through a time window t_{av}. The quasi-stationary averages were computed over a time window varying from $t_{\text{av}} = 10^5$ to 10^8, after a relaxation

time of $t_{\mathrm{rlx}} = 10^5$ units. The longest time intervals were used for the lowest densities, where fluctuations are more relevant. In the following, we briefly describe specific quasi-stationary methods employed in this work.

2.2.1 The standard quasi-stationary method (SQS)

A list of M configurations is built and constantly updated replacing one of its instances, selected at random, by the current state with probability P_{rep} by unit time. Typical values include $M = 50$ and $P_{\mathrm{rep}} = 0.01$.

2.2.2 The hub-reactivation method (HR)

This method consists in bringing back the most connected node, and thus most infectious, into the infectious state ($\sigma = 1$). This method is shown to be fully compatible with the SQS method, in which it captures localization effects, having the advantage of being simpler to implement.

Appendix C – QMF theory for the SIRS dynamics

Critical quantities associated with the QMF theory can be obtained by performing linear stability analysis around the absorbing state $\rho_i^* = 0$, which is a trivial fixed point of the dynamics [110]. In the steady-state, Eq. (3.37) implies $\mu\rho_i = \alpha r_i$ which, combined with the normalization condition $\rho_i + r_i + s_i = 1$, yields:

$$s_i = 1 - \left(1 + \frac{\mu}{\alpha}\right)\rho_i. \tag{3.1}$$

Now, assuming a quasi-stationary state, where $\mu\rho_i \approx \alpha r_i$ holds, by introducing Eq. (3.1) into Eq. (3.36) one obtains:

$$\frac{d\rho_i}{dt} \approx -\mu\rho_i + \lambda\left[1 - \left(1 + \frac{\mu}{\alpha}\right)\rho_i\right]\sum_j A_{ij}\rho_j, \tag{3.2}$$

which, by ignoring the second-order term $\rho_i\rho_j$, becomes:

$$\frac{d\rho_i}{dt} = \sum_j L_{ij}\rho_j, \tag{3.3}$$

where L_{ij} is the Jacobian matrix given by:

$$L_{ij} = \lambda A_{ij} - \delta_{ij}, \tag{3.4}$$

where we fixed $\mu = 1$, without loss of generality, just fixing time scales [94]. Let us expand ρ_i in A_{ij}'s basis of eigenvectors $\{v_i^{(l)}\}$ like $\rho_i = \sum_{l=1}^{N} c_l v_i^{(l)}$, where $v_i^{(l)}$ satisfies $\Lambda^{(l)} v_i^{(l)} = \sum_j A_{ij} v_j^{(l)}$, with $v_i^{(1)}$ corresponding to the i-th PEV component, $v_i^{(2)}$ to the i-th component of the eigenvector associated to the second LEV, and so on. One thus obtains $c_\Lambda(t) = c_\Lambda(0)\exp(\lambda\Lambda - 1)t$. This shows that the absorbing state $\rho_i^* = 0$ loses stability when the largest eigenvalue $\lambda\Lambda - 1$ of the Jacobian is null and, therefore, the threshold of SIRS model assumes the form:

$$\lambda_c = \frac{1}{\Lambda^{(1)}}. \tag{3.5}$$

in which, $\Lambda^{(1)}$ is the largest eigenvalue (LEV) of the adjacency matrix. To understand how localization sets in under the framework of QMF theory, let us recall that the steady-state of Eq. (3.2) yields:

$$\rho_i = \frac{\lambda\sum_j A_{ij}\rho_j}{\mu + \lambda\left(1 + \frac{1}{\alpha}\right)\sum_j A_{ij}\rho_j}. \tag{3.6}$$

Once more, we evoke that the prevalence ρ_i can be expanded in terms of eigenvectors $\{v_i^{(l)}\}$ of A_{ij} [115]. Assuming a large gap between $\Lambda^{(1)}$ and $\Lambda^{(2)}$, we can assume that the dynamic properties are dominated by the PEV near the epidemic threshold $\lambda \gtrsim \lambda_c$ where $\rho_i \ll 1$, i.e.:

$$\rho_i \approx c^{(1)} v_i^{(1)}. \tag{3.7}$$

to the leading order in ρ_i. Introducing Eq. (3.7) into Eq. (3.6) and summing up i from 1 through N, one obtains:

$$\frac{\lambda}{\mu}\Lambda^{(1)} \sum_i^N \frac{\left[v_i^{(1)}\right]^2}{1 + \frac{\lambda}{\mu}\left(1 + \frac{\mu}{\alpha}\right)\Lambda^{(1)} c^{(1)} v_i^{(1)}} \simeq 1. \tag{3.8}$$

Expanding Eq. (3.8) for $\rho_i \approx c^{(1)} v_i^{(1)} \ll 1$, noting that $\frac{\lambda}{\mu}\Lambda^{(1)}$ is $\mathcal{O}(1)$, we obtain:

$$c^{(1)} \simeq \frac{\frac{\lambda}{\mu}\Lambda^{(1)} - 1}{\left(1 + \frac{\mu}{\alpha}\right)\sum_i \left[v_i^{(1)}\right]^3}, \tag{3.9}$$

which is used to compute the epidemic prevalence as:

$$\rho = \frac{1}{N}\sum_i \rho_i \simeq \frac{\alpha}{\mu + \alpha} a(N) \frac{\lambda\Lambda^{(1)} - \mu}{\mu} \tag{3.10}$$

where the pre-factor $a(N)$ is a function of N given by:

$$a(N) = \frac{\sum_i v_i^{(1)}}{N \sum_i \left[v_i^{(1)}\right]^3}, \tag{3.11}$$

implying that $\rho \sim (\lambda - \lambda_c)^\beta$ with critical exponent $\beta = 1$. Comparing Eq. (3.10) with the QMF solution of the SIS model presented in Ref. [115], we obtain a proportionality relation between SIRS and SIS prevalences given by:

$$\rho^{\text{SIRS}} \simeq \left(\frac{\alpha}{\mu + \alpha}\right) \rho^{\text{SIS}}, \tag{3.12}$$

implying that QMF theory predicts the same critical properties for SIRS and SIS models.

Appendix D – A few remarks on the SIRS model with multiple infectious stages

4.1 Stochastic simulations

Gillespie algorithm

Each infectious stage is realized during an interval τ_i following a Poisson distribution $\eta\mu e^{-\eta\mu\tau_i}$, so we are able to use the whole machinery of the Gillespie Algorithm to perform stochastic simulations of the epidemic model with η infectious stages described in Sec. 5.1. To do so, we follow analogous steps to those discussed in Ref. [94]. For the sake of simplicity and comparison with analytically tractable results found in this work, our model deals solely with infected stages evolving spontaneously to the next with a homogeneous evolution/recovery rate $\eta\mu$. This choice allows us to obtain the same mean infectious period $1/\mu$ for any number of stages. Another simplifying assumption present in our model is that infection rates are the same in all $i = 1, ..., \eta$ infectious stages. This is aimed at scrutinizing the effects of Gamma-distributed infectious times on the dynamics and, we reinforce, for the sake of simplicity. In the following, we present a brief explanation of the Optimized Gillespie algorithm (OGA).

First, one determines the probability of events taking place in the dynamics. This is possible through the present number of infected N_{inf} nodes, the totality of their emanating infectious edges N_{e} and the sum of recovered nodes N_{rec} in the present time. Since the absorbing state is the only actual stationary state in finite-size systems, a quasi-stationary method is employed to keep the dynamics away from the inactive state. For convenience, the hub reinfection method was implemented [134], especially for its desired characteristics, such as the possibility of sampling localized meta-stable states. In a few words, the most connected agent in the dynamics gets reinfected whenever the last infected node recovers, independent of the number of recovered still present. Coming back to the OGA, in each time step, with probability:

$$P_{\text{I}\to\text{R}} = \frac{\mu\eta N_{\text{inf}}}{\mu\eta N_{\text{inf}} + \lambda N_{\text{e}} + \alpha N_{\text{rec}}}, \tag{4.1}$$

an infected node is selected at random and recovers if its infectious stage is η. Otherwise, it remains infected and evolves to the next stage $\sigma \leq \eta$. Alternatively, to a recovery/evolving event, an immunity waning event is chosen with probability:

$$P_{\text{R}\to\text{S}} = \frac{\alpha N_{\text{rec}}}{\mu\eta N_{\text{inf}} + \lambda N_{\text{e}} + \alpha N_{\text{rec}}}, \tag{4.2}$$

in which a recovered node is chosen randomly and returns to a susceptible state. Finally, an infection event is chosen with probability:

$$P_{I\to S} = \frac{\lambda N_{\mathrm{e}}}{\mu\eta N_{\mathrm{inf}} + \lambda N_{\mathrm{e}} + \alpha N_{\mathrm{rec}}}, \tag{4.3}$$

then an infected node i is chosen randomly and accepted with probability proportional to its degree. A neighbor j is chosen at random and, if susceptible, it becomes infected, otherwise, nothing happens. This virtual event is referred to as a *phantom process* [94]. Before going on, at this point, optimizations should be sought and emphatically advised, since recursive rejections of low-degree nodes may slow down the algorithm since they are the huge majority in typical heterogeneous networks. We refer the interested reader to optimization schemes such as the *Improved Gillespie Algorithm* [94]. Finally, time is incremented by:

$$\delta t = \frac{-\ln u}{\mu\eta N_{\mathrm{inf}} + \lambda N_{\mathrm{SI}} + \alpha N_{\mathrm{rec}}}, \tag{4.4}$$

in which u is a pseudo-random number uniformly distributed in the open interval $(0, 1)$. If there is no recovered compartment, the implementation above corresponds to the SIS model with η infectious stages.

4.2 Asymptotic solutions of Eq. (5.10) to determine the average lifetime through the saddle point method

In order to compute the asymptotic limit of Eq. (5.10), we define a variable:

$$Z_\eta(K) = \alpha \int_0^\infty e^{-\alpha t_2}(1 - p_1^2 p_2)^K dt_2. \tag{4.5}$$

where p_1 is given by Eq. (5.4), being a constant, and p_2, according to Eqs. (5.2) and (5.3), is represented as:

$$p_2 = P_{\mathrm{inf}}(t_2) \quad = 1 - \frac{\widetilde{\gamma}(\eta, \eta\mu t_2)}{(\eta - 1)!}, \tag{4.6}$$

where $\widetilde{\gamma}$ is the incomplete Gamma function [152], is represented by:

$$\widetilde{\gamma}(n, x) = \int_0^x y^{n-1} e^{-y} dy = (n-1)! \left[1 - e^{-x} \sum_{m=0}^{n-1} \frac{x^m}{m!}\right]. \tag{4.7}$$

Here, the right-hand side is the series expansion of $\widetilde{\gamma}$ [152]. Now, by replacing $(1-p_1^2 p_2)^K \simeq \exp(-K p_1^2 p_2)$, Eq. (4.6), and Eq. (4.7) in Eq. (4.5) we obtain:

$$Z_\eta(K) = \frac{\alpha}{\eta\mu} \int_0^\infty \exp\left[-\frac{\alpha z}{\eta\mu} - K p_1^2 e^{-z} \sum_{m=0}^{\eta-1} \frac{z^m}{m!}\right] dz, \tag{4.8}$$

where we performed the change of variable $z = \eta\mu t_2$. Notice that Eq. (4.8) has the proper form to apply the saddle-point method [153]:

$$Z_\eta(K) = \frac{\alpha}{\eta\mu}\int_0^\infty \exp\left(-f(z)\right) dz, \tag{4.9}$$

where:

$$f(z) = \frac{\alpha z}{\eta\mu} + Kp_1^2 e^{-z}\sum_{m=0}^{\eta-1}\frac{z^m}{m!}. \tag{4.10}$$

The extrema of Eq. (4.10), $f'(z_*) = 0$, are given by the solutions of transcendent equation:

$${z_*}^{\eta-1}e^{-z_*} = \frac{(\eta-1)!}{\eta}\frac{\alpha}{\mu K p_1^2}. \tag{4.11}$$

For $\eta = 1$, Eq. (4.11) has a single solution which is a minimum:

$$z_* = \ln\left(\frac{\mu K p_1^2}{\alpha}\right). \tag{4.12}$$

For $\eta \geq 2$, there are two solutions since $Kp_1^2 \gg 1$. Since

$$f''(z_*) = \frac{\alpha}{\mu\eta}\left(1 - \frac{\eta-1}{z_*}\right), \tag{4.13}$$

the solution for small z_* is a local maximum, not relevant for the saddle-point method. So, to the leading order in K, the minimum is then given by

$$z_* \simeq \ln\left(Kp_1^2\right) + (\eta-1)\ln\left[\ln\left(Kp_1^2\right)\right]. \tag{4.14}$$

Now that we have settled things, we can perform the saddle-point method, which consists in expanding $f(z)$ around its minimum z_* up to the second order and plug it into Eq. (4.9) to obtain

$$Z_\eta(K) = \frac{\alpha}{\eta\mu}e^{-f(z_*)}\sqrt{\frac{2\pi}{f''(z_*)}}. \tag{4.15}$$

Since $z_* \gg 1$, using Eq. (4.13), we have $f''(z_*) \simeq \alpha/\mu\eta$ and, using Eqs. (4.10) and (4.11),

$$\begin{aligned} f(z_*) &= \frac{\alpha z_*}{\eta\mu} + \frac{\alpha}{\mu\eta}\frac{(\eta-1)!}{z_*^{\eta-1}}\sum_{m=0}^{\eta-1}\frac{z_*^m}{m!} \\ &= \frac{\alpha z_*}{\eta\mu}\left[1 + \frac{1}{z_*} + \mathcal{O}(z_*^{-1})\right] \simeq \frac{\alpha z_*}{\eta\mu}. \end{aligned} \tag{4.16}$$

to the leading order. Therefore, introducing $f(z_*)$ and $f''(z_*)$ in Eq. (4.15) leads to

$$Z_\eta(K) \sim \exp\left(-\frac{\alpha z_*}{\mu\eta}\right) = \left[Kp_1^2\right]^{-\frac{\alpha}{\eta\mu}}\left[\ln\left(Kp_1^2\right)\right]^{-\frac{\alpha(\eta-1)}{\eta\mu}}. \tag{4.17}$$

4.3 Homogeneous mean-field analysis for $SI_\eta RS$

Since the transition between infectious stages is a Poisson process, the set of mean-field equations for the $\mathrm{SI}_\eta\mathrm{RS}$ dynamics for k contacts is given by:

$$\begin{aligned}
\frac{dI_1}{dt} &= \lambda k(1-I-R)I - \mu\eta I_1, \\
\frac{dI_j}{dt} &= \mu\eta I_{j-1} - \mu\eta I_j, \quad j = 2,\ldots,\eta \\
\frac{dR}{dt} &= \mu\eta I_\eta - \alpha R,
\end{aligned} \tag{4.18}$$

where $I = \sum_{j=1}^{\eta} I_\eta$ and $S+I+R = 1$ for a closed population. Performing a linear stability around the absorbing state fixed point $R = I_j = 0$, we obtain the Jacobian matrix given by:

$$\mathbf{L} = \begin{pmatrix}
\lambda k - \mu\eta & \lambda k & \lambda k & \cdots & \lambda k & \lambda k & 0 \\
\mu\eta & -\mu\eta & 0 & \cdots & 0 & 0 & 0 \\
0 & \mu\eta & -\mu\eta & \ddots & 0 & 0 & 0 \\
\vdots & \ddots & & \ddots & -\mu\eta & 0 & 0 \\
0 & 0 & \cdots & 0 & \mu\eta & -\mu\eta & 0 \\
0 & 0 & \cdots & 0 & 0 & \mu\eta & -\alpha
\end{pmatrix}. \tag{4.19}$$

The epidemic threshold corresponds to the value of λ in which the largest eigenvalue of this matrix is null. Note that, from a linear stability analysis, one can see that the Eq.4.18 converges to the $\mathrm{SI}_\eta\mathrm{S}$ model. Therefore, the results in Ref. [147] holds and the epidemic threshold is given by $\lambda_\mathrm{c} = \mu/k$.

References

[1] V. Colizza, A. Barrat, M. Barthelemy, A.-J. Valleron, and A. Vespignani, "Modeling the worldwide spread of pandemic influenza: Baseline case and containment interventions," *PLOS Medicine*, vol. 4, pp. 1–16, 2007.

[2] M. F. C. Gomes, A. P. Piontti, L. Rossi, D. L. Chao, I. M. Longini, M. E. Halloran, and A. Vespignani, "Assessing the international spreading risk associated with the 2014 west african ebola outbreak," *PLoS Currents*, vol. 6, 2014.

[3] A. G. Muñoz, M. C. Thomson, A. M. Stewart-Ibarra, G. A. Vecchi, X. Chourio, P. Nájera, Z. Moran, and X. Yang, "Could the recent zika epidemic have been predicted?," *Frontiers in Microbiology*, vol. 8, p. 1291, 2017.

[4] A. N. Desai, M. U. G. Kraemer, S. Bhatia, A. Cori, P. Nouvellet, M. Herringer, E. L. Cohn, M. Carrion, J. S. Brownstein, L. C. Madoff, and B. Lassmann, "Real-time epidemic forecasting: Challenges and opportunities," *Health Security*, vol. 17, no. 4, pp. 268–275, 2019.

[5] A. Arenas, W. Cota, J. Gómez-Gardeñes, S. Gómez, C. Granell, J. T. Matamalas, D. Soriano-Paños, and B. Steinegger, "Modeling the spatiotemporal epidemic spreading of covid-19 and the impact of mobility and social distancing interventions," *Phys. Rev. X*, vol. 10, p. 041055, 2020.

[6] G. S. Costa, W. Cota, and S. C. Ferreira, "Outbreak diversity in epidemic waves propagating through distinct geographical scales," *Phys. Rev. Research*, vol. 2, p. 043306, 2020.

[7] A. T. Levin, W. P. Hanage, N. Owusu-Boaitey, K. B. Cochran, S. P. Walsh, and G. Meyerowitz-Katz, "Assessing the age specificity of infection fatality rates for covid-19: systematic review, meta-analysis, and public policy implications," *European Journal of Epidemiology*, vol. 35, pp. 1123–1138, 2020.

[8] R. Verity, L. C. Okell, I. Dorigatti, P. Winskill, C. Whittaker, N. Imai, G. Cuomo-Dannenburg, H. Thompson, P. G. T. Walker, H. Fu, A. Dighe, J. T. Griffin, M. Baguelin, S. Bhatia, A. Boonyasiri, A. Cori, Z. Cucunubá, R. FitzJohn, K. Gaythorpe, W. Green, A. Hamlet, W. Hinsley, D. Laydon, G. Nedjati-Gilani, S. Riley, S. van Elsland, E. Volz, H. Wang, Y. Wang, X. Xi, C. A. Donnelly, A. C. Ghani, and N. M. Ferguson, "Estimates of the severity of coronavirus disease 2019: a model-based analysis," *The Lancet Infectious Diseases*, vol. 20, pp. 669–677, 2020.

[9] T. Cerqueira-Silva, V. d. A. Oliveira, J. Pescarini, J. Bertoldo Júnior, T. M. Machado, R. Flores-Ortiz, G. Penna, M. Y. Ichihara, J. V. de Barros, V. S. Boaventura, M. L. Barreto, G. L. Werneck, and M. Barral-Netto, "Influence of age on the effectiveness and duration of protection in vaxzevria and coronavac vaccines," *medRxiv*, 2021.

[10] A. Schulenburg, W. Cota, G. S. Costa, and S. C. Ferreira, "Effects of infection fatality ratio and social contact matrices on vaccine prioritization strategies," 2022.

[11] K. Dietz and J. Heesterbeek, "Daniel bernoullis epidemiological model revisited," *Mathematical biosciences*, vol. 180, no. 1-2, pp. 1–21, 2002.

[12] T. Duclos and T. Reichert, "A solution to the kermack and mckendrick integro-differential equations which accurately projects covid-19 case data using google mobility data as an input," *medRxiv*, 2023.

[13] A.-L. Barabási and R. Albert, "Emergence of scaling in random networks," *Science*, vol. 286, pp. 509–512, oct 1999.

[14] A.-L. Barabâsi, H. Jeong, Z. Néda, E. Ravasz, A. Schubert, and T. Vicsek, "Evolution of the social network of scientific collaborations," *Physica A: Statistical mechanics and its applications*, vol. 311, no. 3-4, pp. 590–614, 2002.

[15] R. Pastor-Satorras and A. Vespignani, "Epidemic dynamics in finite size scale-free networks," *Phys. Rev. E*, vol. 65, p. 035108, Mar 2002.

[16] A. Calvó-Armengol, "Job contact networks," *Journal of economic Theory*, vol. 115, no. 1, pp. 191–206, 2004.

[17] M. O. Jackson, "Chapter 12 - an overview of social networks and economic applications*," in *Handbook of Social Economics*, North-Holland, 2011.

[18] R. Pastor-Satorras, C. Castellano, P. V. Mieghem, and A. Vespignani, "Epidemic processes in complex networks," *Rev. Mod. Phys.*, vol. 87, pp. 925–979, aug 2015.

[19] S. Boccaletti, V. Latora, Y. Moreno, M. Chavez, and D.-U. Hwang, "Complex networks: Structure and dynamics," *Physics Reports*, 2006.

[20] A. Arenas, A. Díaz-Guilera, J. Kurths, Y. Moreno, and C. Zhou, "Synchronization in complex networks," *Physics Reports*, vol. 469, 2008.

[21] R. Lu, W. Yu, J. Lü, and A. Xue, "Synchronization on complex networks of networks," *IEEE transactions on neural networks and learning systems*, 2014.

[22] R. Albert and A.-L. Barabási, "Statistical mechanics of complex networks," *Rev. Mod. Phys.*, vol. 74, pp. 47–97, jan 2002.

[23] B. Quoitin and S. Uhlig, "Modeling the routing of an autonomous system with c-bgp," *IEEE Network*, 2005.

[24] A. Celaj, U. Schlecht, J. D. Smith, W. Xu, S. Suresh, M. Miranda, A. M. Aparicio, M. Proctor, R. W. Davis, F. P. Roth, *et al.*, "Quantitative analysis of protein interaction network dynamics in yeast," *Molecular Systems Biology*, 2017.

[25] K. Tarassov, V. Messier, C. R. Landry, S. Radinovic, M. M. S. Molina, I. Shames, Y. Malitskaya, J. Vogel, H. Bussey, and S. W. Michnick, "An in vivo map of the yeast protein interactome," *Science*, vol. 320, no. 5882, pp. 1465–1470, 2008.

[26] A. Huett, A. Ng, Z. Cao, P. Kuballa, M. Komatsu, M. J. Daly, D. K. Podolsky, and R. J. Xavier, "A Novel Hybrid Yeast-Human Network Analysis Reveals an Essential Role for FNBP1L in Antibacterial Autophagy 1," *The Journal of Immunology*, 2009.

[27] O. Sporns, "The human connectome: origins and challenges," *Neuroimage*, vol. 80, pp. 53–61, 2013.

[28] H. Anderson and T. Britton, *Stochastic Epidemic Models and Their Statistical Analysis*. New York: Springer, 2000.

[29] M. Boguná, C. Castellano, and R. Pastor-Satorras, "Nature of the epidemic threshold for the susceptible-infected-susceptible dynamics in networks," *Physical review letters*, vol. 111, no. 6, p. 068701, 2013.

[30] S. C. Ferreira, R. S. Sander, and R. Pastor-Satorras, "Collective versus hub activation of epidemic phases on networks," *Physical Review E*, vol. 93, no. 3, p. 032314, 2016.

[31] C. Castellano and R. Pastor-Satorras, "Competing activation mechanisms in epidemics on networks," *Scientific reports*, vol. 2, p. 371, 2012.

[32] Y. Wang, D. Chakrabarti, C. Wang, and C. Faloutsos, "Epidemic spreading in real networks: an eigenvalue viewpoint," in *22nd International Symposium on Reliable Distributed Systems, 2003. Proceedings.*, pp. 25–34, 2003.

[33] D. Chakrabarti, Y. Wang, C. Wang, J. Leskovec, and C. Faloutsos, "Epidemic thresholds in real networks," *ACM Trans. Inf. Syst. Secur.*, vol. 10, no. 4, 2008.

[34] P. Van Mieghem, J. Omic, and R. Kooij, "Virus spread in networks," *IEEE/ACM Transactions on Networking*, vol. 17, no. 1, pp. 1–14, 2009.

[35] P. Van Mieghem, "The viral conductance of a network," *Computer Communications*, vol. 35, no. 12, pp. 1494 – 1506, 2012.

[36] P. Van Mieghem, "Epidemic phase transition of the sis type in networks," *Europhysics Letters*, vol. 97, no. 4, p. 48004, 2012.

[37] R. Pastor-Satorras, C. Castellano, P. Van Mieghem, and A. Vespignani, "Epidemic processes in complex networks," *Rev. Mod. Phys.*, vol. 87, pp. 925–979, 2015.

[38] A. S. Mata and S. C. Ferreira, "Pair quenched mean-field theory for the susceptible-infected-susceptible model on complex networks," *EPL (Europhysics Letters)*, vol. 103, no. 4, p. 48003, 2013.

[39] D. H. Silva, S. C. Ferreira, W. Cota, R. Pastor-Satorras, and C. Castellano, "Spectral properties and the accuracy of mean-field approaches for epidemics on correlated power-law networks," *Phys. Rev. Research*, vol. 1, p. 033024, 2019.

[40] D. H. Silva, F. A. Rodrigues, and S. C. Ferreira, "High prevalence regimes in the pair-quenched mean-field theory for the susceptible-infected-susceptible model on networks," *Phys. Rev. E*, vol. 102, p. 012313, 2020.

[41] M. Shrestha, S. V. Scarpino, and C. Moore, "Message-passing approach for recurrent-state epidemic models on networks," *Physical Review E*, vol. 92, no. 2, p. 022821, 2015.

[42] B. Karrer and M. E. Newman, "Message passing approach for general epidemic models," *Physical Review E*, vol. 82, no. 1, p. 016101, 2010.

[43] C. Castellano and R. Pastor-Satorras, "Relevance of backtracking paths in recurrent-state epidemic spreading on networks," *Phys. Rev. E*, vol. 98, p. 052313, 2018.

[44] T. Mountford, D. Valesin, and Q. Yao, "Metastable densities for the contact process on power law random graphs," *Electronic Journal of Probability*, vol. 18, no. 103, p. 36 pp., 2013.

[45] S. Chatterjee and R. Durrett, "Contact processes on random graphs with power law degree distributions have critical value 0," *The Annals of Probability*, vol. 37, no. 6, pp. 2332–2356, 2009.

[46] J.-D. Bancal and R. Pastor-Satorras, "Steady-state dynamics of the forest fire model on complex networks," *Eur. Phys. J. B*, vol. 76, pp. 109–121, 2010.

[47] S. C. Ferreira, C. Castellano, and R. Pastor-Satorras, "Epidemic thresholds of the susceptible-infected-susceptible model on networks: A comparison of numerical and theoretical results," *Physical Review E*, vol. 86, no. 4, p. 041125, 2012.

[48] J. C. M. Silva, D. H. Silva, F. A. Rodrigues, and S. C. Ferreira, "Comparison of theoretical approaches for epidemic processes with waning immunity in complex networks," *Physical Review E*, vol. 106, no. 3, p. 034317, 2022.

[49] J. C. M. Silva, D. H. Silva, F. A. Rodrigues, and S. C. Ferreira, "Consequences of non-markovian healing processes on epidemic models with recurrent infections on networks," *New Journal of Physics*, vol. 27, no. 1, p. 013009, 2025.

[50] A.-L. Barabási and M. Pósfai, *Network science*. Cambridge, UK: Cambridge University Press, 2016.

[51] M. Newman, *Networks: an introduction*. Oxford university press, 2010.

[52] A. Barrat, M. Barthelemy, and A. Vespignani, *Dynamical processes on complex networks*. Cambridge University Press, 2008.

[53] G. Caldarelli, *Large scale structure and dynamics of complex networks: from information technology to finance and natural science*, vol. 2. World Scientific, 2007.

[54] "What does autonomous system mean?." https://www.techopedia.com/definition/11063/autonomous-system-as. Accessed: 2024-03-26.

[55] "Autonomous systems." https://www.ibm.com/docs/fr/aix/7.1?topic=protocol-autonomous-systems. Accessed: 2024-03-26.

[56] R. Pastor-Satorras, A. Vázquez, and A. Vespignani, "Dynamical and correlation properties of the internet," *Phys. Rev. Lett.*, vol. 87, p. 258701, Nov 2001.

[57] G. Bianconi and A.-L. Barabási, "Bose-einstein condensation in complex networks," *Physical review letters*, vol. 86, no. 24, p. 5632, 2001.

[58] R. Albert and A.-L. Barabási, "Statistical mechanics of complex networks," *Reviews of modern physics*, vol. 74, no. 1, p. 47, 2002.

[59] M. Boguná, R. Pastor-Satorras, and A. Vespignani, "Cut-offs and finite size effects in scale-free networks," *The European Physical Journal B*, vol. 38, no. 2, pp. 205–209, 2004.

[60] M. Boguná, C. Castellano, and R. Pastor-Satorras, "Langevin approach for the dynamics of the contact process on annealed scale-free networks," *Physical Review E*, vol. 79, no. 3, p. 036110, 2009.

[61] A. S. Mata and S. C. Ferreira, "Multiple transitions of the susceptible-infected-susceptible epidemic model on complex networks," *Physical Review E*, vol. 91, no. 1, p. 012816, 2015.

[62] F. Chung, L. Lu, and V. Vu, "The spectra of random graphs with given expected degrees," *Internet Mathematics*, vol. 1, no. 3, pp. 257–275, 2004.

[63] D. H. Silva, S. C. Ferreira, W. Cota, R. Pastor-Satorras, and C. Castellano, "Spectral properties and the accuracy of mean-field approaches for epidemics on correlated power-law networks," *Phys. Rev. Res.*, 2019.

[64] Y. Wang, J. Ma, J. Cao, and L. Li, "Edge-based epidemic spreading in degree-correlated complex networks," *Journal of theoretical biology*, vol. 454, pp. 164–181, 2018.

[65] X.-H. Chen, S.-M. Cai, W. Wang, M. Tang, and H. E. Stanley, "Predicting epidemic threshold of correlated networks: A comparison of methods," *Physica A: Statistical Mechanics and its Applications*, 2018.

[66] C. Kittel and P. McEuen, *Introduction to solid state physics*. John Wiley & Sons, 2018.

[67] S.-H. Yook, H. Jeong, and A.-L. Barabási, "Modeling the internet's large-scale topology," *Proceedings of the National Academy of Sciences*, vol. 99, no. 21, pp. 13382–13386, 2002.

[68] A.-L. Barabási, "The physics of the web," *Physics World*, vol. 14, no. 7, p. 33, 2001.

[69] F. Arrigo, D. J. Higham, and V. Noferini, "Beyond non-backtracking: non-cycling network centrality measures," *Proceedings of the Royal Society A*, 2020.

[70] F. Bloch, M. O. Jackson, and P. Tebaldi, "Centrality measures in networks," *Social Choice and Welfare*, vol. 61, no. 2, pp. 413–453, 2023.

[71] M. E. Newman, "A measure of betweenness centrality based on random walks," *Social networks*, vol. 27, no. 1, pp. 39–54, 2005.

[72] D. Vilone and C. Castellano, "Solution of voter model dynamics on annealed small-world networks," *Physical Review E*, vol. 69, no. 1, p. 016109, 2004.

[73] S. N. Dorogovtsev and J. F. F. Mendes, "Evolution of networks," *Adv. Phys.*, vol. 51, pp. 1079–1187, jun 2002.

[74] M. Kitsak, L. K. Gallos, S. Havlin, F. Liljeros, L. Muchnik, H. E. Stanley, and H. A. Makse, "Identification of influential spreaders in complex networks," *Nature physics*, vol. 6, no. 11, p. 888, 2010.

[75] T. Tomé, *Dinâmica Estocástica e Irreversibilidade Vol. 35*. Edusp, 2001.

[76] J. Jimenez-Martinez and C. F. Negre, "Eigenvector centrality for geometric and topological characterization of porous media," *Physical Review E*, vol. 96, no. 1, p. 013310, 2017.

[77] C. Castellano and R. Pastor-Satorras, "Relevance of backtracking paths in recurrent-state epidemic spreading on networks," *Physical Review E*, vol. 98, no. 5, p. 052313, 2018.

[78] D. H. Silva and S. C. Ferreira, "Dissecting localization phenomena of dynamical processes on networks," *Journal of Physics: Complexity*, 2021.

[79] R. Pastor-Satorras and C. Castellano, "The localization of non-backtracking centrality in networks and its physical consequences," *Scientific reports*, vol. 10, no. 1, pp. 1–12, 2020.

[80] F. Arrigo, D. J. Higham, and V. Noferini, "Non-backtracking alternating walks," *SIAM Journal on Applied Mathematics*, 2019.

[81] N. Alon, I. Benjamini, E. Lubetzky, and S. Sodin, "Non-backtracking random walks mix faster," *Communications in Contemporary Mathematics*, 2007.

[82] M. E. J. Newman, "Spread of epidemic disease on networks," *Phys. Rev. E*, vol. 66, p. 016128, Jul 2002.

[83] T. Martin, X. Zhang, and M. E. Newman, "Localization and centrality in networks," *Physical review E*, 2014.

[84] C. Glover and M. Kempton, "Some spectral properties of the non-backtracking matrix of a graph," *Linear Algebra and its Applications*, vol. 618, pp. 37–57, 2021.

[85] C. Merger, J. Albers, C. Honerkamp, and M. Helias, "Spurious self-feedback of mean-field predictions inflates infection curves," *Physical Review E*, 2024.

[86] C. Castellano and R. Pastor-Satorras, "Thresholds for epidemic spreading in networks," *Physical review letters*, vol. 105, no. 21, p. 218701, 2010.

[87] N. G. Van Kampen, *Stochastic processes in physics and chemistry*, vol. 1. Elsevier, 1992.

[88] C. Graham and D. Talay, *Stochastic simulation and Monte Carlo methods: mathematical foundations of stochastic simulation*, vol. 68. Springer Science & Business Media, 2013.

[89] M. E. Newman and G. T. Barkema, *Monte Carlo methods in statistical physics*. Clarendon Press, 1999.

[90] V. Balakrishnan, *Elements of nonequilibrium statistical mechanics*, vol. 3. Springer, 2008.

[91] J. Marro and R. Dickman, *Nonequilibrium phase transitions in lattice models*. Cambridge University Press, 2005.

[92] J. Marro and R. Dickman, *Nonequilibrium Phase Transitions in Lattice Models*. Aléa-Saclay, Cambridge University Press, 2005.

[93] M. Henkel, H. Hinrichsen, and S. Lübeck, *Non-Equilibrium Phase Transitions*, vol. I. Netherlands: Springer, Dordrecht, 2008.

[94] W. Cota and S. C. Ferreira, "Optimized Gillespie algorithms for the simulation of Markovian epidemic processes on large and heterogeneous networks," *Computer Physics Communications*, 2017.

[95] I. Z. Kiss, J. C. Miller, P. L. Simon, *et al.*, "Mathematics of epidemics on networks," *Cham: Springer*, vol. 598, 2017.

[96] M. J. Keeling and P. Rohani, *Modeling infectious diseases in humans and animals*. Princeton university press, 2011.

[97] W. Cota, *Spreading phenomena on complex networks and social systems*. Thesis, Universidade Federal de Viçosa, 2020.

[98] G. S. Costa and S. C. Ferreira, "Simple quasistationary method for simulations of epidemic processes with localized states," *Comput. Phys. Commun.*, vol. 267, p. 108046, 2021.

[99] R. Dickman and R. Vidigal, "Quasi-stationary distributions for stochastic processes with an absorbing state," *Journal of Physics A: Mathematical and General*, vol. 35, no. 5, p. 1147, 2002.

[100] C. Deroulers and R. Monasson, "Field-theoretic approach to metastability in the contact process," *Physical Review E*, 2004.

[101] K. J. Sharkey, "Deterministic epidemic models on contact networks: Correlations and unbiological terms," *Theoretical population biology*, vol. 79, no. 4, pp. 115–129, 2011.

[102] G. Jenkinson and J. K. Goutsias, "Numerical integration of the master equation in some models of stochastic epidemiology," *PLoS ONE*, vol. 7, 2012.

[103] G. StOnge, V. Thibeault, A. Allard, L. J. Dubé, and L. Hébert-Dufresne, "Master equation analysis of mesoscopic localization in contagion dynamics on higher-order networks.," *Physical review. E*, vol. 103 3-1, p. 032301, 2020.

[104] G. S. Costa, M. M. de Oliveira, and S. C. Ferreira, "Heterogeneous mean-field theory for two-species symbiotic processes on networks," *Physical Review E*, vol. 106, no. 2, p. 024302, 2022.

[105] A. S. Mata, R. S. Ferreira, and S. C. Ferreira, "Heterogeneous pair-approximation for the contact process on complex networks," *New Journal of Physics*, vol. 16, no. 5, p. 053006, 2014.

[106] D. H. Silva and S. C. Ferreira, "Activation thresholds in epidemic spreading with motile infectious agents on scale-free networks," *Chaos: An Interdisciplinary Journal of Nonlinear Science*, vol. 28, no. 12, p. 123112, 2018.

[107] D. H. Silva, F. A. Rodrigues, and S. C. Ferreira, "High prevalence regimes in the pair-quenched mean-field theory for the susceptible-infected-susceptible model on networks," *Physical Review E*, vol. 102, no. 1, p. 012313, 2020.

[108] B. Munsky and M. Khammash, "The finite state projection algorithm for the solution of the chemical master equation," *The Journal of chemical physics*, vol. 124, no. 4, 2006.

[109] R. B. Sidje and W. J. Stewart, "A numerical study of large sparse matrix exponentials arising in markov chains," *Computational statistics & data analysis*, vol. 29, no. 3, pp. 345–368, 1999.

[110] S. H. Strogatz, *Nonlinear dynamics and chaos: with applications to physics, biology, chemistry, and engineering*. CRC press, 2018.

[111] R. Pastor-Satorras and A. Vespignani, "Epidemic spreading in scale-free networks," *Phys. Rev. Lett.*, vol. 86, pp. 3200–3203, apr 2001.

[112] A. S. da Mata, R. S. Ferreira, and S. C. Ferreira, "Heterogeneous pair-approximation for the contact process on complex networks," *New Journal of Physics*, 2014.

[113] R. Pastor-Satorras and A. Vespignani, "Immunization of complex networks," *Physical review E*, vol. 65, no. 3, p. 036104, 2002.

[114] M. Boguá, R. Pastor-Satorras, and A. Vespignani, "Epidemic spreading in complex networks with degree correlations," in *Statistical mechanics of complex networks*, pp. 127–147, Springer, 2003.

[115] A. V. Goltsev, S. N. Dorogovtsev, J. G. Oliveira, and J. F. Mendes, "Localization and spreading of diseases in complex networks," *Physical review letters*, vol. 109, no. 12, p. 128702, 2012.

[116] G. Kozyreff and T. Erneux, "Contagious photons: Laser dynamics and the susceptible-infected-recovered model," *Physical Review E*, vol. 108, no. 2, p. 024218, 2023.

[117] R. Criado, J. Flores, E. García, A. J. G. del Amo, Á. Pérez, and M. Romance, "On the α-nonbacktracking centrality for complex networks: Existence and limit cases," *Journal of Computational and Applied Mathematics*, vol. 350, pp. 35–45, 2019.

[118] C. Widder and T. Schilling, "Generating functions for message passing on weighted networks: Directed bond percolation and susceptible, infected, recovered epidemics," *Physical Review E*, vol. 104, no. 5, p. 054305, 2021.

[119] D. Aleja, R. Criado, A. J. G. del Amo, Á. Pérez, and M. Romance, "Non-backtracking pagerank: From the classic model to hashimoto matrices," *Chaos, Solitons & Fractals*, vol. 126, pp. 283–291, 2019.

[120] F. R. Gantmacher and J. L. Brenner, *Applications of the Theory of Matrices*. Courier Corporation, 2005.

[121] R. Pastor-Satorras and C. Castellano, "Distinct types of eigenvector localization in networks," *Scientific reports*, vol. 6, no. 1, pp. 1–9, 2016.

[122] R. Pastor-Satorras and C. Castellano, "Eigenvector localization in real networks and its implications for epidemic spreading," *J. Stat. Phys.*, vol. 173, pp. 1110–1123, feb 2018.

[123] F. Chung, L. Lu, and V. Vu, "Spectra of random graphs with given expected degrees," *Proc. Natl. Acad. Sci. U.S.A.*, vol. 100, pp. 6313–6318, may 2003.

[124] D. J. Watts and S. H. Strogatz, "Collective dynamics of small-worldnetworks," *nature*, vol. 393, no. 6684, pp. 440–442, 1998.

[125] J. A. Hołyst, J. Sienkiewicz, A. Fronczak, P. Fronczak, and K. Suchecki, "Universal scaling of distances in complex networks," *Physical Review E*, vol. 72, no. 2, p. 026108, 2005.

[126] J. C. de Moraes Silva, "O papel de sítios periféricos no processo epidêmico sis," master's thesis, Universidade Federal de Viçosa, 2019. Available at https://www.locus.ufv.br/handle/123456789/28444.

[127] J. Joo and J. L. Lebowitz, "Pair approximation of the stochastic susceptible-infected-recovered-susceptible epidemic model on the hypercubic lattice," *Phys. Rev. E*, vol. 70, p. 036114, 2004.

[128] D. ben Avraham and J. Köhler, "Mean-field (n,m)-cluster approximation for lattice models," *Phys. Rev. A*, vol. 45, pp. 8358–8370, Jun 1992.

[129] T. Friedrich, A. Göbel, N. Klodt, M. S. Krejca, and M. Pappik, "Analysis of the survival time of the SIS and SIRS process on stars and cliques," *arXIv 2205.02653*, 2022.

[130] T. Friedrich, A. Göbel, N. Klodt, M. S. Krejca, and M. Pappik, "Analysis of the survival time of the SIRS process via expansion," *Electronic Journal of Probability*, vol. 29, 2024.

[131] F. Krzakala, C. Moorec, E. Mosseld, J. Neemand, A. Slyd, L. Zdeborováe, and P. Zhanga, "Spectral redemption in clustering sparse networks," *Proceedings of the National Academy of Sciences of the United States of America*, vol. 110, pp. 20935–20940, 2013.

[132] K.-i. Hashimoto, "Zeta functions of finite graphs and representations of p-adic groups," *Advanced Studies in Pure Mathematics*, vol. 15, pp. 211–280, 1989.

[133] M. M. de Oliveira and R. Dickman, "How to simulate the quasistationary state," *Phys. Rev. E*, vol. 71, p. 016129, 2005.

[134] R. S. Sander, G. S. Costa, and S. C. Ferreira, "Sampling methods for the quasistationary regime of epidemic processes on regular and complex networks," *Phys. Rev. E*, vol. 94, p. 042308, 2016.

[135] R. Pastor-Satorras and C. Castellano, "The localization of non-backtracking centrality in networks and its physical consequences," *Scientific Reports*, vol. 10, p. 21639, 2020.

[136] M. Catanzaro, M. Boguná, and R. Pastor-Satorras, "Generation of uncorrelated random scale-free networks," *Physical review e*, vol. 71, no. 2, p. 027103, 2005.

[137] S. N. Dorogovtsev, A. V. Goltsev, and J. F. F. Mendes, "K-core organization of complex networks," *Physical review letters*, vol. 96, no. 4, p. 040601, 2006.

[138] D. R. de Souza and T. Tomé, "Stochastic lattice gas model describing the dynamics of the SIRS epidemic process," *Phys. A Stat. Mech. its Appl.*, vol. 389, pp. 1142–1150, 2010.

[139] S. Chatterjee and R. Durrett, "Contact processes on random graphs with power law degree distributions have critical value 0," *The Annals of Probability*, 2009.

[140] R. Durrett, *Probability: theory and examples*. Belmont, CA: Duxbury Press, second ed., 1996.

[141] M. J. Keeling and P. Rohani, *Modeling infectious diseases in humans and animals*. Princeton University Press, 9 2011.

[142] H. J. Wearing, P. Rohani, and M. J. Keeling, "Appropriate models for the management of infectious diseases," *PLOS Medicine*, vol. 2, p. null, 07 2005.

[143] H. T. Nguyen and P. Rohani, "Noise, nonlinearity and seasonality: the epidemics of whooping cough revisited," *Journal of The Royal Society Interface*, vol. 5, no. 21, pp. 403–413, 2008.

[144] P. Van Mieghem and R. van de Bovenkamp, "Non-markovian infection spread dramatically alters the susceptible-infected-susceptible epidemic threshold in networks," *Phys. Rev. Lett.*, vol. 110, p. 108701, Mar 2013.

[145] J. A. Hołyst, J. Sienkiewicz, A. Fronczak, P. Fronczak, and K. Suchecki, "Universal scaling of distances in complex networks," *Phys. Rev. E*, vol. 72, p. 026108, Aug 2005.

[146] C. Castellano and R. Pastor-Satorras, "Cumulative merging percolation and the epidemic transition of the susceptible-infected-susceptible model in networks," *arXiv:1906.06300v1*, 2019.

[147] G. Röst and T. Tekeli, "Stability and oscillations of multistage sis models depend on the number of stages," *Applied Mathematics and Computation*, vol. 380, p. 125259, 2020.

[148] E. Cator, R. van de Bovenkamp, and P. Van Mieghem, "Susceptible-infected-susceptible epidemics on networks with general infection and cure times," *Phys. Rev. E*, vol. 87, p. 062816, Jun 2013.

[149] P. Van Mieghem and Q. Liu, "Explicit non-markovian susceptible-infected-susceptible mean-field epidemic threshold for weibull and gamma infections but poisson curings," *Phys. Rev. E*, vol. 100, p. 022317, Aug 2019.

[150] G. G. Jensen, F. Uekermann, and K. Sneppen, "Multi stability and global bifurcations in epidemic model with distributed delay sirns-model," *The European Physical Journal B*, vol. 92, pp. 28–33, 2019.

[151] C. D. Meyer, *Matrix analysis and applied linear algebra*. SIAM, 2023.

[152] D. Zwillinger, *Table of Integrals, Series, and Products*. Elsevier, 2015.

[153] G. Arfken and H. Weber, *Mathematical Methods for Physicists*. Mathematical Methods for Physicists, Elsevier Science, 2013.